Optimal Estimation and Passivity based Control for Human Friendly Robots

Cao, Sheng

(Degree)
博士（工学）

(Date of Degree)
2017-09-25

(Date of Publication)
2018-09-01

(Resource Type)
doctoral thesis

(Report Number)
甲第7012号

(URL)
https://hdl.handle.net/20.500.14094/D1007012

Doctoral Dissertation

Optimal Estimation and Passivity based Control for Human Friendly Robots

ヒトに優しいロボットのための
最適推定と受動性に基づく制御
に関する研究

Sheng Cao

July 2017
Graduate School of System Informatics
Kobe University

Content

Chapter 1 Introduction

1.1 Background

1.1.1 The coming aged society

In recent years, due to the decrease of the birthrate and increase of the aged people, many countries in the world have faced the problem of aging population. The rapid declines in mortality and fertility after the World War II accelerated population of aging. Asia and Europe will become the two severely afflicted regions of this problem in the near future. For instance, in Japan, the percentage of people aged over 60s within the total population is the highest in the world: 30.5% in 2010. By 2025, one in every three people will be over 60s. When 2050 comes, 41.5% of Japanese will be elderly people. Population ageing will seriously influence not only the modern industry but also social welfare, medical system, social economy and almost all areas of social activities.

Therefore, it is highly expected that new technologies such as robotics can be developed and come to play a central role to help to solve the serious social problems.

1.1.2 From industrial robot to human friendly robot

The word robot is originated from a Czech word ‘robota’ which means forced laborer. The Robotic Institute of America defines robot as a reprogrammable multi-functional manipulator designed to move materials, parts, tools, or specialized devices, through variable programmed motions for the performance of a variety of tasks. Nowadays, robots can help people complete desired works in many areas.

The initial purpose of the robot was to liberate human from the heavy work in production lines of factories. In Japan, since 1960s, teaching playback based industrial robots has been already used in many factories. The industrial robot elevates the production efficiency and creates more economical value.

However, recent advances in the robotic technology, on the other hand, try to carry robots out of the factories to help people in more aspects. As the rhythm of the modern life speeds up and the aged society is coming, human friendly robot, which

can directly interact with the human, such as in rescue, amusement, household, medical and welfare, becomes more and more important. In order to better solve the problems exerting in the coming aged society, how to develop human-friendly robot to support many aspects in aged people's daily life needs to be carefully considered. By now, in the research field of human friendly robot for aged people, it appears many kinds of robot with different functions, respectively. They can be divided into two groups:

- Human friendly robot which can provide mental support: in order to release the mental pressure or decrease the lonely feelings of the aged people, some amusement robots which can dance or perform as a pet has been researched.
- Human friendly robot which can provide physical support: in order to take care of the physical ability loss of the aged people, some physical supporting robot, such as nursing care robot or rehabilitation robot, has been researched.

In this thesis, we focus on the research of the second group: how to make robot provide human-friendly physical support to aged or disabled people.

1.1.3 Physical interaction problem of the human friendly robot

In order to realize the friendly physical interaction between the robot and human, it is important to solve the following three key technical problems:

- Firstly, robot should measure and recognize its surrounding unknown environment as well as physically interacted objects. Among a lot of effective measurement designs, it is necessary to choose a rational design which can balance all tradeoff factors including accuracy of the measurement, efficiency of the measurement and cost of the design, etc.
- Secondly, during the physical interaction, the robot should avoid any kinds of harms to human subjects, that is, the mechanical energy from the robot to the interacted objects should be kept limited.
- Finally, structure design of the robot should fit with human's physical and psychological properties. From the mechanical point of view, this structure

should fit with the complex joint structures of the human body so as to avoid any limitation acting on human joint's motion.

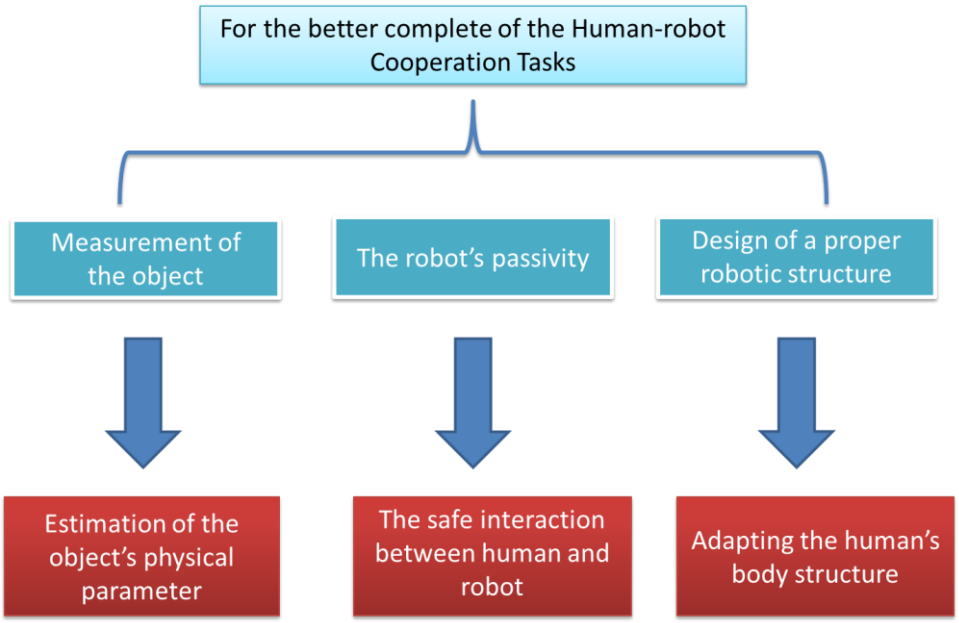

Fig. 1.1 Problems required to be solved for Human Friendly Robot Design

In detail, as shown in Fig. 1.1, the three problems can be discussed as follows:

- Measurement of the object: to estimate the object's physical parameter

Obviously, in human-robot physical interaction tasks, especially for those full-body manipulation tasks, as the first step, it is important to obtain the object's physical properties. For example, when the robot is required to carry up a patient, the patient's body information, such as center position of the mass, length of the body and so on, are necessary so as to control the total human-robot system. We can use a lot of sensors to measure the object's information, such as the size of force or the contact position and so on, so that we can further estimate the object's physical parameter. In the traditional industrial robot's design, the force sensors are designed to equip at almost same location of the contact point, however, when we consider the contact problem in the human-robot physical interaction, for instance, when a nursing care robot is lifting up a person, it is required to perform full body manipulation with a lot of contact points between the robot and the person. The location of sensors and the position of the contact points may not coincide with each other, leading the new problem of object estimation.

- The robot's passivity

During the human robot interaction, the safety problem is a big issue that we need to consider. In the traditional industrial robot design, since the robot does not contact directly with the human, compared with some features which can prompt the effective production, the safety contact problem of the robot manipulator was not so crucial in those days. However, as the increasing needs of the human-robot friendly cooperation, the safety problem becomes more and more important in the robotic research. Fortunately, we can achieve this desired control purpose by focusing on the robot's passivity. If we take the point of view of energy, once the energy exerted by the robot to the environment is limited under a certain value, the robot is passive and obviously, since there's no more surplus energy, the robot's motion can be safe.

- Design of an appropriate robotic structure which is capable to adapt the human body's structure

Furthermore, it is also important to discuss on how to design a proper mechanical structure of a human friendly robot.

In traditional industrial robot's design, every motor equipped at a robot's joint actually defines one rotation axis. These motors provide the strong power to the robot while prevent the joint's motion in the extra D.O.F.s. Since the structure of each joint of human body is more complex with more than one D.O.F, when considering the case that human-robot directly connected with each other and need to complete one certain task with the cooperation, it is required that design of robot's joint should perfect fit the human body's structure. Obviously, the traditional mechanical design is difficult to satisfy this requirement. One solution to make robot's design better fit the human body is to apply cable driven mechanism rather than using the system directly driven by a fixed axis motor. In this thesis, we propose a passivity based control method for a proper robot's structure which has better fit with complex human body's joint structure.

1.2 Previous Researches

1.2.1 Estimation of the object's physical parameter

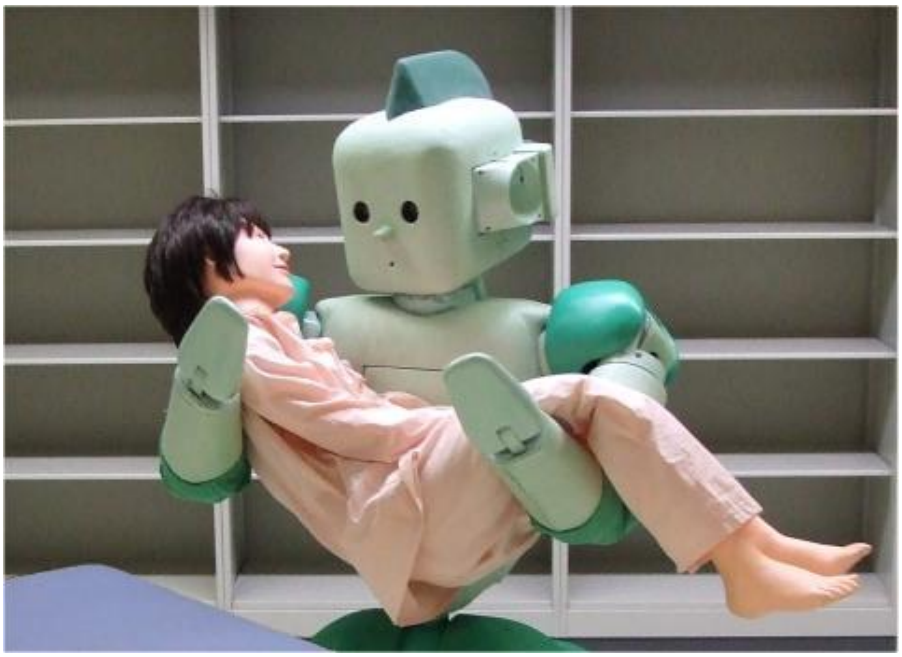

Fig. 1.1 RI-MAN carries up a person

Considering the full body manipulation, such as to carry up a person by full robot arm and body of RI-MAN as shown in Fig.1.2 of [1] to [5], the previous research proposed to attach tactile sensor sheets onto the robot surface so as to measure the contact point positions as well as contact forces directly from the sensor sheet. However, such sensor sheet is not only too expensive but also easily be harmed during direct interaction. In addition, more time is required to sampling and process of the data from the two dimensional sensor sheets.

On the other hand, Nagase proposed a method of estimating a contact point between a robot finger and an object by using a force sensor which is equipped at different location of the contact point [6]. By taking into account of measurement noise, the research formulated an objective function represented the error and introduced the Lagrange multipliers to choose an optimal solution so as the error be as small as possible. However, this research did not consider the case of multiple contact points.

In nursing care job, human body is a redundant system due to its lots of D.O.Fs. This makes the computation to control of the cared person very difficult. In [7], Dong

proposed to reduce the unnecessary D.O.Fs of the human body to make the human model be simple. He also proposed an adaptive force control method to handle the human model uncertainties.

Therefore, when we analyze the situation of the person be lifted up, we can regard his/her body as a simple geometrical shape so that the robot can complete the task at the real time.

1.2.2 Passivity: Keep the Safe human-robot interaction

In order to keep safe contact between the robot and human, many researches have been proposed such that to design the light weight of the robot body [8],[9], to design the high-performance torque-controlled joints[10], to design the impedance control [11].

For impedance control, if the impedance center is time constant, then it can keep the robot's passivity, however, in the case when the impedance is time varying, the robot may lost its passivity.

In order to realize the robot's trajectory tracking as well as maintaining passivity, P. Li et al. proposed passive velocity field control (called PVFC[12] to [16]). This method first augments the robot system by creating a virtual passive energy storage element, such as a flywheel or a spring. Then, it creates a desired velocity field based on a desired trajectory so that the robot and the augmented system can correctly complete the trajectory tracking. After some proper design of the controller, the robot can asymptotically track the desired trajectory and satisfy the passivity. However, this control law is too complicated for real time control.

In order to overcome the influence of time-varying desired trajectory to the impedance control, Kishi et al. proposed passive impedance control by adjusting the scalar parameter of the desired velocity [17]. However, the approach could not cover the robot's model uncertainties' problem.

In addition, although sliding mode control [19] is also proposed to realize robust tracking control of time-varying reference trajectory under the robot's model

uncertainties, it is impossible to keep the robot's passivity. P. Li et al. proposed adaptive PVFC [14] to take into account the robot's model uncertainties' problem. However, like the previous PVFC, this control law is too complicated for real time computation.

1.2.3 Proper Structure Design: Cable-Driven Exoskeleton

To realize better fit of a robot to human, recently, exoskeleton robot has been focused. Exoskeleton robots can be utilized on human's activity support, rehabilitation works and so on. Compared to traditional planar robotic manipulator which support the user's activity only depending on the connecting of end-effector and the human hand, the exoskeleton possesses a lot of superiorities [20]-[25]. Simply speaking, it can provide 3D interaction at the joint level while the traditional planar robot only supervised human hand motion. However, unfortunately, since the joints of human body are too complex, the fitness between the exoskeleton devices and human remains to be improved.

In recent years, research of cable-driven exoskeleton robot becomes popular. Compared to other researches of exoskeleton [26]-[29], the cable-driven system is well known for their lightweight, low moving inertia, ease of the transformation and cheap. These features are desirable in human friendly devices and is started to be used in many kinds of applications, such as rehabilitation.

However, Similar with the muscular system, cable-driven robots have two important characteristics:

1) Cable has an inability that it can only actuate robots with positive tension force but not push.

2) In order to make the system completely restrained, it is necessary to add the redundant cables into the system.

Lack of the compression ability of the cables affects some abilities of the cable-driven robot, such as

1. It affects the achievable place of the robot, which need to be considered both

in the construction of the cable's distribution and in the control scheme of the cable-driven robot.

2. It makes tension be necessary to be nonnegative and creates a big barrier for the control scheme.

Considering the first term, there are some different classifications of the limited workspace, such as the Static Equilibrium Workspace [32], the Wrench Closure Workspace [33][34] and the Wrench Feasible Workspace [35][36].

In fact, there are many researches focusing on the construction of the cable-driven robot's appropriate control scheme for overcoming its problems shown in 1 and 2. Oh and Agrawal [37] proposed a method which handle the nonnegative tension problem of the cable-driven robot using both LP (Linear Programming) and QP (Quadratic Programming) programming solver. Fang et al. [39] suggested a method of using PD control law to control the motion of cable-driven robot considering the optimal tension distribution. However, the admissible zone mentioned in these researches paper may not exist in some situations, which makes computer unable to complete the calculation of the tension distribution. Besides, optimization method used in the tension distribution would cause a lot of calculation time. Borgstrom [40] proposed a method which introduces a slack variable to enable the explicit computation of the near-optimal feasible start point leading to the rapid calculation of tension distribution. In order to handle the dynamical position tracking task of the cable-driven robot, Oh and Agrawal[38] have attempted to build iterative computational framework which first calculate the reachable domain based on the initial position considering the nonnegative tension input constraint and then determine the most appropriate desired position which is the closest one toward to the final desired position in this feasible domain. However, the algorithm proposed in this research is too complicated leading a lot of calculation time. Moreover, the computation difficulty would increase fast along with the augment of the cable's quantity. This research also left the problem that the final desired position moves in a trajectory was not considered.

1.3 Research Purposes of the Thesis

The research work presented in this thesis addresses the issues related to the design of human friendly robot. The major research purposes of this thesis are outlined as follows.

Firstly, this thesis studies optimal estimation of interacted object's physical parameters, such as the center of gravity of the object based on the contact point and contact force estimation from force sensors equipped on the robot arms. Considering the case when we are asking a robot to perform nursing care tasks, such as to carry up a person by two arms, it is clear that, in order for a robot to realize physical interaction with a heavy person, full body manipulation is effective. During full body manipulation, the cared person's center of gravity should be estimated so as to avoid dropping of him or her. On the other hand, full body manipulation also cause that the robot may contact human with multiple contact points. The position of the sensor may not coincide with the contact points. In this research, multi axed force sensor that is located at different position from the contact points to estimate optimally the interacted object's physical parameters is used. Two cases, (1)when a robot arm is contacting with an object at one point or two points, and (2) when two robot arms is holding an common object, are studied. Experiments and simulations are performed to show the effectiveness of our approach.

The second research in this thesis focuses on the robot's safety problem from the view of the passivity meaning that robots do not add any surplus energy to the environment. It is clear that, there are two factors that influence the robot's passivity. One comes from the time-varying reference trajectory of robot. Another is due to the robot's model uncertainties when performing nonlinear dynamic control. To reduce the effect from the robot's model uncertainties, in this thesis, two control methods are proposed. Firstly, by carefully adjusting the estimation parameters of the robot, it shows possibility to use simple PD like control to keep the robot's passivity. However, since the trajectory tracking performance as well as the force response result are not improved even by using this PD like control method, we further design observer

based passive impedance control method to observe the effect from the model uncertainties so as to keep the robot's passivity as well as desired impedance control's results. The effectiveness of these approaches is evaluated using computer simulations.

Considering the possibility of the robotic rehabilitation, the last study of the thesis pay attention to the fitness between the robot and human, a passivity based control design is performed for a robot with cable-driven structure to realize better fitness with the complex human body joint structure. Taking into account of the limitations that the cable driven robot has high redundant actuation and cable tension needs to be kept in a certain range, the passive velocity field control (PVFC) method is extended for the redundant cable-driven robot system to realize not only passivity but also tracking performance. The effectiveness of these approaches is also evaluated using computer simulations.

Chapter 2 Robot Dynamics and Control

This Chapter describes basic dynamics and control approaches for a robot manipulator that will be used in the following chapters.

2.1 Property of Robot Dynamics

2.1.1 Lagrange Equation

Considering a mass-point system with n D.O.F, the generalized coordinate can be set as $q_1, q_2 \cdots q_n$. A three-dimensional position vector $\boldsymbol{x_v}$ in an inertial coordinate system $\sum_U$ of an arbitrary mass point P_v belonging to this system is represented as

$$\boldsymbol{x_v} = \boldsymbol{x_v}(q_1, q_2 \cdots q_n, t) \tag{2.2.1}$$

From the Newton's rule of motion, we have

$$m_v \ddot{\boldsymbol{x_v}} = \boldsymbol{F_v} \tag{2.2.2}$$

where F_v is applied force on the mass point P_v and m_v is the mass of this point. The force $\boldsymbol{F_{vg}}$exerted by the potential energy U can be denoted as

$$\boldsymbol{F_{vg}} = -\frac{\partial U}{\partial \boldsymbol{x_v}} \tag{2.2.3}$$

The kinetic energy T can be shown as

$$T = \sum_v \frac{1}{2} m_v \dot{\boldsymbol{x_v}}^{\boldsymbol{T}} \dot{\boldsymbol{x_v}} \tag{2.2.4}$$

The Lagrangian is calculated as

$$L = T - U = \sum_v \frac{1}{2} m_v \dot{\boldsymbol{x_v}}^{\boldsymbol{T}} \dot{\boldsymbol{x_v}} - U(\boldsymbol{x}, \boldsymbol{y}) \tag{2.2.5}$$

where

$$\dot{\boldsymbol{x_v}} = \sum_v \frac{\partial \boldsymbol{x_v}}{\partial q_i} \dot{q}_\iota + \frac{\partial \boldsymbol{x_v}}{\partial t} \tag{2.2.6}$$

$$\frac{\partial \dot{x_v}}{\partial \dot{q_i}} = \frac{\partial x_v}{\partial q_i} \tag{2.2.7}$$

$$\frac{\partial L}{\partial \dot{q_i}} = \sum_v m_v (\dot{x}_v)^T \frac{\partial \dot{x_v}}{\partial \dot{q_i}} = \sum_v m_v (\dot{x}_v)^T \frac{\partial x_v}{\partial q_i} \tag{2.2.8}$$

$$\frac{\partial L}{\partial q_i} = \frac{\partial (T-U)}{\partial q_i} = -\frac{\partial U}{\partial q_i} \tag{2.2.9}$$

From the Eq. 2.2.2 ,Eq. 2.2.3,Eq. 2.2.8 and Eq. 2.2.9, it can be derived that

$$\frac{d}{dt}\left(\frac{\partial L}{\partial \dot{q_i}}\right) - \frac{\partial L}{\partial q_i} = \sum_v m_v \ddot{x}_v^{\ T} \frac{\partial x_v}{\partial q_i} + \frac{\partial U}{\partial x_v}\frac{\partial x_v}{\partial q_i}$$

$$= \sum_v (F_v - F_{vg}) \frac{\partial x_v}{\partial q_i} = Q_i \tag{2.2.10}$$

where Q_i represent the generalized force corresponding to q_i. Eq. 2.2.10 is called the Lagrange Equation.

2.1.2 Robot Dynamic Model derived from the Lagrange Equation

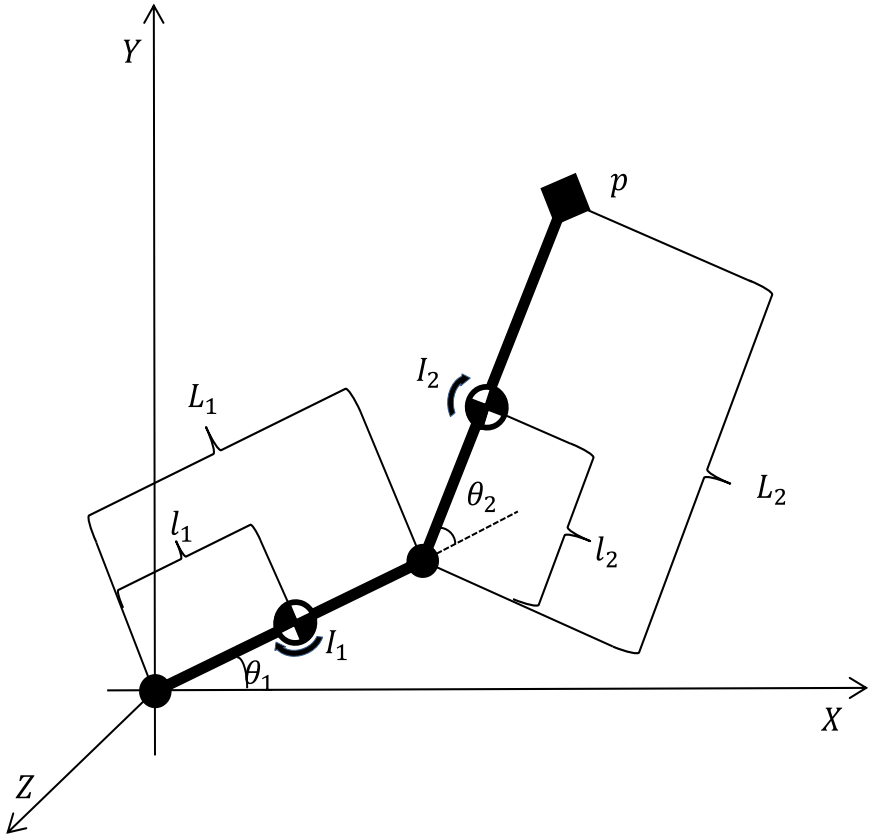

Fig.2.1.1 Physical parameters of a 2 D.O.F robot

Fig. 2.1.1 shows a manipulator model with 2 D.O.F, each physical parameter can be denoted as below:

- q_i : Rotation angle of the joint i
- m_i : Mass of the link i
- I_i : Moment of the inertial of link i which have the direction parallel to the z axis and pass through the center of mass
- L_i : The length of the link i
- l_i : The length between the joint i and the center of the mass of link i

Generally, the kinetic energy of a rigid body is denoted as

$$T = \frac{1}{2} m \dot{s}^T \dot{s} + \frac{1}{2} w^T I w \tag{2.2.11}$$

where m is the mass of the rigid body, wis the rotation velocity, $\dot{s}$ denote the translational velocity, I represent the inertial tensor. Considering the motion of the link 1, the kinetic energy T_1 and the position energy P_1 (potential energy) can be computed as

$$\begin{cases} T_1 = \frac{1}{2} m_1 {l_1}^2 {\dot{q}_1}^2 + \frac{1}{2} I_1 {\dot{q}_1}^2 \\ P_1 = m_1 g l_1 sin(q_1) \end{cases} \tag{2.2.12}$$

where g represents the gravity acceleration. Then, the position of the center of the mass of link 2 can be calculated as

$$S_2 = \begin{bmatrix} L_1\, cos(q_1) + l_2\, cos(q_1 + q_2) \\ L_1\, sin(q_1) + l_2\, sin(q_1 + q_2) \end{bmatrix}$$

The kinetic energy T_2 and position energy (potential energy) of link 2 can thus be shown as

$$\begin{cases} T_2 = \frac{1}{2} m_2 \dot{S}_2^{\,T} \dot{S}_2 + \frac{1}{2} I_2 (\dot{q}_1 + \dot{q}_2)^2 \\ P_2 = m_2 g (L_1\, sin(q_1) + l_2\, sin(q_1 + q_2)) \end{cases} \tag{2.2.13}$$

Afterwards, by using the Lagrangian L calculated as $L = T_1 + T_2 - P_1 - P_2$ and

using Eq. 2.1.10, Equation of the robot's dynamic motion can be derived as

$$\begin{cases} \tau_1 = M_{11}\ddot{q_1} + M_{12}\ddot{q_2} + C_{122}\dot{q_2} + 2C_{112}\dot{q_1}\dot{q_2} + g_1 \\ \tau_2 = M_{21}\ddot{q_1} + M_{22}\ddot{q_2} + C_{211}\dot{q_1} + g_2 \end{cases} \quad (2.2.14)$$

where

$$M_{11} = m_1 {l_1}^2 + I_1 + m_2\left({L_1}^2 + {l_2}^2 + 2L_1 l_2\, cos(q_2)\right) + I_2$$

$$M_{12} = M_{21} = m_2\left({l_2}^2 + 2L_1 l_2\, cos(q_2)\right) + I_2$$

$$M_{22} = m_2 {l_2}^2 + I_2$$

$$C_{122} = C_{112} = -C_{211} = -m_2 L_1 l_2\, sin(q_2)$$

$$g_1 = m_1 g l_1\, cos(q_1) + m_2 g(L_1\, cos(q_1) + l_2\, cos(q_1 + q_2))$$

$$g_2 = m_2 g l_2\, cos(q_1 + q_2)$$

Rewrite Eq. 2.2.14, we can get

$$\boldsymbol{M(q)\ddot{q} + C(q,\dot{q})\dot{q} + g(q) = \tau} \quad (2.2.15)$$

where $\boldsymbol{M(q)} \in \Re^{n\times n}$ is the inertial matrix, $\boldsymbol{C(q,\dot{q})\dot{q}} \in \Re^{1\times n}$ is the Coriolis and centrifugal force vector. $\boldsymbol{\tau}$ is the applied joint torque

Note that, in Eq. 2.2.15, the relation between $\boldsymbol{M}$ and $\boldsymbol{C}$ satisfies

$$\boldsymbol{\dot{M}(q) - 2C(q,\dot{q}) = -\left(\dot{M}(q) - 2C(q,\dot{q})\right)^T} \quad (2.2.16)$$

That is, $\boldsymbol{\dot{M}(q) - 2C(q,\dot{q})}$ is a skew-symmetric matrix.

2.2 Trajectory Tracking: Construction of the Desired Velocity Field

For the robot dynamics in Eq.2.2.15, it is well known that, by PD control [42]

$$\boldsymbol{\tau = -D_0\dot{q} - K_0(q - q_d)} \quad (2.3.1)$$

the robot's position $\boldsymbol{q}$ can convergence to the desired constant position $\boldsymbol{q_d}$. Where $\boldsymbol{D}_0, \boldsymbol{K}_0$ is the ratio of damping and stiffness respectively. The tracking ability of this method can be proved as follows:

We can construct an Lyapunov function as

$$V_L = \frac{1}{2}\dot{q}^T M\dot{q} + \frac{1}{2}(q - q_d)^T K_0 (q - q_d) \tag{2.3.2}$$

and its derivative can be formulated as

$$\dot{V}_L = \dot{q}^T M\ddot{\boldsymbol{q}} + \frac{1}{2}\dot{q}^T \dot{M}\dot{q} + \dot{q}^T K_0 (q - q_d) \tag{2.3.3}$$

after substituting (2.2.15), (2.2.16) and (2.3.1), we can obtain

$$\dot{V}_L = -\dot{q}^T D_0 \dot{q} \tag{2.3.4}$$

It is obvious that $\dot{V}_L$ is semi-positive definite, which means that robot's tracking system is stable and robot's position $\boldsymbol{q}$ is able to convergence to the desired constant position $\boldsymbol{q_d}$.

On another hand, when the robot is required to track a time varying trajectory, if we only use PD control, with the change of the desired position, robot performs the simple point-to-point tracking control to minimize the trajectory tracking error $\boldsymbol{e}$ at every instant of time.

As pointed out in Li's research [12] and others, trajectory tracking error does not reflect how well the contour is being followed. As seen from Fig. 3, by using Eq. (2.3.1), the robot in fact leaves the desired contour to catch up the desired location specified by the timed trajectory. When the robot is required to complete a certain contour following, PD control based on the trajectory tracking error is invaluable. On the other hand, from Fig. 3, the contour error, which denotes the error between robot's position and the nearest position in the desired contour, actually can describe whether the contour is being followed or not.

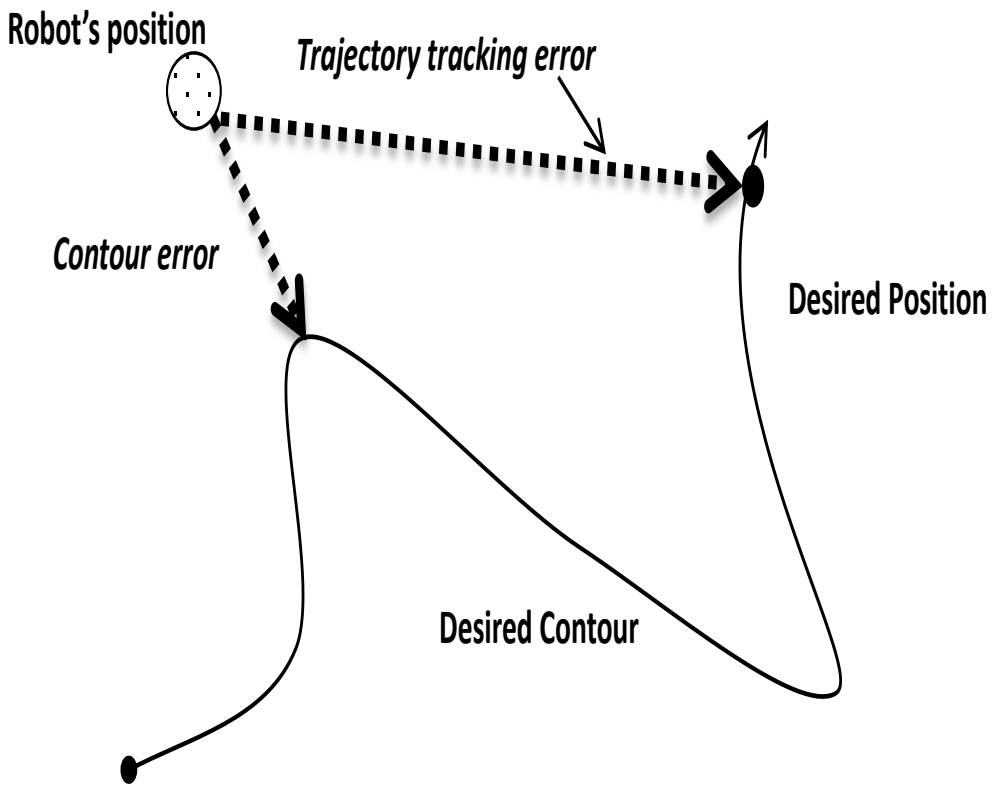

Fig. 3 Position based Desired Velocity Field

In order to trace the trajectory, it is proposed to formulate the objective motion of the robot as a velocity vector field $\mathbf{V}(\mathbf{q})$ (time invariant) with respect to the robot's position vector $\mathbf{q}$. As shown in Li's work [10], if $\mathbf{q} \in \mathcal{g}$ (a m-dimension configuration manifold), then we can denote the tangent space of $\mathcal{g}$ as $\mathrm{T}_{\mathrm{q}}\mathcal{g}$ at one $\mathbf{q}$ and desired velocity field $\mathbf{V}$ is a map $\mathbf{V}: \mathcal{g} \to \mathrm{T}\mathcal{g}$; $\mathbf{q} \to \mathbf{V}(\mathbf{q})$ where $\mathrm{T}\mathcal{g} = \bigcup_{\mathrm{q}\in\mathcal{g}} \mathrm{T}_{\mathrm{q}}\mathcal{g}$, $\mathrm{T}\mathcal{g}$ is the tangent bundle of the manifold $\mathcal{g}$.

Note that, $\boldsymbol{V}(\boldsymbol{q})$ is a desired velocity vector at each point in the workspace, which replaces the task of tracking the final trajectory by the tracing of the desired vector at each point.

In order to build the map $\boldsymbol{V}(\boldsymbol{q})$, firstly, we construct a potential function $P_o(\boldsymbol{q})$ with respect to $\boldsymbol{q}$ and this function is required to have the maximum value at the desired trajectory leading $P_o(\boldsymbol{q})$'s gradient can have the minimum size zero at the desired trajectory and can represent the normal vectors of the desired trajectory.

Therefore, gradient of $P_o(\boldsymbol{q})$ can be used as one part of V and can be denoted as $\boldsymbol{V^n}$. On the another side, we can also design a perpendicular vector of this gradient as the tangential vector of the desired trajectory which is required to have smaller size at points away from desired trajectory and have maximum size at the desired trajectory. This vector can be denoted as $\boldsymbol{V^t}$.Both normal and tangential desired vector constitute a desired velocity vector $\boldsymbol{V}$ at each point ($\boldsymbol{V = V^t + V^n}$).

For example, when the robot is required to trace a desired circle, the contour error can be represented as

$$d \equiv \left|\sqrt{(x_r - x_0)^2 + (y_r - y_0)^2} - R\right|$$

where (x_r, y_r) denotes the robot's position and (x_0, y_0) denotes the center point of the desired circle, R is the radius of the circle.

Then, potential function $P_o(\boldsymbol{q})$ can be chosen as

$$P(x_r, y_r) = exp\left(-\frac{d^2}{\sigma^2}\right) \tag{2.3.5}$$

$\boldsymbol{V^n}$ and $\boldsymbol{V^t}$ can be designed as

$$\boldsymbol{V^n} = gradP(x_r, y_r) = \frac{-2d}{\sigma^2} exp\left(-\frac{d^2}{\sigma^2}\right)\left(\frac{(x_r - x_0)}{\sqrt{(x_r - x_0)^2 + (y_r - y_0)^2}}, \frac{(y_r - y_0)}{\sqrt{(x_r - x_0)^2 + (y_r - y_0)^2}}\right)^T \tag{2.3.6}$$

$$\boldsymbol{V^t} = exp\left(-\frac{d^2}{\sigma^2}\right)\left(\frac{y_r - y_d}{\sqrt{(x_r - x_0)^2 + (y_r - y_0)^2}}, \frac{-(x_r - x_d)}{\sqrt{(x_r - x_0)^2 + (y_r - y_0)^2}}\right)^T \tag{2.3.7}$$

The desired velocity vector at each point can be calculated as

$$\boldsymbol{V = V^n + V^t}$$

The desired trajectory is set as a circle (shown in Fig. 5 (a)) with center point [0.8;0.8] and radius $r = 0.5$.

The following chapter will consider the tracking control based on such velocity vector field.

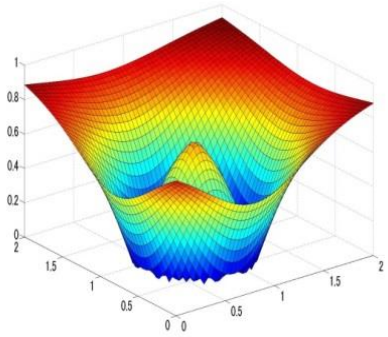

(a) Size of the Gradient of $\mathbf{exp}\left(-\frac{d^2}{\sigma^2}\right)$

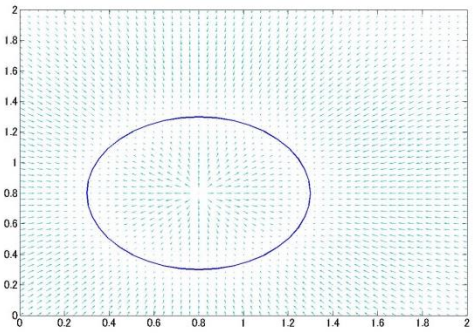

(b) V^n

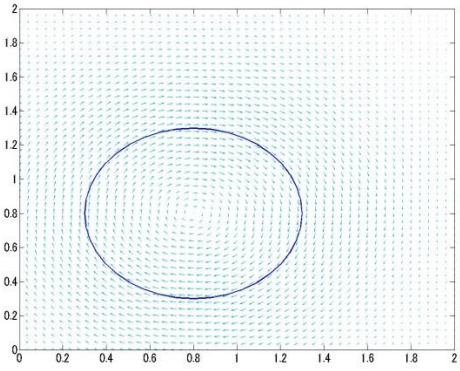

(c) V^t

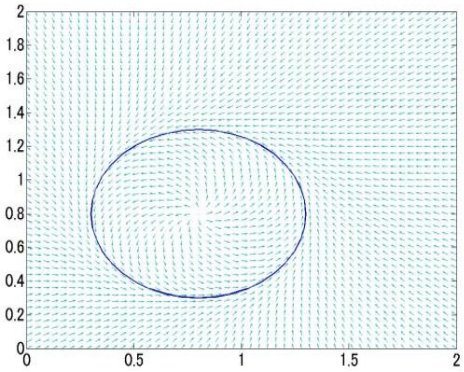

(d) Velocity Field of the Desired Circle

Fig.5 Design of the Velocity Field

2.3 Impedance Control

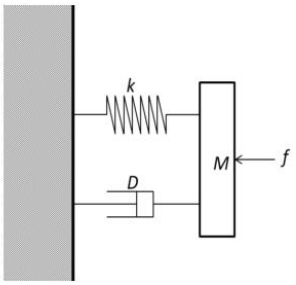

Fig. 6 A Mass Spring Damper System

In the case when the robot is required to make physical interaction with its environment[8], Impedance control was proposed. Impedance control actually makes the end-effector of the robot perform a desired dynamics. The desired performance of the robot is specified through a generalized dynamic impedance as shown in Fig. 6, namely a complete set of mass-spring-damper equations (typically chosen as linear and decoupled, but also nonlinear). It is usually formulated as

$$\boldsymbol{M_d\ddot{x} + D_d\dot{x} + K_d(x - x_d) = f_e} \tag{2.4.1}$$

where $\boldsymbol{M_d, D_d, K_d}$ are the desired mass, damping ratio and stiffness of the impedance in Fig. 6, respectively; $\boldsymbol{x} \in \Re^m$ is the position of the robot, $\boldsymbol{x_d}$ denotes the desired position of the robot. We can set the parameter presented above as

$$\boldsymbol{M_d} = diag[m_{d1,\ldots,}m_{dm}] \quad \boldsymbol{D_d} = diag[d_{d1,\ldots,}d_{dm}] \quad \boldsymbol{K_d} = diag[k_{d1,\ldots,}k_{dm}]$$

which are constant matrices and designed concerning the task requirement.

Note that, robot's dynamics represented in eq. (2.2.15) is a nonlinear system. In order to make the end-effector of the robot mimic the linear impedance behavior of eq. (2.4.1), if the dynamics of the robot is known, we can set the control input torque with a properly designed nonlinear compensation as

$$\boldsymbol{\tau = M(q)J^{-1}(q)\{M_d{}^{-1}(-D_d\dot{x} - K_d(x - x_d) + f_e) - J(\dot{q})\dot{q}\} + C(q,\dot{q})\dot{q} - J^T f_e} \tag{2.4.2}$$

In the following chapter, the cases when the desired position x_d is time varying and when the dynamics of the robot is unknown will be studied.

Chapter 3 Estimation of an Object's Physical Parameter by Force Sensors of a Dual-arm Robot

In this chapter, the thesis first studied on optimal estimation of the interacted object's physical parameters, such as the center of gravity of the object based on the contact point and contact force estimation from force sensors equipped on the robot arms. Considering the case when we are asking a robot to perform nursing care tasks, such as to carry up a person by two arms, it is clear that, in order for a robot to realize physical interaction with a heavy person, full body manipulation is effective. During full body manipulation, the robot may contact with human at multiple contact points, the cared person's center of gravity should be estimated so as to avoid dropping of him or her.

Previous researches usually use tactile sensor sheets to measure the interaction position and force, directly. However, such sensor sheet is not only too expensive but also easily be harmed during direct interaction. In addition, more time is required to sampling and process of the data from the two dimensional sensor sheet.

In this research, the thesis proposed to use multi axed force sensor that is located at different position from the contact points to estimate optimally the interacted object's physical parameters. Two cases, (1)when a robot arm is contacting with an object at one point or two points, and (2) when two robot arms is holding an common object, are studied. Experiments and simulations are performed to show the effectiveness of our approach.

In detail, the thesis considers the object lift up motion by a nursing care robot, such as the robot shown in Fig.3.1

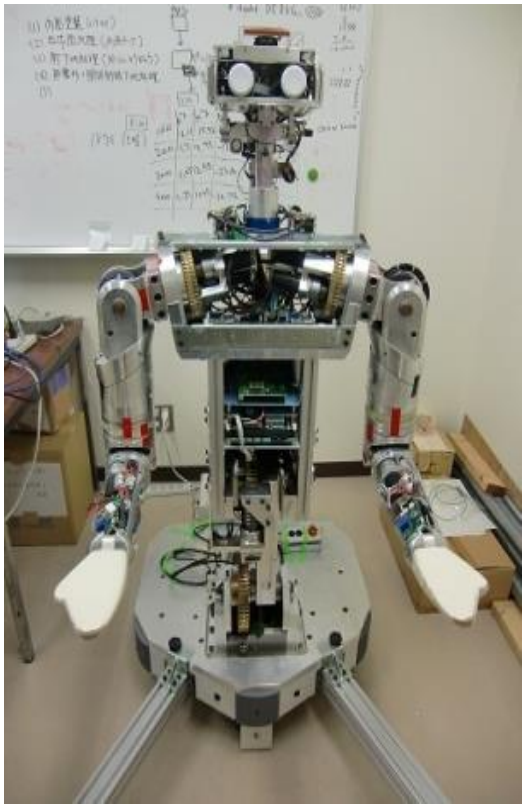

Fig.3.1　A nursing-care robot

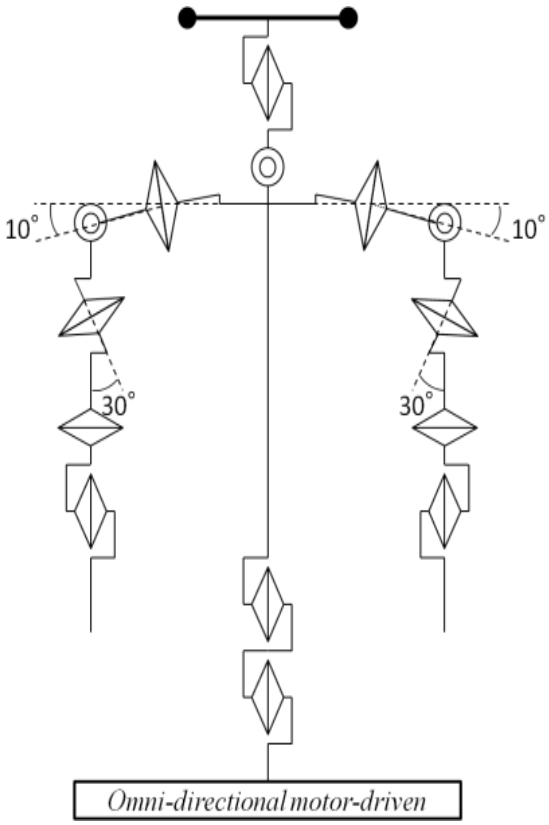

Fig.3.2 Degree of freedoms of the robot

The upper body of the nursing care robot is designed in a humanoid type with 14 degrees of freedom as shown in Fig.3.2. The 14 degrees of freedom contains 2 D.O.F of the neck joint of the head, 3 D.O.F of shoulders joints both on left and right side, 2 D.O.F of elbow joints both on left and right side, 2 D.O.F of hip joints. The total length of the robot is 1.5m high with the mass of about 100kg. In order to measure the interaction with the external objects, two force sensors with 6 D.O.F. are equipped at the upper arms of the robot.

The following Section 1 shows our method on estimation of object's center of gravity. Section 2 shows simulation settings and result. In section 3, we show the experiment results which indicate that we can steady estimate the position of center of gravity with little error.

3.1 Estimation of an Object's Physical Parameter

3.1.1 Estimation of the Contact Position when contact with one point

a) The Model and Formulation

In order to estimate the contact position between the robot arm and the object by using the 6-axis force sensor which is installed on the upper arm part of the robot, the model can be assumed as Fig.3. 3.

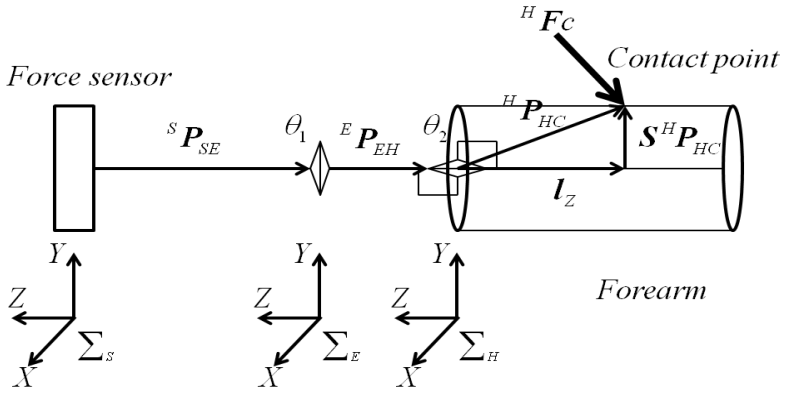

Fig.3.3 Contact between a robot arm and an object

For simplicity, here the robot arm can be assumed as a cylinder with radius r. The origin of the sensor coordinate system $\Sigma_s$is set as the center of the sensor. In addition, there are two coordinate systems of the elbow (the pivot axis coordinate system Σ_E

and the flexion axis coordinate system Σ_H). The rotation matrix performing coordinate transformation can be represented as ${}^{H}\boldsymbol{R}_{E}$, ${}^{E}\boldsymbol{R}_{S}$. Moreover, the vector from the origin of the flexion axis coordinate system to the contact point and the contact force can be set as ${}^{\mathbf{H}}\mathbf{P}_{\mathbf{HC}}$ and ${}^{\mathbf{H}}\mathbf{F}_{\mathbf{C}}$, respectively. S is a projecting matrix from XYZ space to the XY plane. The force and moment acted on the origin of the flexion coordinate system is represented as ${}^{H}\boldsymbol{F}_{S}$, ${}^{H}\boldsymbol{M}_{f}$. Moreover, ${}^{S}\boldsymbol{F}_{S}$ ${}^{S}\boldsymbol{M}_{f}$ are the force and the moment observed from the origin of the force sensor coordinate. Thus, the coordinate transformation from the sensor coordinate system to the flexion axis coordinate system can be

$$\begin{pmatrix} {}^{H}\boldsymbol{F}_{S} \\ {}^{H}\boldsymbol{M}_{f} \end{pmatrix} = \begin{pmatrix} {}^{H}\boldsymbol{R}_{E} & \mathbf{0} \\ [\,{}^{H}\boldsymbol{P}_{EH}\times]\,{}^{H}\boldsymbol{R}_{E} & {}^{H}\boldsymbol{R}_{E} \end{pmatrix} \begin{pmatrix} {}^{E}\boldsymbol{R}_{S} & \mathbf{0} \\ [\,{}^{E}\boldsymbol{P}_{SE}\times]\,{}^{E}\boldsymbol{R}_{S} & {}^{E}\boldsymbol{R}_{S} \end{pmatrix} \begin{pmatrix} {}^{S}\boldsymbol{F}_{S} \\ {}^{S}\boldsymbol{M}_{f} \end{pmatrix} \tag{3.1.1}$$

If there exists no noise, then

$$ {}^{H}\boldsymbol{F}_{S} = {}^{H}\boldsymbol{F}_{C} $$

$$ {}^{H}\boldsymbol{M}_{f} = {}^{H}\boldsymbol{P}_{HC} \times {}^{H}\boldsymbol{F}_{C} \tag{3.1.2}$$

Since the contact point is on the surface of cylinder, thus

$$ \boldsymbol{g}\left(\boldsymbol{S}\,{}^{H}\boldsymbol{P}_{HC}\right) = \left\|\boldsymbol{S}\,{}^{H}\boldsymbol{P}_{HC}\right\|^{2} - r^{2} = \mathbf{0} \tag{3.1.3}$$

Because the contact force only exist on the direction into the cylinder, it is concluded that

$$ \left(\boldsymbol{S}\,{}^{H}\boldsymbol{P}_{HC}\right)^{T}\,{}^{H}\boldsymbol{F}_{S} \leq \mathbf{0} \tag{3.1.4}$$

Here, ${}^{H}\boldsymbol{P}_{EH}$ and ${}^{E}\boldsymbol{P}_{SE}$ are already known. If there exists some noises, the determination of the contact position ${}^{H}\boldsymbol{P}_{HC}$ becomes a problem.

Since the existence of the noises, the balance of the eq. (3.1.2) has been broken and the error $\boldsymbol{e}$ can be calculated as

$$\boldsymbol{e} = {}^{\boldsymbol{H}}\boldsymbol{F_S} \times {}^{\boldsymbol{H}}\boldsymbol{P_{HC}} + {}^{\boldsymbol{H}}\boldsymbol{M_f} \tag{3.1.5}$$

From Eq. (3.1.5), it is obvious that there exists an optimal estimation of ${}^{\boldsymbol{H}}\boldsymbol{P_{HC}}$ minimizing the error value $\boldsymbol{e}$. We can form an objective function subjected to two constraints to solve error e's minimization problem.

$$\begin{cases} Objective\ Function: \quad \|\boldsymbol{e}\|^2 = \left\| {}^{\boldsymbol{H}}\boldsymbol{F_S} \times {}^{\boldsymbol{H}}\boldsymbol{P_{HC}} + {}^{\boldsymbol{H}}\boldsymbol{M_f} \right\|^2 \\ S.T. \quad \boldsymbol{I}.\ g\left(\boldsymbol{S}\,{}^{\boldsymbol{H}}\boldsymbol{P_{HC}}\right) = \left\|\boldsymbol{S}\,{}^{\boldsymbol{H}}\boldsymbol{P_{HC}}\right\|^2 - r^2 = 0 \\ \quad\ \ \boldsymbol{II}.\ \left(\boldsymbol{S}\,{}^{\boldsymbol{H}}\boldsymbol{P_{HC}}\right)^T {}^{\boldsymbol{H}}\boldsymbol{F_S} \le 0 \end{cases} \tag{3.1.6}$$

The method of Lagrange multipliers can be used to solve this optimization problem.

b) Derivation of analytical solution

Firstly, in order to solve the optimization problem of Eq. (3.1.6), it is necessary to only consider the objective function and the constraint Ⅰ. Then, by imposing constraint Ⅱ, we can get the solution of Eq.(3.1.6). The Lagrange function can be formed based on the objective function and constraint Ⅰ.

$$L = \frac{1}{2}\left\|\left[{}^{\boldsymbol{H}}\boldsymbol{F_S}\times\right]{}^{\boldsymbol{H}}\boldsymbol{P_{HC}} + {}^{\boldsymbol{H}}\boldsymbol{M_f}\right\|^2 + \frac{1}{2}\lambda\left(\left\|\boldsymbol{S}\,{}^{\boldsymbol{H}}\boldsymbol{P_{HC}}\right\|^2 - r^2\right) \tag{3.1.7}$$

The first necessary condition of the Lagrange function for calculating the optimal solution of ${}^{\mathrm{H}}\mathrm{P}_{\mathrm{HC}}$ is that

$$\frac{\partial L}{\partial\, {}^{\boldsymbol{H}}\boldsymbol{P_{HC}}} = \left[{}^{\boldsymbol{H}}\boldsymbol{F_S}\times\right]^{\boldsymbol{T}}\left(\left[{}^{\boldsymbol{H}}\boldsymbol{F_S}\times\right]{}^{\boldsymbol{H}}\boldsymbol{P_{HC}} + {}^{\boldsymbol{H}}\boldsymbol{M_f}\right) + \lambda \tag{3.1.8}$$

$$\frac{\partial L}{\partial \lambda} = \frac{1}{2}\left(\left\|\boldsymbol{S}\,{}^{\boldsymbol{H}}\boldsymbol{P_{HC}}\right\|^2 - r^2\boldsymbol{S}\,{}^{\boldsymbol{H}}\boldsymbol{P_{HC}} = \boldsymbol{0}\right) \tag{3.1.9}$$

Furthermore, the second order partial derivative of the Lagrange function about the ${}^{\mathrm{H}}\mathrm{P}_{\mathrm{HC}}$ can be formulated as

$$\frac{\partial^2 L}{\partial {}^H P_{HC}{}^2} = \left[{}^H F_S \times\right]^T \left[{}^H F_S \times\right] + \lambda S \tag{3.1.10}$$

Thus,

$$x^T \frac{\partial^2 L}{\partial {}^H P_{HC}{}^2} x = \left\| {}^H F_S \times x \right\|^2 + \lambda \|Sx\|^2 \tag{3.1.11}$$

The second necessary condition of the Lagrange function can be described as

$$x^T \frac{\partial^2 L}{\partial {}^H P_{HC}{}^2} x > 0 \quad x \neq 0 \in X$$

$$X \coloneqq \left\{ x \middle| \left(S {}^H P_{HC}\right)^T x = 0 \right\} \tag{3.1.12}$$

It is possible to derive the analytical solution of the problem to satisfy these two conditions.

By multiplying the ${}^H F_S{}^T$ on the left side of the eq. (3.1.8), we get

$${}^H F_S{}^T \left\{ - {}^H F_S \times \left({}^H F_S \times {}^H P_{HC} + {}^H M_f \right) + \lambda S {}^H P_{HC} \right\} = \lambda {}^H F_S{}^T S {}^H P_{HC} = 0 \tag{3.1.13}$$

Therefore, it is obvious that the optimal solution can be solved in terms of two situations $\lambda = 0$ and ${}^H F_S{}^T S {}^H P_{HC} = 0$.

***case* 1**: $\lambda = 0$

Eq. (3.1.8) becomes

$$- {}^H F_S \times \left({}^H F_S \times {}^H P_{HC} + {}^H M_f \right) = 0 \tag{3.1.14}$$

Based on Eq. (3.1.14), ${}^H \mathbf{P}_{\mathbf{HC}}$ can be formulated as

$${}^H P_{HC} = \frac{1}{\left\| {}^H F_S \right\|^2} \left\{ {}^H F_S \times {}^H M_f + \left({}^H F_S{}^T {}^H P_{HC} \right) {}^H F_S \right\} \tag{3.1.15}$$

By substituting Eq. (3.1.15) into $g\left(S {}^H P_{HC}\right)$ of the Constraint I and solving the new $g\left(S {}^H P_{HC}\right)$ with variable ${}^H F_S{}^T {}^H P_{HC}$, we can get the ${}^H F_S{}^T {}^H P_{HC}$. Therefore,

Eq. (3.1.15) becomes to Eq. (3.1.16).

$$^{H}\boldsymbol{P}_{\boldsymbol{HC}} = \frac{^{H}\boldsymbol{F}_{\boldsymbol{S}} \times ^{H}\boldsymbol{M}_{\boldsymbol{f}}}{\left\| ^{H}\boldsymbol{F}_{\boldsymbol{S}} \right\|^{2}} + \frac{^{H}\boldsymbol{F}_{\boldsymbol{S}}}{\left\| ^{H}\boldsymbol{F}_{\boldsymbol{S}} \right\|^{2}} \left\{ \frac{-\,^{H}\boldsymbol{F}_{\boldsymbol{S}}^{\ T}\boldsymbol{S}(^{H}\boldsymbol{F}_{\boldsymbol{S}} \times ^{H}\boldsymbol{M}_{\boldsymbol{f}}) \pm \sqrt{\boldsymbol{W}}}{\left\| \boldsymbol{S}\,^{H}\boldsymbol{F}_{\boldsymbol{S}} \right\|^{2}} \right\} \tag{3.1.16}$$

where $\boldsymbol{W} = \left\| ^{H}\boldsymbol{F}_{\boldsymbol{S}}^{\ T}\boldsymbol{S}\left(^{H}\boldsymbol{F}_{\boldsymbol{S}} \times ^{H}\boldsymbol{M}_{\boldsymbol{f}}\right) \right\|^{2} - \left\| \boldsymbol{S}\,^{H}\boldsymbol{F}_{\boldsymbol{S}} \right\|^{2} \left(\left\| \boldsymbol{S}\left(^{H}\boldsymbol{F}_{\boldsymbol{S}} \times ^{H}\boldsymbol{M}_{\boldsymbol{f}}\right) \right\|^{2} - r^{2} \left\| ^{H}\boldsymbol{F}_{\boldsymbol{S}} \right\|^{4} \right)$

By multiplying Eq. (3.1.16) with $^{H}\boldsymbol{F}_{\boldsymbol{S}}^{\ T}\boldsymbol{S}$ and imposing the Constraint Ⅱ, we will get Eqs. (3.1.17) and (3.1.18).

$$^{H}\boldsymbol{F}_{\boldsymbol{S}}^{\ T}\boldsymbol{S}\,^{H}\boldsymbol{P}_{\boldsymbol{HC}} = \frac{-\sqrt{W}}{\left\| \boldsymbol{S}\,^{H}\boldsymbol{F}_{\boldsymbol{S}} \right\|^{2}} \tag{3.1.17}$$

$$^{H}\boldsymbol{P}_{\boldsymbol{HC}} = \frac{^{H}\boldsymbol{F}_{\boldsymbol{S}} \times ^{H}\boldsymbol{M}_{\boldsymbol{f}}}{\left\| ^{H}\boldsymbol{F}_{\boldsymbol{S}} \right\|^{2}} + \frac{^{H}\boldsymbol{F}_{\boldsymbol{S}}}{\left\| ^{H}\boldsymbol{F}_{\boldsymbol{S}} \right\|^{2}} \left\{ \frac{-\,^{H}\boldsymbol{F}_{\boldsymbol{S}}^{\ T}\boldsymbol{S}(^{H}\boldsymbol{F}_{\boldsymbol{S}} \times ^{H}\boldsymbol{M}_{\boldsymbol{f}}) - \sqrt{\boldsymbol{W}}}{\left\| \boldsymbol{S}\,^{H}\boldsymbol{F}_{\boldsymbol{S}} \right\|^{2}} \right\} \tag{3.1.18}$$

Note that in eq. (3.1.18), since that it is necessary to make interior of the square root be positive so that we can get the optimal solution, eq. (3.1.19) need to be satisfied.

$$\alpha = \frac{1}{\left\| \boldsymbol{S}\,^{H}\boldsymbol{F}_{\boldsymbol{S}} \right\|^{2}} \sqrt{N} \ , \qquad r \left\| ^{H}\boldsymbol{F}_{\boldsymbol{S}} \right\|^{2} > \alpha \tag{3.1.19}$$

where $\boldsymbol{N} = \left\| \boldsymbol{S}\,^{H}\boldsymbol{F}_{\boldsymbol{S}} \right\|^{2} \left\| \boldsymbol{S}\left(^{H}\boldsymbol{F}_{\boldsymbol{S}} \times ^{H}\boldsymbol{M}_{\boldsymbol{f}}\right) \right\|^{2} - \left\| ^{H}\boldsymbol{F}_{\boldsymbol{S}}^{\ T}\boldsymbol{S}\left(^{H}\boldsymbol{F}_{\boldsymbol{S}} \times ^{H}\boldsymbol{M}_{\boldsymbol{f}}\right) \right\|^{2}$

***case* 2**: $^{H}\boldsymbol{F}_{\boldsymbol{S}}^{\ T}\boldsymbol{S}\,^{H}\boldsymbol{P}_{\boldsymbol{HC}} = 0$

Because $^{H}\boldsymbol{F}_{\boldsymbol{S}}^{\ T}\boldsymbol{S}\,^{H}\boldsymbol{P}_{\boldsymbol{HC}} = 0$, the Constraint Ⅱ is satisfied. The inner product of eq. (3.1.8) and can $\boldsymbol{S}\,^{H}\boldsymbol{P}_{\boldsymbol{HC}}$ be formulated as

$$\left(\boldsymbol{S}\,^{H}\boldsymbol{P}_{\boldsymbol{HC}}\right)^{T} \left\{ -\,^{H}\boldsymbol{F}_{\boldsymbol{S}} \times \left(^{H}\boldsymbol{F}_{\boldsymbol{S}} \times ^{H}\boldsymbol{P}_{\boldsymbol{HC}} + ^{H}\boldsymbol{M}_{\boldsymbol{f}} \right) + \lambda \boldsymbol{S}\,^{H}\boldsymbol{P}_{\boldsymbol{HC}} \right\}$$

$$= \left(\left\| ^{H}\boldsymbol{F}_{\boldsymbol{S}} \right\|^{2} + \lambda \right) r^{2} - \left(\boldsymbol{S}\,^{H}\boldsymbol{P}_{\boldsymbol{HC}}\right)^{T} \left(^{H}\boldsymbol{F}_{\boldsymbol{S}} \times ^{H}\boldsymbol{M}_{\boldsymbol{f}} \right) = 0 \tag{3.1.20}$$

Considering the fact that $^{H}\boldsymbol{P}_{\boldsymbol{HC}} = \boldsymbol{S}\,^{H}\boldsymbol{P}_{\boldsymbol{HC}} + \boldsymbol{l}_{\boldsymbol{Z}}$, the cross product of eq. (3.1.8)

and $\boldsymbol{S}^{\boldsymbol{H}}\boldsymbol{P}_{\boldsymbol{HC}}$ is

$$\left(\boldsymbol{S}^{\boldsymbol{H}}\boldsymbol{P}_{\boldsymbol{HC}}\right)\times\left\{-{}^{\boldsymbol{H}}\boldsymbol{F}_{\boldsymbol{S}}\times\left({}^{\boldsymbol{H}}\boldsymbol{F}_{\boldsymbol{S}}\times{}^{\boldsymbol{H}}\boldsymbol{P}_{\boldsymbol{HC}}+{}^{\boldsymbol{H}}\boldsymbol{M}_{\boldsymbol{f}}\right)+\lambda\boldsymbol{S}^{\boldsymbol{H}}\boldsymbol{P}_{\boldsymbol{HC}}\right\}$$
$$=\left(\boldsymbol{S}^{\boldsymbol{H}}\boldsymbol{P}_{\boldsymbol{HC}}\right)\times\left\{-\left({}^{\boldsymbol{H}}\boldsymbol{F}_{\boldsymbol{S}}{}^{\boldsymbol{T}}\boldsymbol{l}_{\boldsymbol{Z}}\right){}^{\boldsymbol{H}}\boldsymbol{F}_{\boldsymbol{S}}+\left\|{}^{\boldsymbol{H}}\boldsymbol{F}_{\boldsymbol{S}}\right\|^{2}\boldsymbol{l}_{\boldsymbol{Z}}-\left({}^{\boldsymbol{H}}\boldsymbol{F}_{\boldsymbol{S}}\times{}^{\boldsymbol{H}}\boldsymbol{M}_{\boldsymbol{f}}\right)\right\}=\boldsymbol{0} \tag{3.1.21}$$

The inner product of $\boldsymbol{l}_{\boldsymbol{Z}}$ and Eq. (3.1.8) can be formulated as

$$-\left({}^{\boldsymbol{H}}\boldsymbol{F}_{\boldsymbol{S}}{}^{\boldsymbol{T}}\boldsymbol{l}_{\boldsymbol{Z}}\right)\boldsymbol{l}_{\boldsymbol{Z}}^{\boldsymbol{T}}{}^{\boldsymbol{H}}\boldsymbol{F}_{\boldsymbol{S}}+\left\|{}^{\boldsymbol{H}}\boldsymbol{F}_{\boldsymbol{S}}\right\|^{2}\boldsymbol{l}_{\boldsymbol{Z}}^{\boldsymbol{T}}\boldsymbol{l}_{\boldsymbol{Z}}-\boldsymbol{l}_{\boldsymbol{Z}}^{\boldsymbol{T}}\left({}^{\boldsymbol{H}}\boldsymbol{F}_{\boldsymbol{S}}\times{}^{\boldsymbol{H}}\boldsymbol{M}_{\boldsymbol{f}}\right)=0 \tag{3.1.22}$$

by considering ${}^{\boldsymbol{H}}\boldsymbol{P}_{\boldsymbol{HC}}=\boldsymbol{S}^{\boldsymbol{H}}\boldsymbol{P}_{\boldsymbol{HC}}+\boldsymbol{l}_{\boldsymbol{Z}}$.

Set the $\boldsymbol{l}_{\boldsymbol{Z}}=\boldsymbol{p}_{\boldsymbol{Z}}\boldsymbol{e}_{\boldsymbol{z}}$, where $\boldsymbol{e}_{\boldsymbol{z}}=[0\ 0\ 1]^{\mathrm{T}}$. Based on the eq. (3.1.22), the solution of p_Z can be concluded as

$$\boldsymbol{P}_{\boldsymbol{Z}}=\boldsymbol{0},\quad \boldsymbol{P}_{\boldsymbol{Z}}=\frac{\boldsymbol{e}_{\boldsymbol{z}}{}^{\boldsymbol{T}}\left({}^{\boldsymbol{H}}\boldsymbol{F}_{\boldsymbol{S}}\times{}^{\boldsymbol{H}}\boldsymbol{M}_{\boldsymbol{f}}\right)}{\left\|\boldsymbol{S}^{\boldsymbol{H}}\boldsymbol{P}_{\boldsymbol{HC}}\right\|^{2}} \tag{3.1.23}$$

Let $\boldsymbol{C}=-\left({}^{\boldsymbol{H}}\boldsymbol{F}_{\boldsymbol{S}}{}^{\boldsymbol{T}}\boldsymbol{l}_{\boldsymbol{Z}}\right){}^{\boldsymbol{H}}\boldsymbol{F}_{\boldsymbol{S}}+\left\|{}^{\boldsymbol{H}}\boldsymbol{F}_{\boldsymbol{S}}\right\|^{2}\boldsymbol{l}_{\boldsymbol{Z}}-\left({}^{\boldsymbol{H}}\boldsymbol{F}_{\boldsymbol{S}}\times{}^{\boldsymbol{H}}\boldsymbol{M}_{\boldsymbol{f}}\right)$. From Eq. (3.1.21), $\boldsymbol{C}$ is parallel to the $\boldsymbol{S}^{\boldsymbol{H}}\boldsymbol{P}_{\boldsymbol{HC}}$. Based on the Constraint I

$$\boldsymbol{S}^{\boldsymbol{H}}\boldsymbol{P}_{\boldsymbol{HC}}=\pm r\frac{\boldsymbol{C}}{\|\boldsymbol{C}\|} \tag{3.1.24}$$

In term of calculating the inner product of the $\boldsymbol{S}^{\boldsymbol{H}}\boldsymbol{P}_{\boldsymbol{HC}}$ and $\boldsymbol{C}$, we get

$$\left(\boldsymbol{S}^{\boldsymbol{H}}\boldsymbol{P}_{\boldsymbol{HC}}\right)^{\boldsymbol{T}}\boldsymbol{C}=-\left(\boldsymbol{S}^{\boldsymbol{H}}\boldsymbol{P}_{\boldsymbol{HC}}\right)^{\boldsymbol{T}}\left({}^{\boldsymbol{H}}\boldsymbol{F}_{\boldsymbol{S}}\times{}^{\boldsymbol{H}}\boldsymbol{M}_{\boldsymbol{f}}\right) \tag{3.1.25}$$

Based on Eq. (3.1.20) and Eq. (3.1.25), it is concluded that

$$\lambda=-\left\|{}^{\boldsymbol{H}}\boldsymbol{F}_{\boldsymbol{S}}\right\|^{2}\mp\frac{\|\boldsymbol{C}\|}{r} \tag{3.1.26}$$

On the other hand, by substituting the $\boldsymbol{l}_{\boldsymbol{Z}}=p_Z\boldsymbol{e}_{\boldsymbol{z}}$ into the $\boldsymbol{C}$ and reorganizing the formula, it is found that $\|\boldsymbol{C}\|=\alpha$. Note that, the equation of $\boldsymbol{C}$ after substituting the $\mathrm{l_Z}$ states that the result of which $P_Z=\frac{\boldsymbol{e}_{\boldsymbol{z}}{}^{\boldsymbol{T}}\left({}^{\boldsymbol{H}}\boldsymbol{F}_{\boldsymbol{S}}\times{}^{\boldsymbol{H}}\boldsymbol{M}_{\boldsymbol{f}}\right)}{\left\|\boldsymbol{S}^{\boldsymbol{H}}\boldsymbol{P}_{\boldsymbol{HC}}\right\|^{2}}$ actually contains the result of which $\mathrm{P_Z}=0$.

In order to satisfy the second order necessary condition defined in Eq.(3.1.11) and

(3.1.12), λ becomes $\lambda = -\left\| {}^{H}\boldsymbol{F_S} \right\|^2 + \frac{\|C\|}{r}$ and $r\left\| {}^{H}\boldsymbol{F_S} \right\|^2 < \alpha$ need to be satisfied. ${}^{H}\boldsymbol{P_{HC}}$ can be formulated as

$$ {}^{H}\boldsymbol{P_{HC}} = \boldsymbol{S}\,{}^{H}\boldsymbol{P_{HC}} + \boldsymbol{l_Z} = -r\frac{\boldsymbol{C}}{\|\boldsymbol{C}\|} + \boldsymbol{l_Z} \tag{3.1.27} $$

In conclusion, when $r\left\| {}^{H}\boldsymbol{F_S} \right\|^2 > \alpha$, ${}^{H}\mathrm{P}_{\mathrm{HC}}$ need to satisfy Eq.(3.1.18). When $r\left\| {}^{H}\boldsymbol{F_S} \right\|^2 < \alpha$, ${}^{H}\boldsymbol{P_{HC}}$ need to satisfy Eq.(3.1.27).

3.1.2 Estimation of the Contact Position and Force when contact with two point

As the analysis shown in [7], some D.O.Fs of the human body can be reduced when computing the control input. Thus, in order to analyze easily, we regard the human body as a simple pipe as in Fig.3.4.

Based on the estimation of one point contact, it is possible to estimate the contact position and force when the robot arm contacts the object with two points. When there are two contact positions, according to Fig.3.4, we have

$$ \boldsymbol{F_S} = \boldsymbol{F_A} + \boldsymbol{F_B}, \quad \boldsymbol{M_f} = \boldsymbol{P_A} \times \boldsymbol{F_A} + \boldsymbol{P_B} \times \boldsymbol{F_B} \tag{3.1.28} $$

where $\mathbf{F_S}$ and $\mathbf{M_f}$ represent the force and moment measured by sensor. $\mathbf{P_A}$ and $\mathbf{P_B}$ is the vector from sensor's center to points A and B. $\mathbf{F_A}$ and $\mathbf{F_B}$ are forces acting on the points. Note that, $\boldsymbol{P_A}$,$\boldsymbol{P_B}$,$\boldsymbol{F_A}$,$\boldsymbol{F_B}$ are all located at the sensor coordinate system.

From Fig. 3.4, it is known that

$$ \|\boldsymbol{F_A}\| = \boldsymbol{F_S} \cdot \boldsymbol{I_{OA}} \ , \ \|\boldsymbol{F_B}\| = \boldsymbol{F_S} \cdot \boldsymbol{I_{OB}} \tag{3.1.29} $$

where $\mathrm{I}_{\mathrm{OA}}, \mathrm{I}_{\mathrm{OB}}$ represent two unit vectors of the directions from center of the cylinder to the two contact points and $\boldsymbol{I_{OA}}, \boldsymbol{I_{OB}}$ can be obtained using angles $\theta_3 = \theta_1, \theta_4 = \theta_2$. Thus, we can calculate $\boldsymbol{F_A}, \boldsymbol{F_B}$ as $\boldsymbol{F_A} = \|\boldsymbol{F_A}\| \cdot \boldsymbol{I_{OA}}$, $\boldsymbol{F_B} = \|\boldsymbol{F_B}\| \cdot \boldsymbol{I_{OB}}$

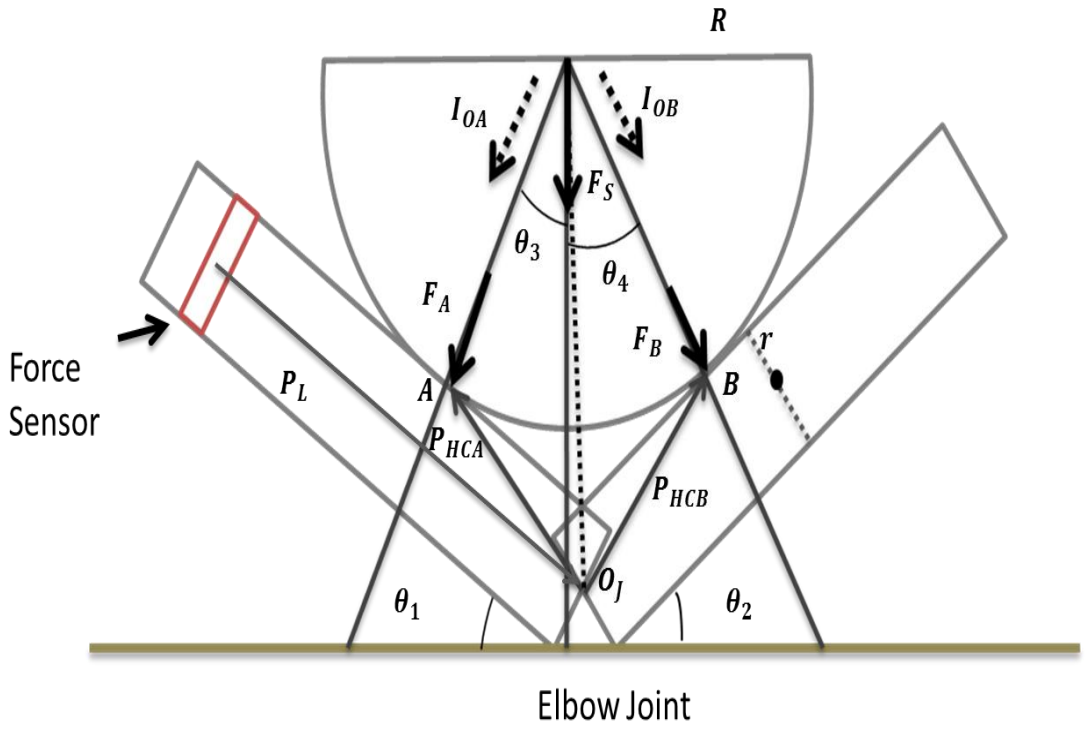

Fig.3.4 Two contact point model

Let the ${}^{H}\boldsymbol{P}_{\boldsymbol{HCA}}$ and ${}^{H}\boldsymbol{P}_{\boldsymbol{HCB}}$ denote the vector from the origin of the flexion axis coordinate system and the points **A** and **B**.

Moreover, based on the analysis of the Fig.3.4, calculation of $\boldsymbol{M_f}$ in (3.1.28) can be rewritten as

$$M_f = \boldsymbol{P_B} \times \boldsymbol{F_S} + ({}^{s}\boldsymbol{P}_{\boldsymbol{HCA}} - {}^{s}\boldsymbol{P}_{\boldsymbol{HCB}}) \times \boldsymbol{F_A} \tag{3.1.30}$$

where ${}^{s}\boldsymbol{P}_{\boldsymbol{HCA}} - {}^{s}\boldsymbol{P}_{\boldsymbol{HCB}} = R \cdot (\boldsymbol{I_{OA}} - \boldsymbol{I_{OB}})$.

Since the existence of the noises, the balance of the Eq. (3.1.30) has been broken and the error $\boldsymbol{e}$ can be calculated as

$$\boldsymbol{e} = \boldsymbol{M_f} - \boldsymbol{P_B} \times \boldsymbol{F_S} - ({}^{s}\boldsymbol{P}_{\boldsymbol{HCA}} - {}^{s}\boldsymbol{P}_{\boldsymbol{HCB}}) \times \boldsymbol{F_A} \tag{3.1.31}$$

Since the third term $(({}^{s}\boldsymbol{P}_{\boldsymbol{HCA}} - {}^{s}\boldsymbol{P}_{\boldsymbol{HCB}}) \times \boldsymbol{F_A})$ in (3.1.31) can be already calculated and $\boldsymbol{M_f}, \boldsymbol{F_S}$ are already known, we also can construct an optimization

problem to get P_B and further get ${}^{H}P_{HCA}$ and ${}^{H}P_{HCB}$

$$\begin{cases} Objective\ Function: & \|e\|^2 = \left\| \boldsymbol{M_f} - \boldsymbol{P_B} \times \boldsymbol{F_S} - ({}^{\boldsymbol{S}}\boldsymbol{P_{HCA}} - {}^{\boldsymbol{S}}\boldsymbol{P_{HCB}}) \times \boldsymbol{F_A} \right\|^2 \\ S.T. & \boldsymbol{I}.\ g\left(\boldsymbol{S}^{\boldsymbol{H}}\boldsymbol{P_{HCB}}\right) = \left\| \boldsymbol{S}^{\boldsymbol{H}}\boldsymbol{P_{HCB}} \right\|^2 - r^2 = 0 \\ & \boldsymbol{II}.\ \left(\boldsymbol{S}^{\boldsymbol{H}}\boldsymbol{P_{HCB}}\right)^T {}^{\boldsymbol{H}}\boldsymbol{F_B} \le 0 \end{cases} \tag{3.1.32}$$

By using the same analysis as in the single contact points' situation in last section, we can calculate P_B and further, it is possible to get ${}^{H}P_{HCA}$ and ${}^{H}P_{HCB}$ by using simple geometry analysis.

$$\boldsymbol{{}^{H}P_{HCA}} = \begin{pmatrix} r \\ R\tan\theta_5 + r\tan\theta_5 \end{pmatrix}$$

$$\boldsymbol{{}^{s}P_{HCB}} = \begin{pmatrix} r \\ -(R\tan\theta_5 + r\tan\theta_5) \end{pmatrix}$$

$$\boldsymbol{{}^{H}P_{HCB}} = {}^{H}R_S\,{}^{S}P_{HCB} \tag{3.1.33}$$

C. Estimation of Physical parameter using dual-arm

Since it is necessary to complete a work in cooperation using dual arm for a nursing care robot, the estimation of physical parameter using dual arm is very important.

a) Coordinate Transformation of the contact position and force

The contact force F_S and contact position P_{HC} in the sensor coordinate system can be represented as

$$\boldsymbol{{}^{S}P_{SC}} = {}^{\boldsymbol{S}}\boldsymbol{R_E}\left({}^{\boldsymbol{E}}\boldsymbol{R_H}\boldsymbol{P_{HC}} + {}^{\boldsymbol{E}}\boldsymbol{P_{EH}}\right) + {}^{\boldsymbol{S}}\boldsymbol{P_{SE}}\ ,\quad \boldsymbol{{}^{S}F_S} = {}^{\boldsymbol{S}}\boldsymbol{R_E}\,{}^{\boldsymbol{E}}\boldsymbol{R_H}\boldsymbol{F_S} \tag{3.1.34}$$

b) *Estimation of the cylinder's center of gravity*

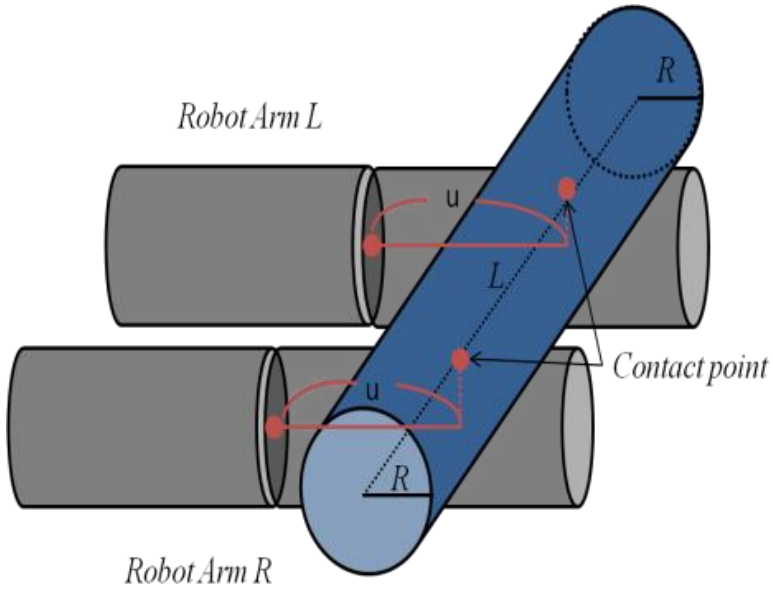

Fig. 3.5 Single contact point

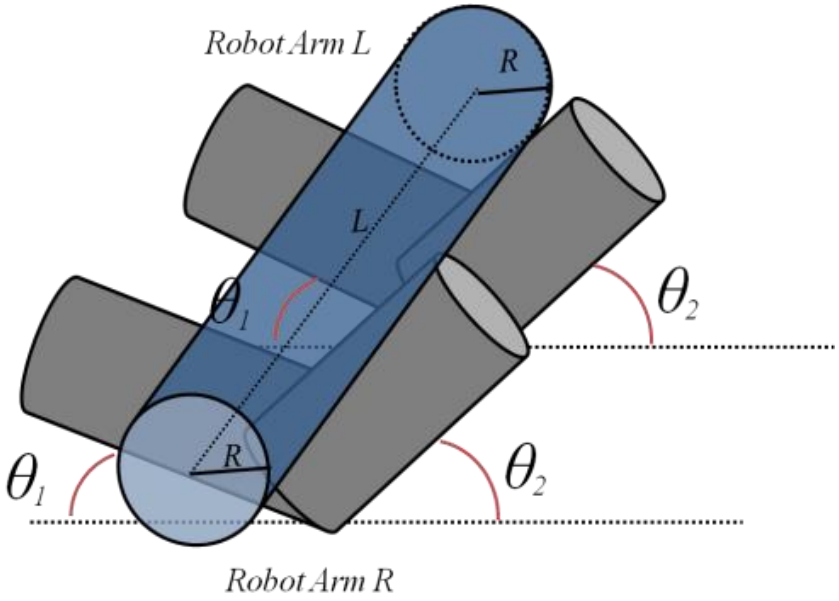

Fig. 3.6 Dual contact point

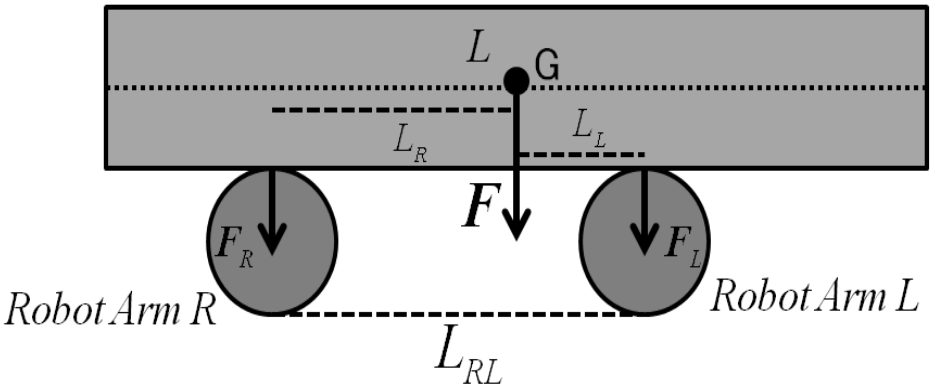

Fig.3.7 Model of robot arms and circular cylinder

$\boldsymbol{F_R}$ and $\boldsymbol{F_L}$ denote respectively the forces action at the right and left arm. $\boldsymbol{L_L, L_R}$ denote the distance from contract position to the center of gravity. Thus, we can get

$$\boldsymbol{L_{RL} = L_L + L_R \ , \quad \|F_R\| L_R = \|F_L\| L_L} \tag{3.1.35}$$

Hence, it is concluded that

$$\boldsymbol{L_R = \frac{\|F_L\|}{\|F_R\| + \|F_L\|} L_{RL} = \frac{F_L}{\|F\|} L_{RL}}$$

$$\boldsymbol{L_L = \frac{\|F_R\|}{\|F_R\| + \|F_L\|} L_{RL} = \frac{F_R}{\|F\|} L_{RL}} \tag{3.1.36}$$

Since the center of gravity $\boldsymbol{{}^oP_G}$ can be represented as

$$\boldsymbol{{}^oP_G = {}^oP_{HC} + {}^oP_{CG}}$$

where $\boldsymbol{{}^oP_{HC}}$ represent the vector from the origin of the origin coordinate system to the contact position, $\boldsymbol{{}^oP_{CG}}$ denote the vector from contact position to center of gravity.

3.2 Simulation Result

3.2.1 The Setting of the Robot's model

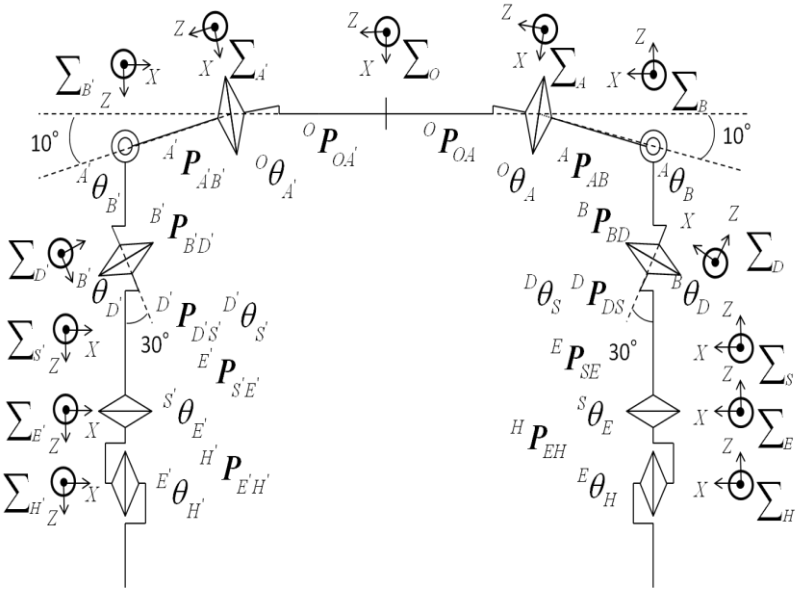

Fig.3.8 Model of robot with arms

The model of the robot is used as a nursing care robot under development as shown in Fig.3.1. The radius of the robot arm which regarded as a cylinder shape is setting as 0.05[m]. The relation parameter between each coordinate system is shown in Table 3.1. The gravity acceleration is $g = 9.8[m/s^2]$. Moreover, since there are noises in the force and moment measured by the 6-axis force sensor, it is necessary to add random noises with a normal distribution.

Right arm	[m]	Left arm	[m]
${}^{O}\mathbf{P}_{OA'}$	$[0 \quad 0 \quad -0.2]^T$	${}^{O}\mathbf{P}_{OA}$	$[0 \quad 0 \quad 0.2]^T$
${}^{A'}\mathbf{P}_{A'B'}$	$[0 \quad 0 \quad -0.1]^T$	${}^{A}\mathbf{P}_{AB}$	$[0 \quad 0 \quad 0.1]^T$
${}^{B'}\mathbf{P}_{B'D'}$	$[0 \quad 0 \quad -0.1]^T$	${}^{B}\mathbf{P}_{BD}$	$[0 \quad 0 \quad -0.1]^T$
${}^{D'}\mathbf{P}_{D'S'}$	$[0 \quad 0 \quad -0.11]^T$	${}^{D}\mathbf{P}_{DS}$	$[0 \quad 0 \quad 0.11]^T$
${}^{S'}\mathbf{P}_{S'E'}$	$[0 \quad 0 \quad -0.045]^T$	${}^{S}\mathbf{P}_{SE}$	$[0 \quad 0 \quad 0.045]^T$
${}^{E'}\mathbf{P}_{E'H'}$	$[0 \quad 0 \quad -0.07]^T$	${}^{E}\mathbf{P}_{EH}$	$[0 \quad 0 \quad 0.07]^T$

Table 3.1 Link vector of robot links

3.2.2 The Model Settings of the Object

The coordinate system as shown in Fig.3.8 is used. The rotation matrix between the coordinate systems is shown in Table 3.2 and the mechanical part that 10°of the shoulder and 30°of the arm has not been shown in the table. The physical parameter which the length $L = 1[m]$, radius is $R = 0.0825[m]$, mass is $M = 3.8[kg]$ has already been known. The distance between two contact point is $L_{RL} = 0.597[m]$. The posture of the robot has already set as two situations: contact object with (1) single point (2) dual points.

	${}^{O}\theta_{A}$ ${}^{O}\theta_{A'}$	${}^{A}\theta_{B}$ ${}^{A'}\theta_{B'}$	${}^{B}\theta_{D}$ ${}^{B'}\theta_{D'}$	${}^{D}\theta_{S}$ ${}^{D'}\theta_{S'}$	${}^{S}\theta_{E}$ ${}^{S'}\theta_{E'}$	${}^{E}\theta_{H}$ ${}^{E'}\theta_{H'}$
(1)	90^o 90^o	-80^o 80^o	0^o 0^o	0^o 0^o	0^o 0^o	0^o 0^o
(2)	60^o 60^o	-80^o 80^o	0^o 0^o	0^o 0^o	0^o 0^o	90^o -90^o

Table 3.2 Rotation matrix of robot links

a) Single point

The posture of robot is shown in the Fig. 3.5 and is fixed. The distance between origin of flexion axis coordinate system and object is denoted as u. This simulation is performed with altering u in two situations: (i) u = 0.10m (ii) u = 0.25m

b) Dual points

As shown in Fig.3.6, each arm contacts the object with two points by bending the arm in order to sandwich the object. Note that,θ_1, θ_2 in Fig. 3.6 is 30°and 60° respectively.

3.2.3 Results of Simulation

In the situation of a), each component of the position vector from the origin of the origin coordinate system to the object's gravity center has been estimated basing on the information measured by left and right sensor.

Besides, in the situation of b), each component of the position vectors from origin of the origin coordinate system to the object's gravity center , denoted as LAPg, LBPg, RAPg and RBPg, are also estimated and shown below.

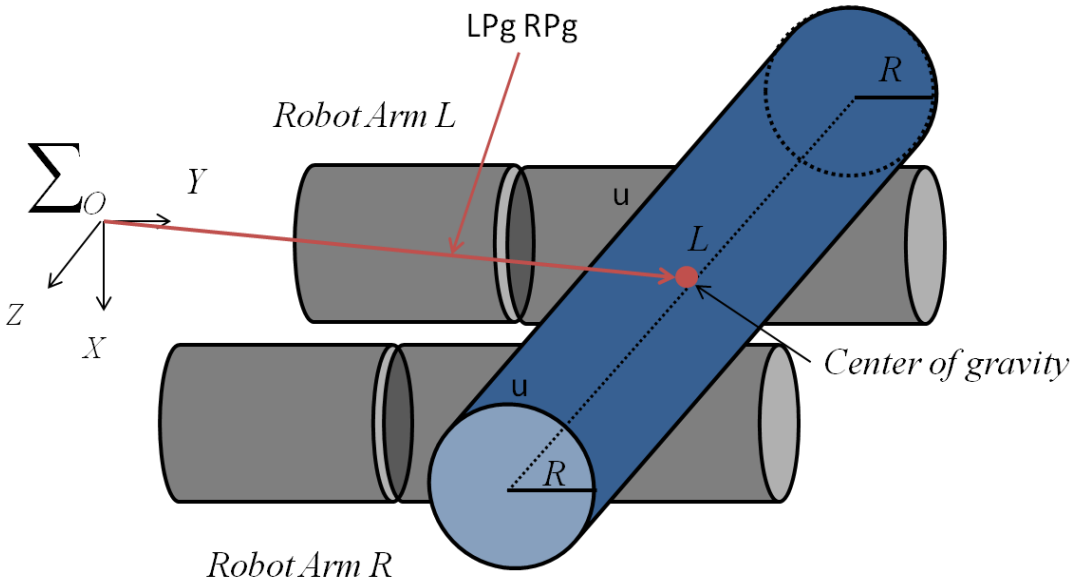

Fig.3.9 Relationship LPg and RPg and model

a) Simulation Result of Single Contact Point

Figs.3.10 and 3.11 show the results of a) with u=0.1m.

From Figs.3.10 and 3.11, none of the components of the position vectors which are estimated by the force sensor has a large fluctuation due to the existence of the noises. The two situations both have the maximum error 0.2mm on z-component.

Figs.3.12 and 3.13 show the results of a) with u=0.25m. There is also none large fluctuation in the results and the maximum error at this situation is also 0.2mm on z-component.

b) Simulation Result of Dual Contact Point.

From Figs. 3.14, 3.15, 3.16 and 3.17, the components of each vectors measured by left and right force sensors contain no large fluctuation. The errors of the estimated vectors mainly come from the z-component. The maximum error is about 0.3mm.

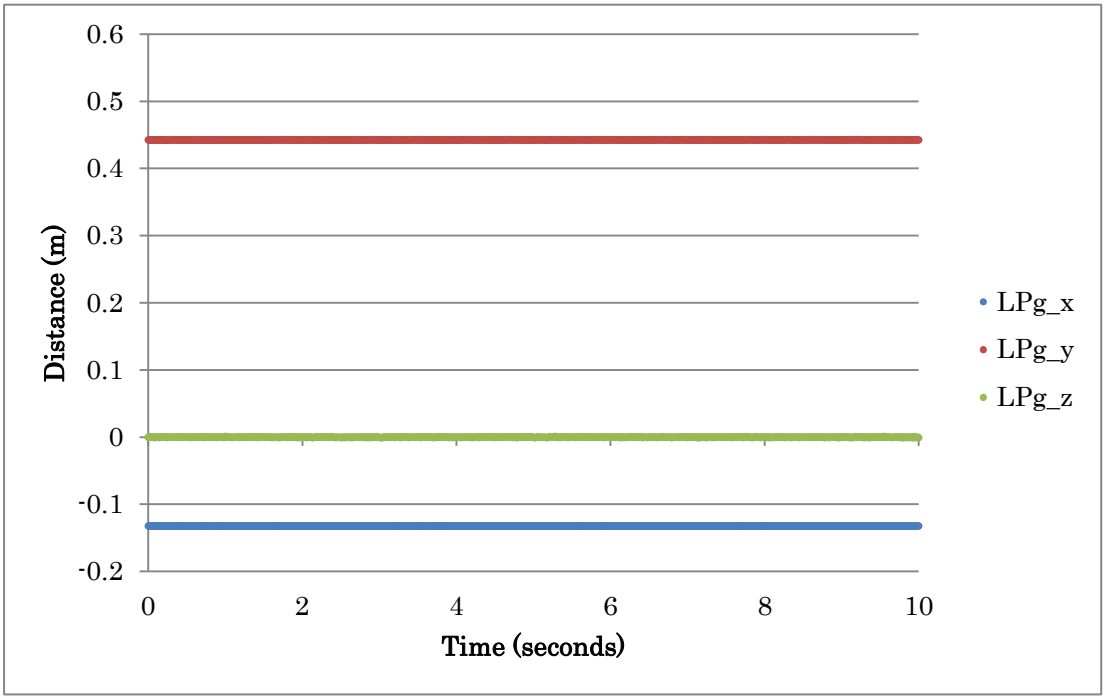

Fig.3.10 Estimated vector from the origin to center of gravity (by left)

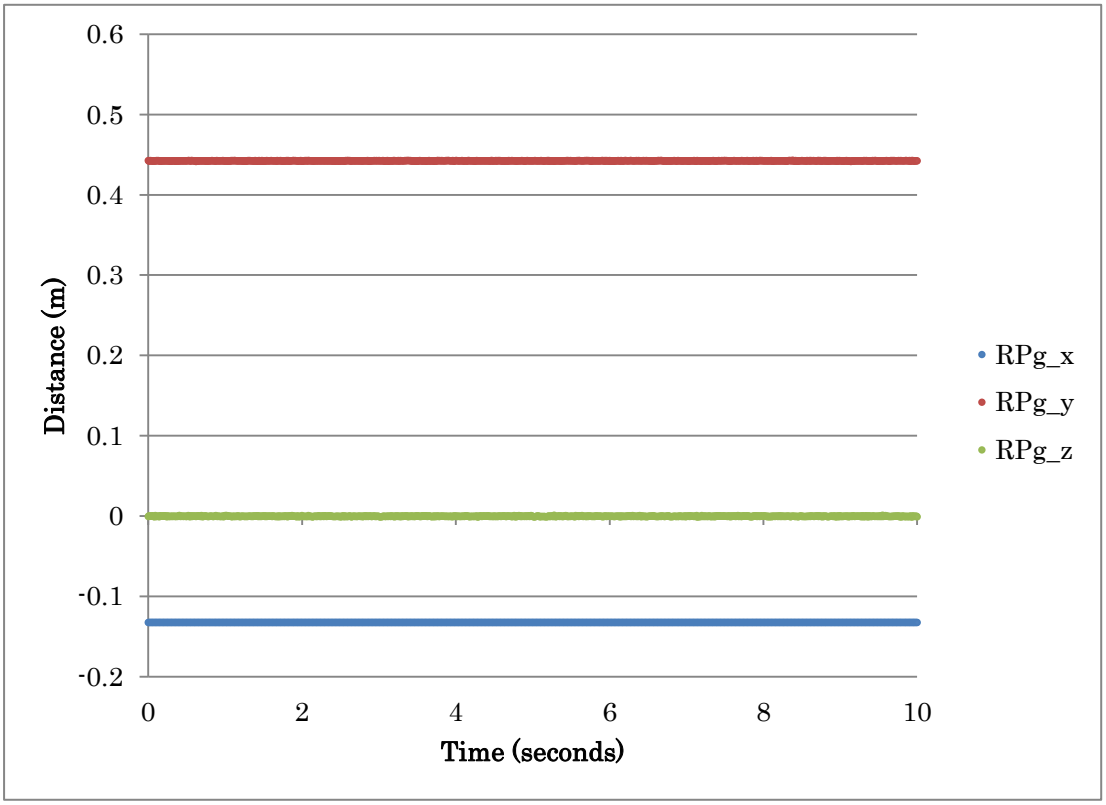

Fig.3.11Estimated vector from the origin to center of gravity (by right)

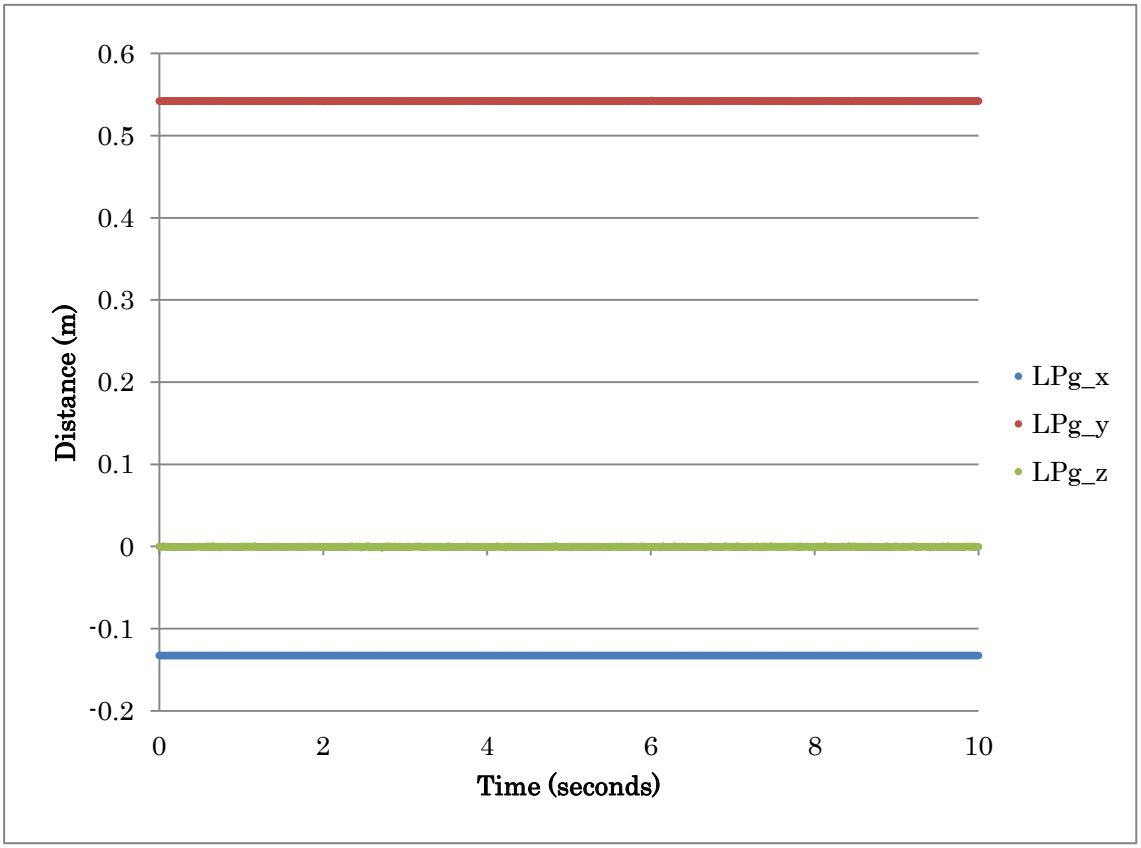

Fig.3.12 Estimated vector from the origin to center of gravity (by left)

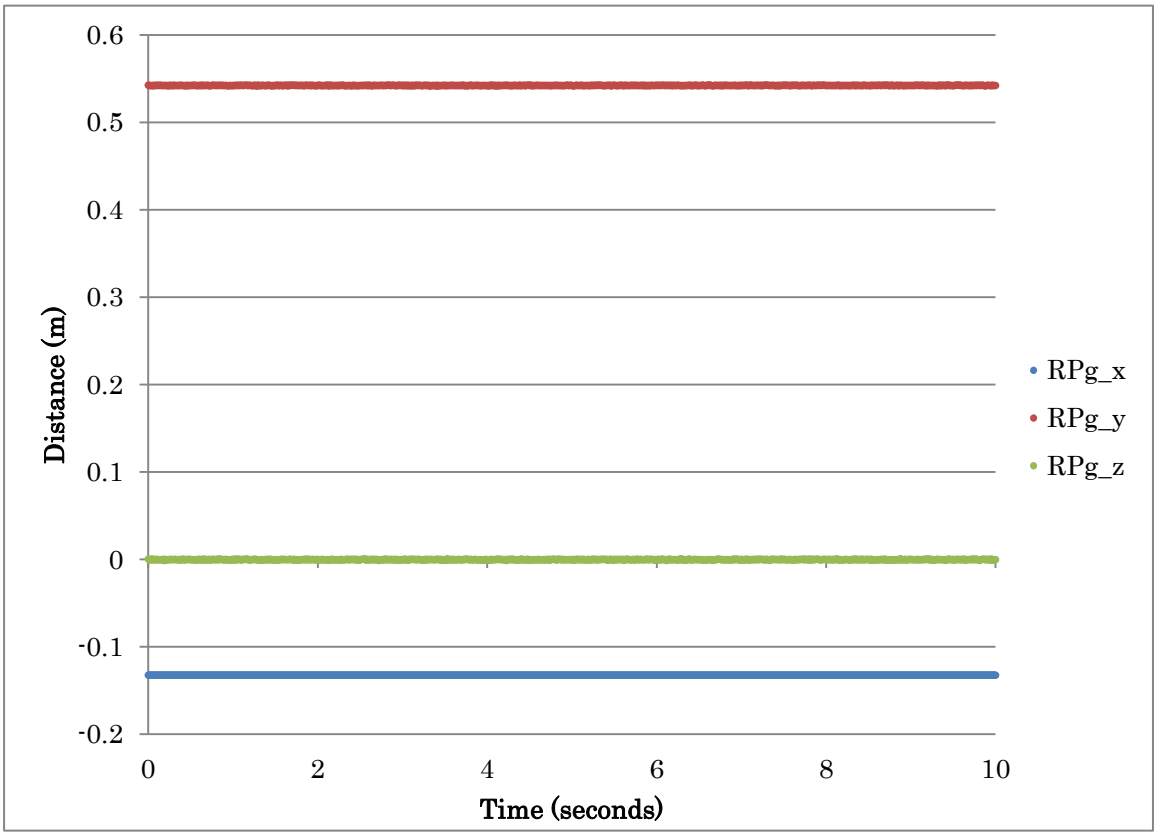

Fig.3.13 Estimated vector from the origin to center of gravity (by right)

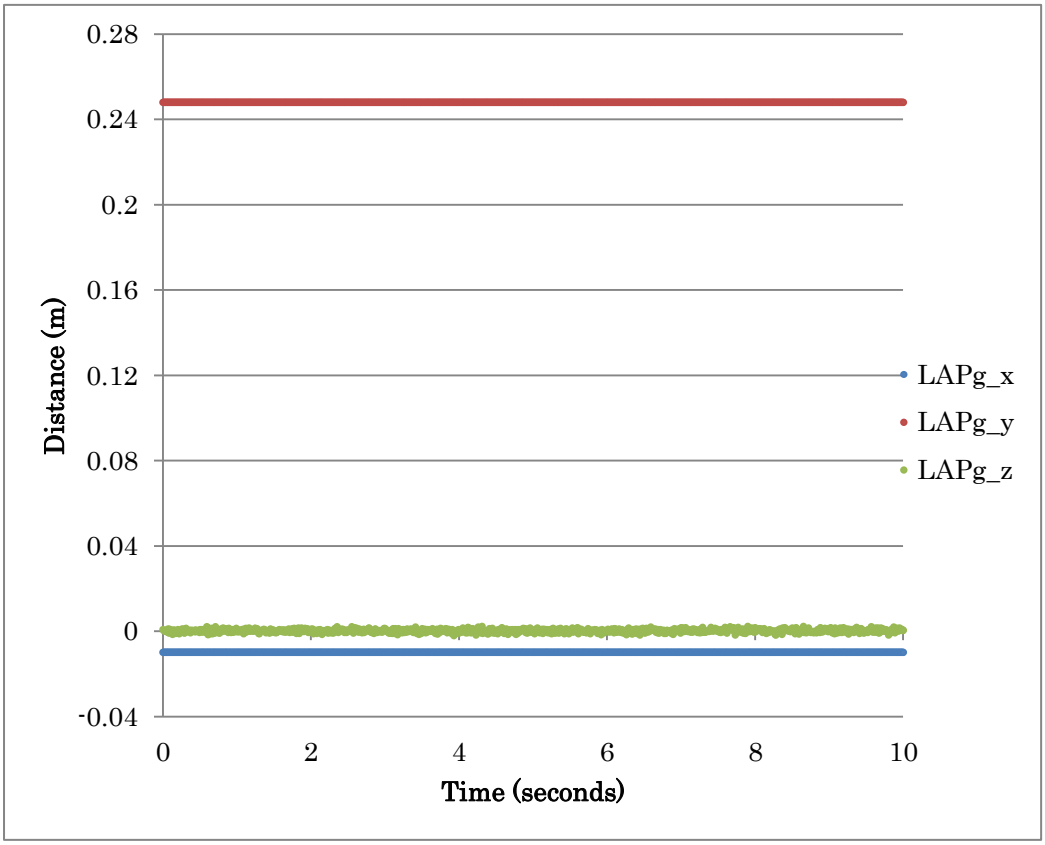

Fig.3.14 Estimated vector from the origin to center of gravity (by left point A)

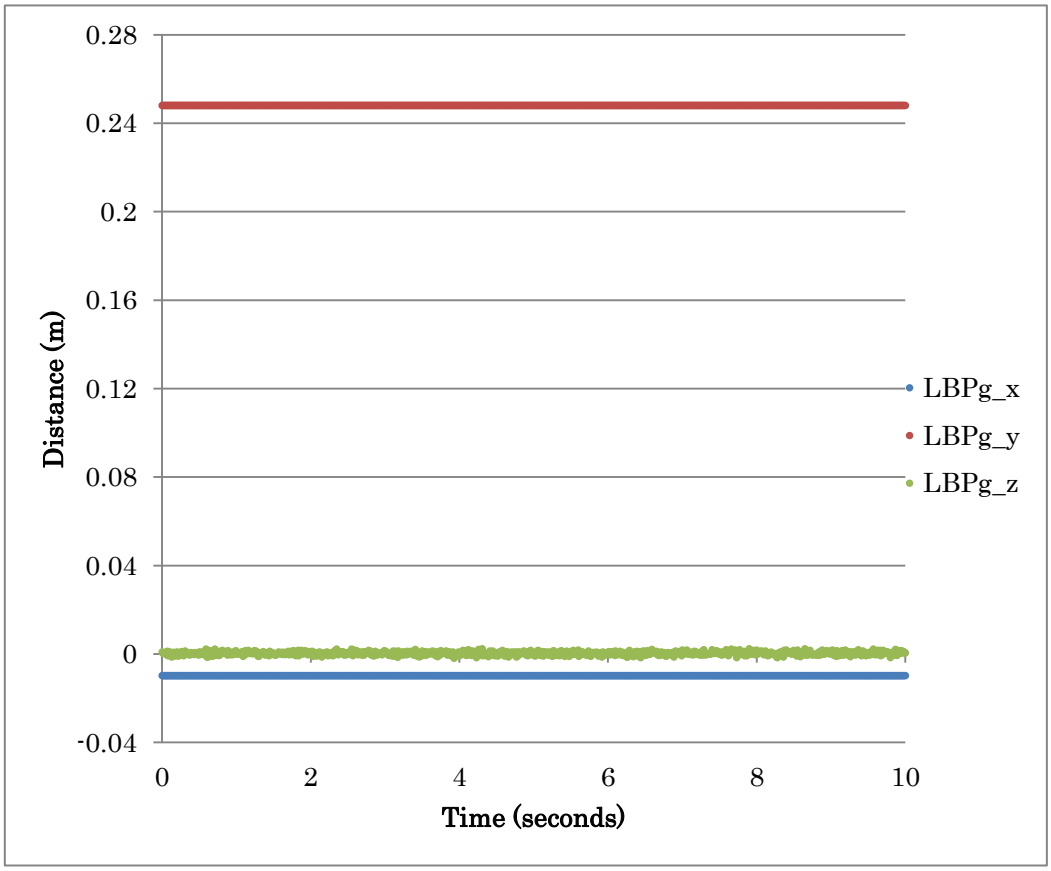

Fig.3.15 Estimated vector from the origin to center of gravity (by left point B)

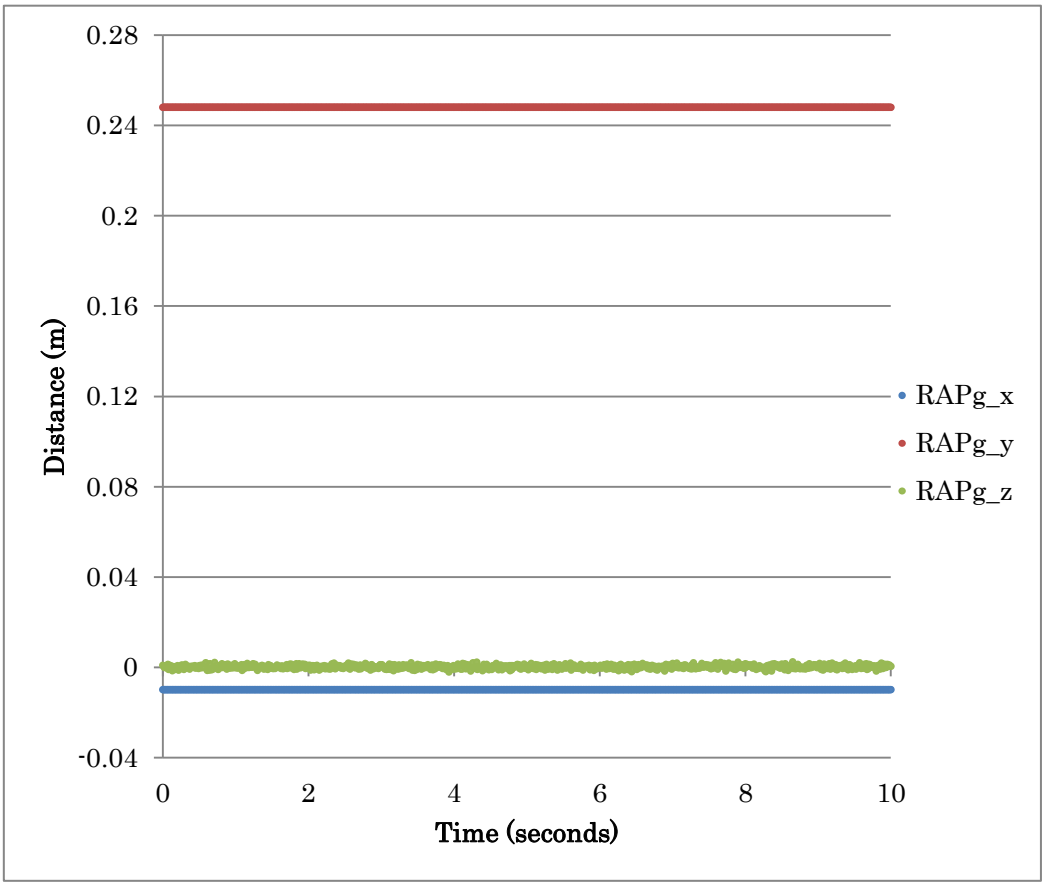

Fig.3.16 Estimated vector from the origin to center of gravity (by right point A)

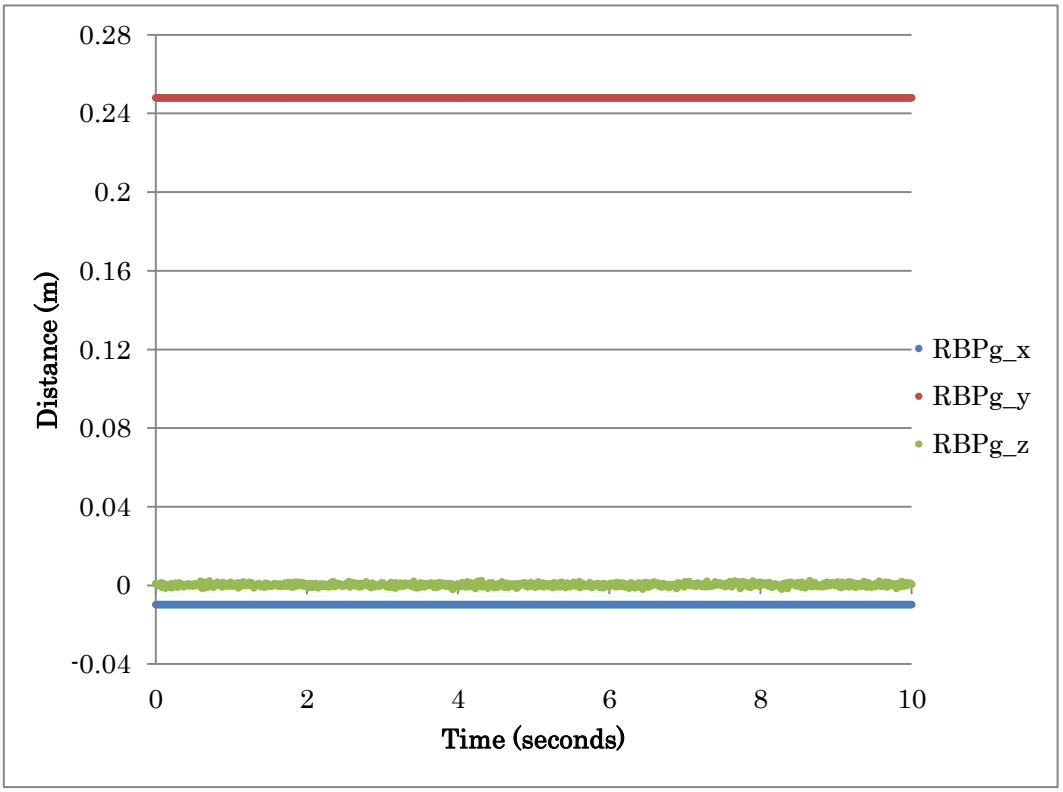

Fig.3.17 Estimated vector from the origin to center of gravity (by right point B)

3.3 Experiment

3.3.1 The Setting of the Experiment

We use the cylindrical object in the experiment as Fig. 3.18. It has the parameters of radius $R = 0.0825[m]$, length $l = 1[m]$, mass $m = 3.8[kg]$.

(a)

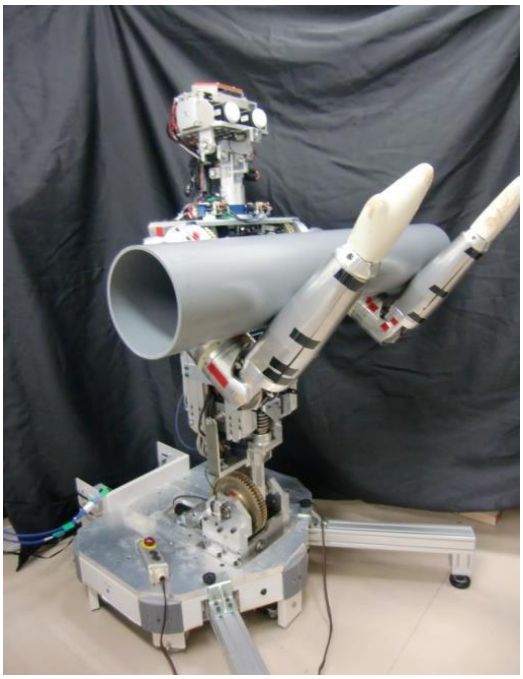

(b)

Fig.3.18 Experiment scene

3.3.2 Results of the Experiment

a) Single Contact Point

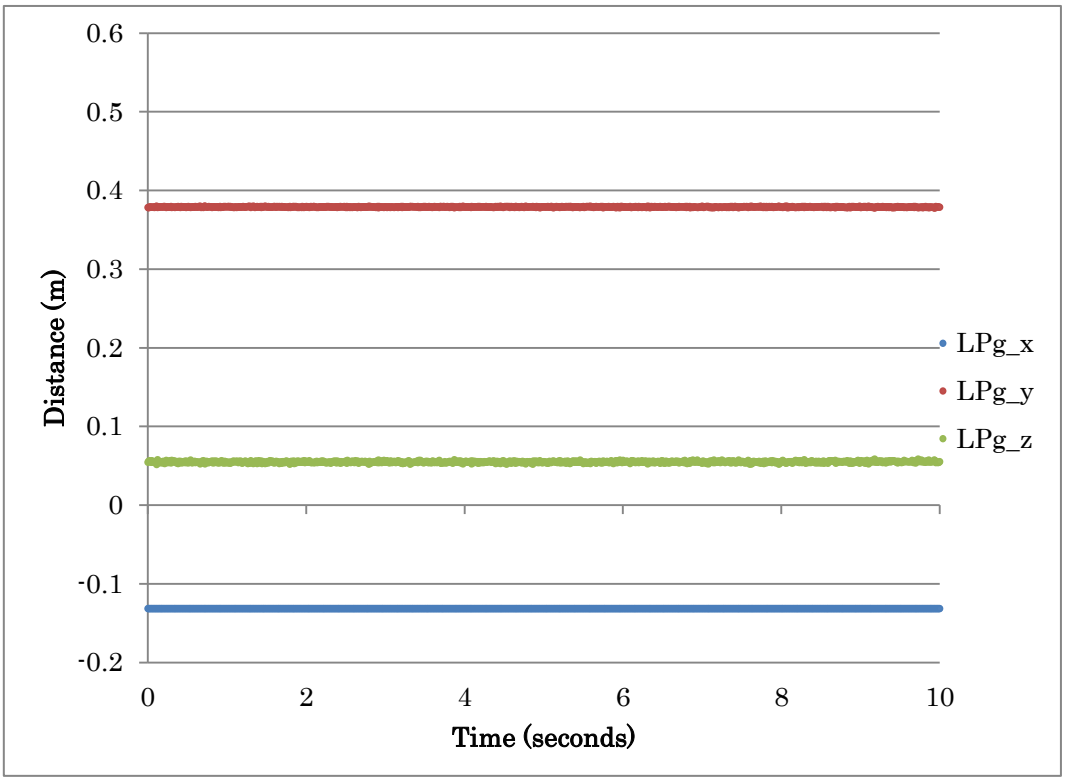

Fig.3.19 Estimated vector from the origin to center of gravity (by left)

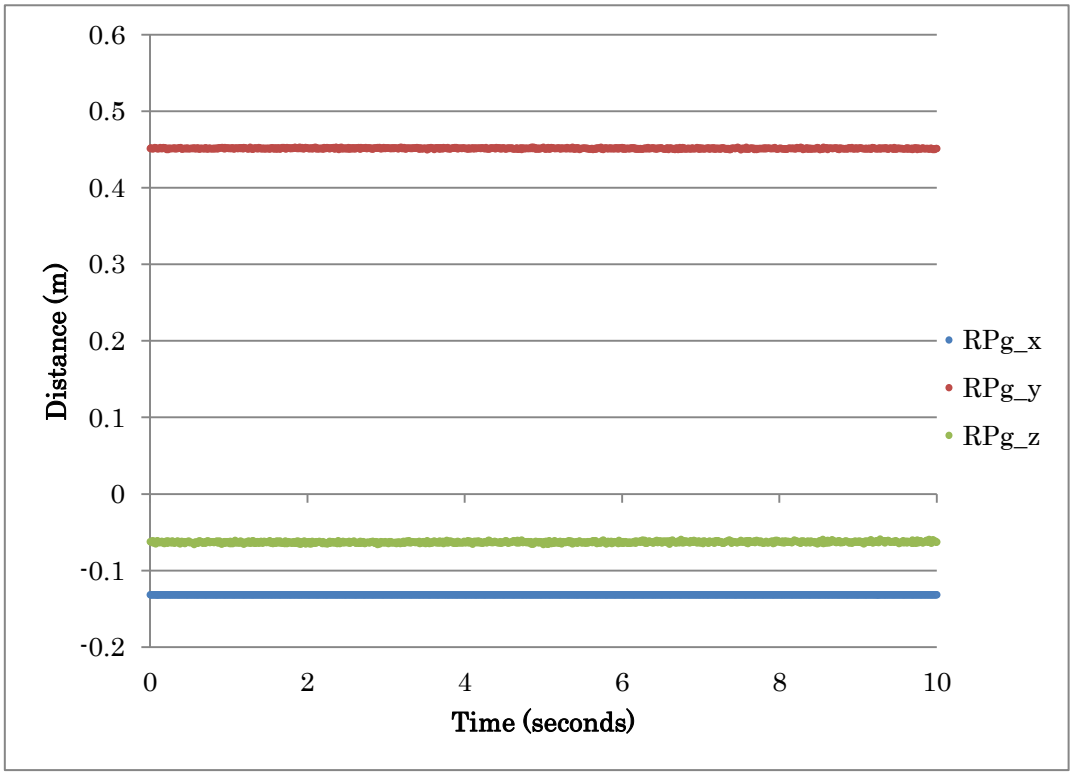

Fig.3.20 Estimated vector from the origin to center of gravity (by right)

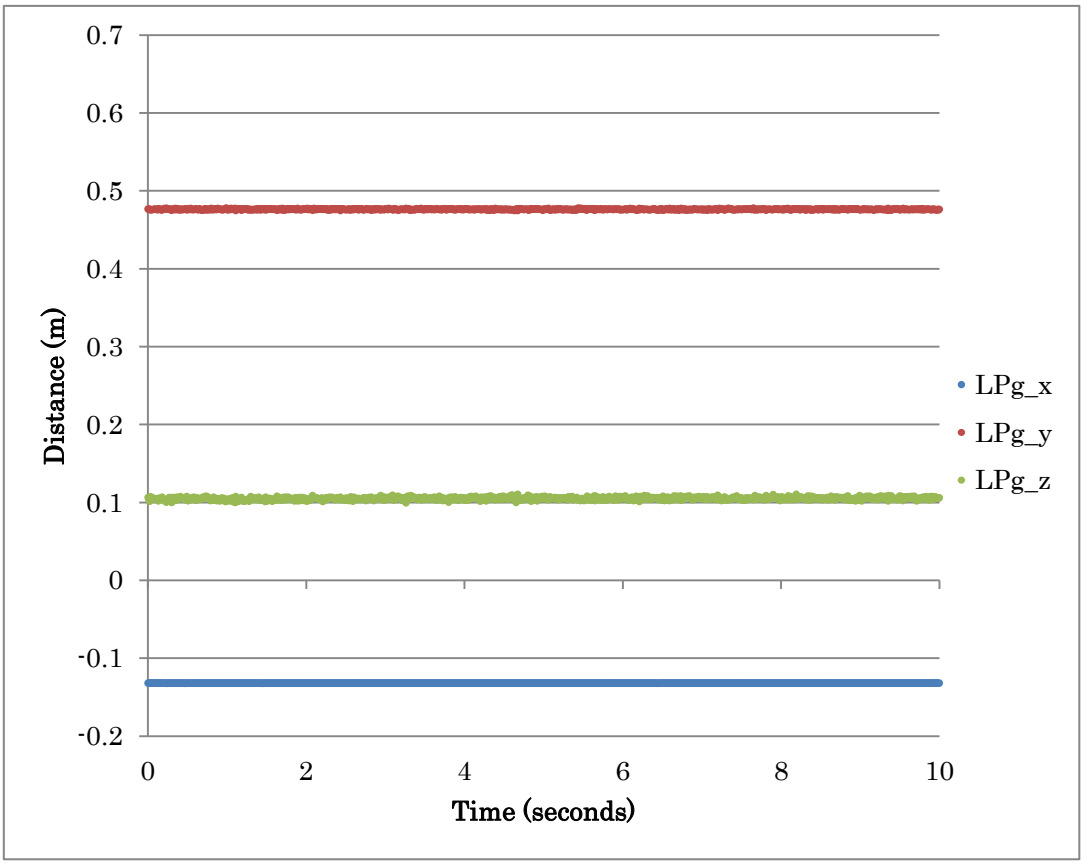

Fig.3.21 Estimated vector from the origin to center of gravity (by left)

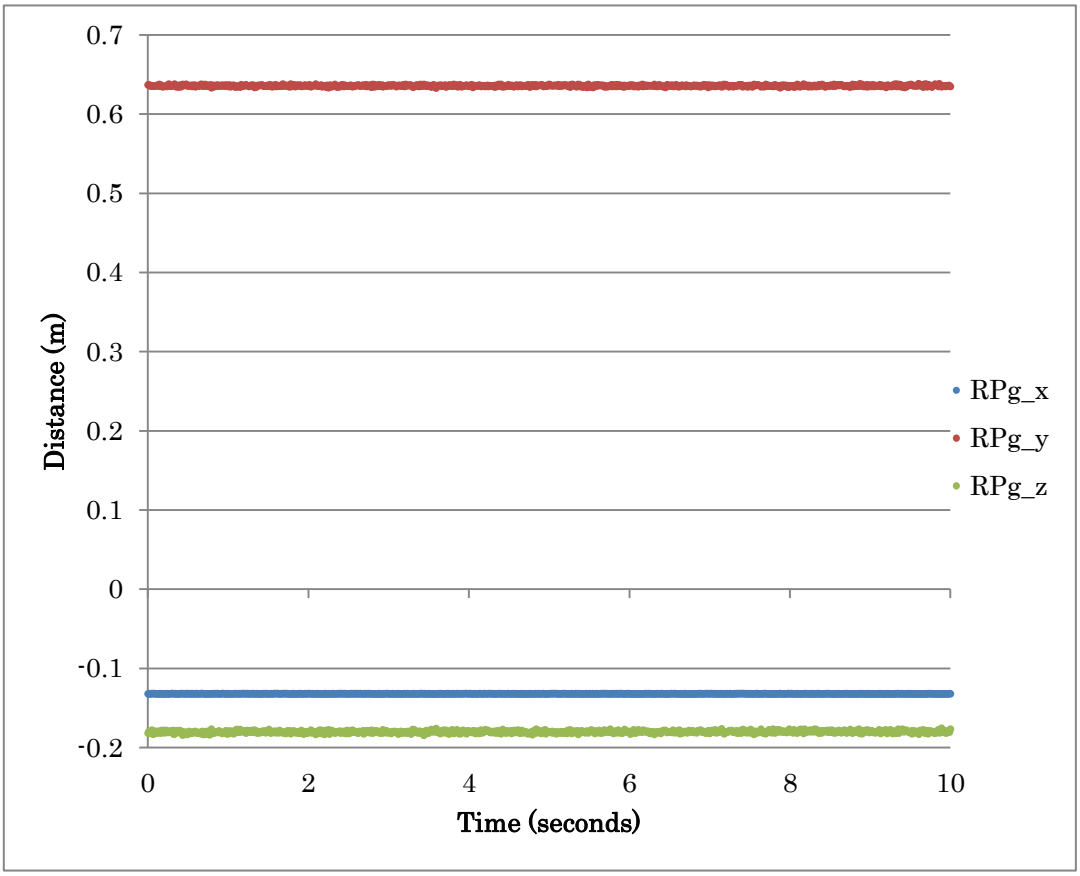

Fig.3.22 Estimated vector from the origin to center of gravity (by right)

Figs.3.19 to 3.22 show the results of the experiment of single contact point with the setting u = 0.10m and u = 0.25m. From these figures, it is known that there is no large fluctuation in the results. The error results show that there is strong correlation between the error and the value of distance u. Error becomes larger with the increase of the value u.

Moreover, since the robot arm is not a perfect cylinder, it appears more errors in y and z component than simulation's result when perform the experiment. We can believe that the model error have a big effect on the result of the estimation.

b) Dual Contact Points

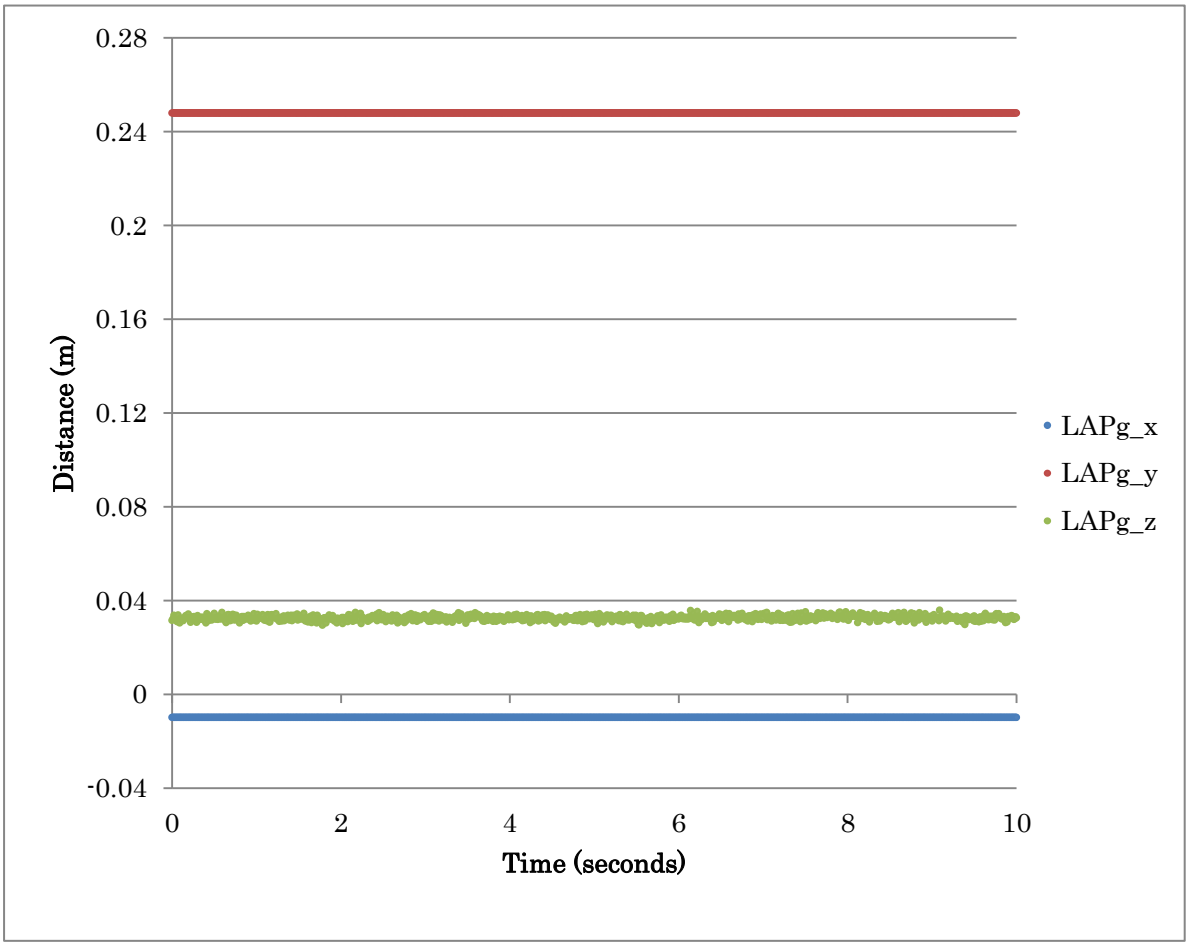

Fig.3.23 Estimated vector from the origin to center of gravity (by left point A)

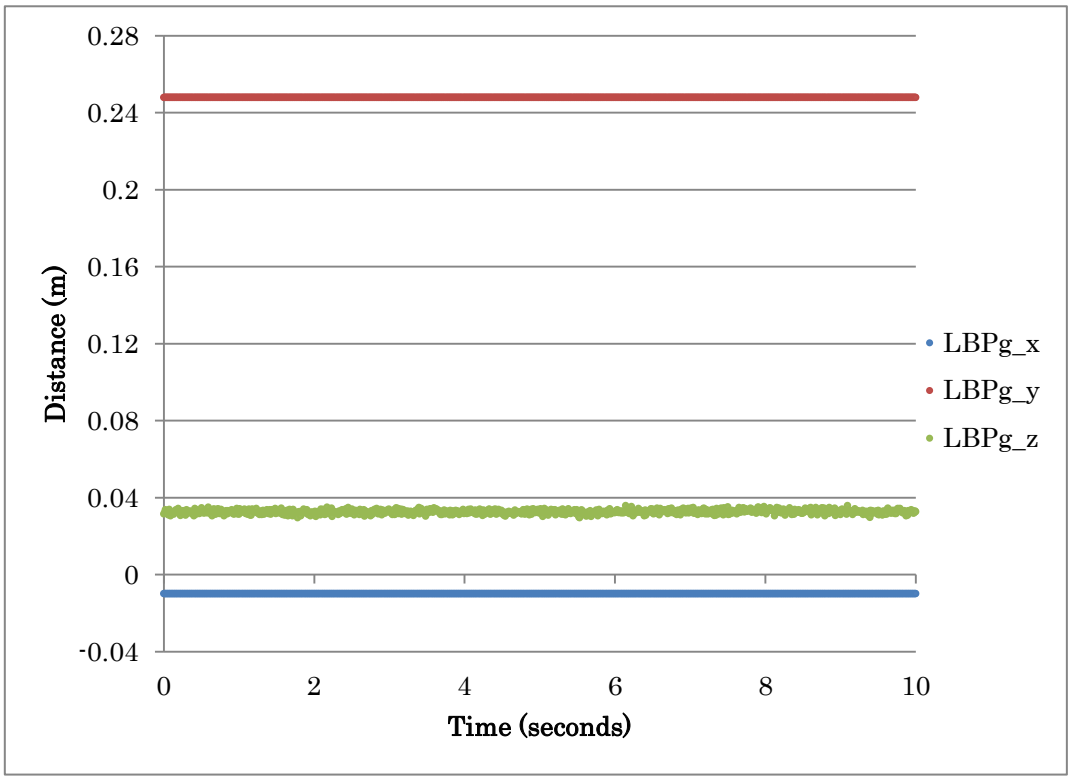

Fig.3.24 Estimated vector from the origin to center of gravity (by left point B)

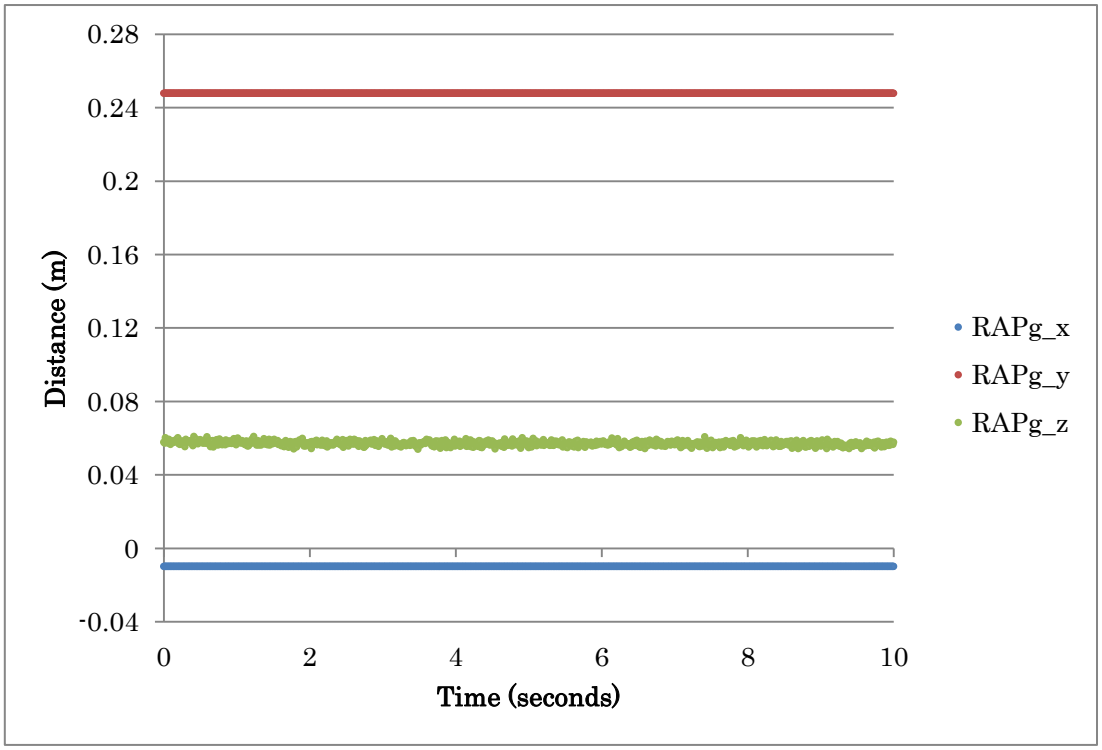

Fig.3.25 Estimated vector from the origin to center of gravity (by right point A)

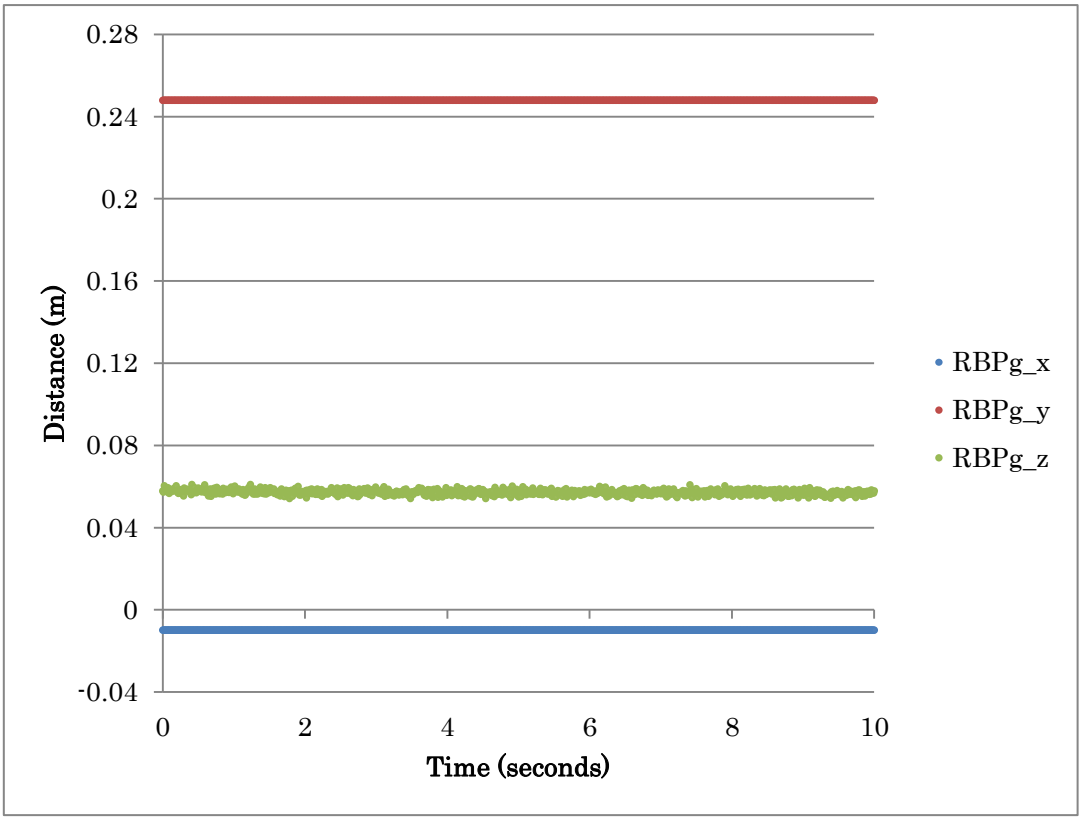

Fig.3.26 Estimated vector from the origin to center of gravity (by right point B)

Figs.3.23 to 3.26 show the results of the experiment of dual contact point with the setting u = 0.10m and u = 0.25m. The results show that there is also no large fluctuation in each component. It is known that there is no error in the x and y component and there are errors of about 3.2cm estimated by left force sensor and 5.7cm estimated by right force sensor in z-component.

Chapter 4 Passivity based Robust Impedance

This chapter focuses on the robot's safety problem from the view of passivity, means that robots do not add any surplus energy to the environment. It is clear that, there are two effectors that influence the robot's passivity. One comes from the time-varying reference trajectory of the robot, another is due to the robot's model uncertainties when performing nonlinear dynamic control. Previous research studied the case when the robot's reference trajectory is time-varying.

To reduce the effect from the robot's model uncertainties, in this thesis, two methods are proposed. Firstly, by carefully setting the estimation parameters of the robot, it shows that a simple PD control can lead to the robot's passivity. However, since the trajectory tracking performance is not improved, the second propose further designed observer based passive impedance control method to observe the effect from the model uncertainties so as to keep the robot's passivity as well as the improvement of the trajectory tracking performance. The effectiveness of these approaches is evaluated using computer simulations.

In the first section, definition of the passivity and previous research on keeping robot's passivity are introduced. Then, the second section shows the passive impedance control method realizing the passivity and impedance without considering the model errors. Furthermore, in the third section, a robust passive impedance control method is proposed, which only utilize a simple parameter adaptation to satisfy the passivity. In the fourth section, an observer based passive robust impedance control method is proposed to realize both the passivity and the impedance of the robot even there are model errors. At last, a series of simulations are performed to verify and compare the effectiveness of two methods.

4.1 Passivity and Passive Velocity Field Control Method

4.1.1 Definition of Robot's Passivity

The problem considered in this section is how to keep the passivity of the robot robustly so as to realize the safety of the robot's movement. The robot's passivity can

be interpreted from the perspective of the robot's energy transformation.

Definition 1 [12]: A dynamic system with input $u \in U$ and output $y \in Y$ is passive with respect to the supply rate $s: U \times Y \to \Re$ if, for any $u: \Re_+ \to U$ and any $t \geq 0$ the following relationship is satisfied

$$\int_0^t s(u(\gamma), y(\gamma))d\gamma \geq -c^2 \tag{4.1.1}$$

where $c \in \Re$ depends on the system's initial conditions.

It is well known that, inputs of the mechanical manipulators interacting with the external environment can be divided into two terms, which are control torques (control inputs) $\boldsymbol{\tau}$ generated by the actuators and the external forces $\boldsymbol{f_e}$ from the environment, respectively. Meanwhile, joint velocity $\dot{\boldsymbol{q}}$ of the manipulators can be regarded as the outputs of the manipulators. When considering the manipulator which is controlled by a closed loop control algorithm with the feedback controller in the process as in Fig. 4.1, then the external forces $\boldsymbol{f_e}$ will be regarded as the inputs and manipulators' velocity $\dot{\boldsymbol{q}}$ the outputs of the system. [12]

The expression in eq. (4.1.1) states that the energy, which is produced by the robot and applied to the environment, should be limited by c^2 so as to keep the robot' passivity and realize the safety of the robot's movement.

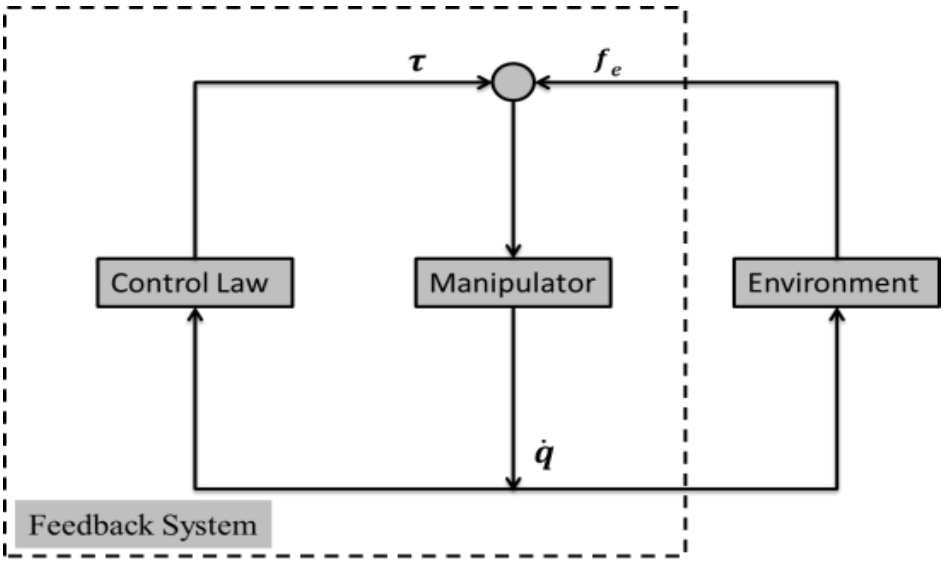

Fig.4.1. Robot interacts with the environment and control

4.1.2 Dynamics of a Robot

The dynamics of a robot in dynamic environment can be described as:

$$\boldsymbol{M}(\boldsymbol{q})\ddot{\boldsymbol{q}} + \boldsymbol{C}(\boldsymbol{q}, \dot{\boldsymbol{q}})\dot{\boldsymbol{q}} = \boldsymbol{\tau} + \boldsymbol{J}^{\boldsymbol{T}}\boldsymbol{f}_{\boldsymbol{e}} \tag{4.1.2}$$

where $\boldsymbol{M}(\boldsymbol{q}) \in \Re^{n\times n}$ is the inertial matrix, $\boldsymbol{C}(\boldsymbol{q}, \dot{\boldsymbol{q}})\dot{\boldsymbol{q}} \in \Re^{1\times n}$ is the Coriolis and centrifugal force vector. $\boldsymbol{\tau}$ is the applied joint torque and $\boldsymbol{f}_{\boldsymbol{e}}$ is the interaction forces exerted at the end-effector from the environment. $\boldsymbol{J}$ is the Jacobi matrix from the robot's joint angle $\boldsymbol{q}$ to the work space $\boldsymbol{x}$.

4.1.3 Passive Velocity Field Control

In order for the robot keep its passivity as well as complete the trajectory tracking task, Li proposed the passive velocity field control method (PVFC) to solve the problem. They firstly augment the system with adding a virtual flywheel and construct a storage function for the surplus energy of the origin system.

Based on the property of the flywheel below,

$$M_F\ddot{q}_{n+1} = \tau_{n+1} \tag{4.1.3}$$

we can formulate the dynamics of the new system as

$$\bar{\boldsymbol{M}}(\bar{\boldsymbol{q}})\ddot{\bar{\boldsymbol{q}}} + \bar{\boldsymbol{C}}(\bar{\boldsymbol{q}}, \dot{\bar{\boldsymbol{q}}})\dot{\bar{\boldsymbol{q}}} = \bar{\boldsymbol{\tau}} + \bar{\boldsymbol{\tau}_{\boldsymbol{e}}} \tag{4.1.4}$$

where

$$\bar{\boldsymbol{M}}(\bar{\boldsymbol{q}}) = \begin{bmatrix} \boldsymbol{M}(\boldsymbol{q}) & \boldsymbol{0} \\ \boldsymbol{0} & \boldsymbol{M_F} \end{bmatrix}, \quad \bar{\boldsymbol{C}}(\bar{\boldsymbol{q}}, \dot{\bar{\boldsymbol{q}}}) = \begin{bmatrix} \boldsymbol{C}(\boldsymbol{q}, \dot{\boldsymbol{q}}) & \boldsymbol{0} \\ \boldsymbol{0} & \boldsymbol{0} \end{bmatrix},$$

$$\bar{\boldsymbol{q}} = \begin{bmatrix} \boldsymbol{q} \\ \boldsymbol{q_{n+1}} \end{bmatrix}, \quad \bar{\boldsymbol{\tau}} = \begin{bmatrix} \boldsymbol{\tau} \\ \boldsymbol{\tau_{n+1}} \end{bmatrix}, \quad \bar{\boldsymbol{\tau_e}} = \begin{bmatrix} \boldsymbol{\tau_e} \\ \boldsymbol{0} \end{bmatrix} \tag{4.1.5}$$

Note that, in order to ensure the trajectory tracking ability of the augmented robot's system, the desired velocity field $\boldsymbol{V}(\boldsymbol{q})$ designed for the original system also needs to be augmented with additional dimension as $\bar{\boldsymbol{V}}(\bar{\boldsymbol{q}}) = [\boldsymbol{V}(\boldsymbol{q})^{\boldsymbol{T}}, V_{n+1}(\boldsymbol{q})]^{\boldsymbol{T}}$. It is known that limiting the energy exerted by the robot can ensure the satisfaction of the robot's

passivity as well as the safety. One possible method is to construct an energy storage function utilizing the augmented system. The kinetic energy of the total system can be shown as

$$k\left(\bar{q},\bar{V}(\bar{q})\right)=\frac{1}{2}\overline{\boldsymbol{V^T}}(\bar{\boldsymbol{q}})\bar{\boldsymbol{M}}(\bar{\boldsymbol{q}})\bar{\boldsymbol{V}}(\bar{\boldsymbol{q}})=\frac{1}{2}\boldsymbol{V^T M(q)V}+\frac{1}{2}M_F{V_{n+1}}^2=\bar{E}>0 \tag{4.1.6}$$

where $\bar{E}$ is a constant value. Thus, based on this setting, the desired velocity of the virtual flywheel system can be designed as

$$V_{n+1}=\sqrt{\frac{\boldsymbol{2}}{\boldsymbol{M_F}}\left(\bar{E}-\frac{\boldsymbol{1}}{\boldsymbol{2}}\boldsymbol{V^T M(q)V}\right)} \tag{4.1.7}$$

In order to realize the passivity and trajectory tracking, control input for the augmented system above can be designed as

$$\bar{\boldsymbol{\tau}}\left(\bar{\boldsymbol{q}},\dot{\bar{\boldsymbol{q}}}\right)=\boldsymbol{G}\dot{\bar{\boldsymbol{q}}}+\gamma\boldsymbol{R}\dot{\bar{\boldsymbol{q}}}=\bar{\boldsymbol{\tau}}_{\boldsymbol{c}}\left(\bar{\boldsymbol{q}},\dot{\bar{\boldsymbol{q}}}\right)+\bar{\boldsymbol{\tau}}_{\boldsymbol{f}}\left(\bar{\boldsymbol{q}},\dot{\bar{\boldsymbol{q}}}\right) \tag{4.1.8}$$

where G and R can respectively be selected as

$$\boldsymbol{G}=\frac{\boldsymbol{1}}{\boldsymbol{2}\bar{E}}(\bar{\boldsymbol{w}}\bar{\boldsymbol{P}}^{\boldsymbol{T}}-\bar{\boldsymbol{P}}\bar{\boldsymbol{w}}^{\boldsymbol{T}}) \tag{4.1.9}$$

$$\boldsymbol{R}=(\bar{\boldsymbol{P}}\bar{\boldsymbol{p}}^{\boldsymbol{T}}-\bar{\boldsymbol{p}}\bar{\boldsymbol{P}}^{\boldsymbol{T}}) \tag{4.1.10}$$

$\bar{\boldsymbol{w}}, \bar{\boldsymbol{P}}, \bar{\boldsymbol{p}}$ can be represented as

$$\bar{\boldsymbol{p}}\left(\bar{\boldsymbol{q}},\dot{\bar{\boldsymbol{q}}}\right)=\bar{\boldsymbol{M}}(\bar{\boldsymbol{q}})\dot{\bar{\boldsymbol{q}}}$$

$$\bar{\boldsymbol{P}}(\bar{\boldsymbol{q}})=\bar{\boldsymbol{M}}(\bar{\boldsymbol{q}})\bar{\boldsymbol{V}}(\bar{\boldsymbol{q}})$$

$$\bar{\boldsymbol{w}}\left(\bar{\boldsymbol{q}},\dot{\bar{\boldsymbol{q}}}\right)=\bar{\boldsymbol{M}}(\bar{\boldsymbol{q}})\dot{\bar{\boldsymbol{V}}}(\bar{\boldsymbol{q}})+\bar{\boldsymbol{C}}\left(\bar{\boldsymbol{q}},\dot{\bar{\boldsymbol{q}}}\right)\bar{\boldsymbol{V}}(\bar{\boldsymbol{q}}) \tag{4.1.11}$$

By this control input, it can be verified that the robot can satisfy the passivity by the value of supply rate $(\dot{\boldsymbol{q}}^{\boldsymbol{T}}\boldsymbol{\tau_e})$. In detail, the supply rate $(\dot{\boldsymbol{q}}^{\boldsymbol{T}}\boldsymbol{\tau_e})$ can satisfy the equation

$$\dot{\boldsymbol{q}}^{\boldsymbol{T}}\boldsymbol{\tau_e} = \dot{\bar{\boldsymbol{q}}}^{\boldsymbol{T}}\bar{\boldsymbol{\tau}}_{\boldsymbol{e}} = \dot{\bar{\boldsymbol{q}}}^{\boldsymbol{T}}\left(\bar{\boldsymbol{M}}(\bar{\boldsymbol{q}})\ddot{\bar{\boldsymbol{q}}} + \boldsymbol{C}(\boldsymbol{q},\bar{\boldsymbol{q}})\dot{\bar{\boldsymbol{q}}}\right) - \dot{\bar{\boldsymbol{q}}}^{\boldsymbol{T}}\bar{\boldsymbol{\tau}}$$

$$= \dot{\boldsymbol{q}}^{\boldsymbol{T}}(\boldsymbol{M}(\boldsymbol{q})\ddot{\boldsymbol{q}} + \boldsymbol{C}(\boldsymbol{q},\dot{\boldsymbol{q}})\dot{\boldsymbol{q}}) + \boldsymbol{M_F}\dot{q}_{n+1}\ddot{q}_{n+1} - \dot{\bar{\boldsymbol{q}}}^{\boldsymbol{T}}\left(\boldsymbol{G}\dot{\bar{\boldsymbol{q}}} + \gamma\boldsymbol{R}\dot{\bar{\boldsymbol{q}}}\right)$$

$$= \frac{\boldsymbol{d}}{\boldsymbol{dt}}\left(\frac{\boldsymbol{1}}{\boldsymbol{2}}\dot{\boldsymbol{q}}^{\boldsymbol{T}}\boldsymbol{M}(\boldsymbol{q})\dot{\boldsymbol{q}} + \frac{\boldsymbol{1}}{\boldsymbol{2}}M_F{\dot{q}_{n+1}}^2\right) + \boldsymbol{0} = \frac{\boldsymbol{d}}{\boldsymbol{dt}}\left(\frac{\boldsymbol{1}}{\boldsymbol{2}}\dot{\bar{\boldsymbol{q}}}^{\boldsymbol{T}}\bar{\boldsymbol{M}}(\bar{\boldsymbol{q}})\dot{\bar{\boldsymbol{q}}}\right) \qquad (4.1.12)$$

Here, since G and R are two skew-symmetric matrixes, the integration from time 0∼t of the eq. (4.1.12) can be written as

$$\int_0^{\mathrm{t}} \dot{\boldsymbol{q}}^{\boldsymbol{T}}\boldsymbol{\tau_e}\,\mathrm{ds} = \left(\frac{1}{2}\dot{\bar{\boldsymbol{q}}}^{\boldsymbol{T}}\bar{\boldsymbol{M}}(\bar{\boldsymbol{q}})\dot{\bar{\boldsymbol{q}}}\right) - \left(\frac{1}{2}\dot{\bar{\boldsymbol{q}}}^{\boldsymbol{T}}\bar{\boldsymbol{M}}(\bar{\boldsymbol{q}})\dot{\bar{\boldsymbol{q}}}\right)\Big|_{\mathrm{t}=0} \geq -\left(\frac{1}{2}\dot{\bar{\boldsymbol{q}}}^{\boldsymbol{T}}\bar{\boldsymbol{M}}(\bar{\boldsymbol{q}})\dot{\bar{\boldsymbol{q}}}\right)\Big|_{\mathrm{t}=0} \qquad (4.1.13)$$

Therefore, the augmented system as well as the original robot system can satisfy passivity. In addition, it was shown that the robot can also realize tracking of an objective velocity field.

Although PVFC method perform well in satisfying the robot's passivity and trajectory tracking, and Adaptive PVFC, the further version of PVFC, overcome the effect from the model errors, the complex calculation of the control input makes it difficult to be applied in those real time task, especially for those manipulator with redundancy.

4.1.4 Passivity of Impedance Control

To overcome the problems of PVFC, Kishi and Luo proposed Passive impedance control. Here, in order for the robot to realize the following impedance

$$\boldsymbol{M_d}\ddot{\boldsymbol{x}} + \boldsymbol{D_d}\dot{\boldsymbol{x}} + \boldsymbol{K_d}(\boldsymbol{x} - \boldsymbol{x_d}) = \boldsymbol{f_e} \qquad (4.1.14)$$

under the condition that the robot's physical parameters are all known, we can specify the robot's control input as

$$\boldsymbol{\tau} = \boldsymbol{M}(\boldsymbol{q})\boldsymbol{J}^{-1}(\boldsymbol{q})\left\{\boldsymbol{M_d}^{-1}(-\boldsymbol{D_d}\dot{\boldsymbol{x}} - \boldsymbol{K_d}(\boldsymbol{x} - \boldsymbol{x_d}) + \boldsymbol{f_e}) - \boldsymbol{J}(\dot{\boldsymbol{q}})\dot{\boldsymbol{q}}\right\} + \boldsymbol{C}(\boldsymbol{q},\dot{\boldsymbol{q}})\dot{\boldsymbol{q}} - \boldsymbol{J}^{\boldsymbol{T}}\boldsymbol{f_e}$$

(4.1.15)

where $\boldsymbol{M_d, D_d, K_d}$ are the desired positive mass , damping and stiffness coefficient. $\boldsymbol{x} \in \Re^m$ is the robot's end-effector position, $\boldsymbol{x_d}$ is the impedance center. Mass ($\boldsymbol{M_d}$) and stiffness ($\boldsymbol{K_d}$) are energy storing elements, while damper ($\boldsymbol{D_d}$) possess the function of dissipating kinetic energy.

From eq. (4.1.14), it is clear that, if the impedance center $\boldsymbol{x_d}$ is constant, then the robot will be passive. However, if $\boldsymbol{x_d}$ is changing with respect to time, then it will influence the robot's passivity as follows. Here, as in [12], to analyze the passivity of the robot with impedance control, we define the mechanic energy as

$$E \coloneqq \frac{1}{2}\dot{\boldsymbol{x}}^T\boldsymbol{M_d}\dot{\boldsymbol{x}} + \frac{1}{2}(\boldsymbol{x}-\boldsymbol{x_d})^T\boldsymbol{K_d}(\boldsymbol{x}-\boldsymbol{x_d}) \tag{4.1.16}$$

It is clear that E is positive. The first and the second term represent the kinetic and potential energy, respectively.

Using eq. (4.1.14), the time change of the mechanic energy can be derived as

$$\frac{d}{dt}E = \dot{\boldsymbol{x}}^T\boldsymbol{M_d}\ddot{\boldsymbol{x}} + (\dot{\boldsymbol{x}}-\dot{\boldsymbol{x}_d})^T\boldsymbol{K_d}(\boldsymbol{x}-\boldsymbol{x_d}) = -\dot{\boldsymbol{x}}^T\boldsymbol{D_d}\dot{\boldsymbol{x}} - \dot{\boldsymbol{x}_d}\boldsymbol{K_d}(\boldsymbol{x}-\boldsymbol{x_d}) + \dot{\boldsymbol{x}}^T\boldsymbol{f_e} \tag{4.1.17}$$

By integrating the eq. (4.1.17), we get

$$\int_0^t \dot{\boldsymbol{x}}^T\boldsymbol{f_e}\,\boldsymbol{ds} = E - E|_{t=0} + \int_0^t \left(\dot{\boldsymbol{x}}^T\boldsymbol{D_d}\dot{\boldsymbol{x}} + \dot{\boldsymbol{x}_d}\boldsymbol{K_d}(\boldsymbol{x}-\boldsymbol{x_d})\right)\boldsymbol{ds}$$

$$\geq -E|_{t=0} + \int_0^t \left(\dot{\boldsymbol{x}_d}\boldsymbol{K_d}(\boldsymbol{x}-\boldsymbol{x_d})\right)\boldsymbol{ds} \tag{4.1.18}$$

From eq. (4.1.18), it is apparent that if $\boldsymbol{x_d}$ don't change with the time variation, that is, if $\dot{x}_d$ is 0, then

$$\int_0^t \dot{\boldsymbol{x}}^T\boldsymbol{f_e}\,ds \geq -E|_{t=0} \tag{4.1.19}$$

That is, the energy served by the robot to the environment can be controlled less than the initial kinetic energy so that the surplus energy will not supply to the

environment. From the definition of the passivity (i.e. eq. (4.1.1)), the impedance controlled robot is passive.

However, if the impedance center x_d varies with respect to time (i.e. tracking a trajectory), that is, if $\dot{x_d}$ is not 0, then the right side of the eq. (4.1.18) may not satisfy the passivity condition of eq. (4.1.1), which implies that robot may impose surplus energy to environment so as to approach to the desired position as shown in Fig.4.2.

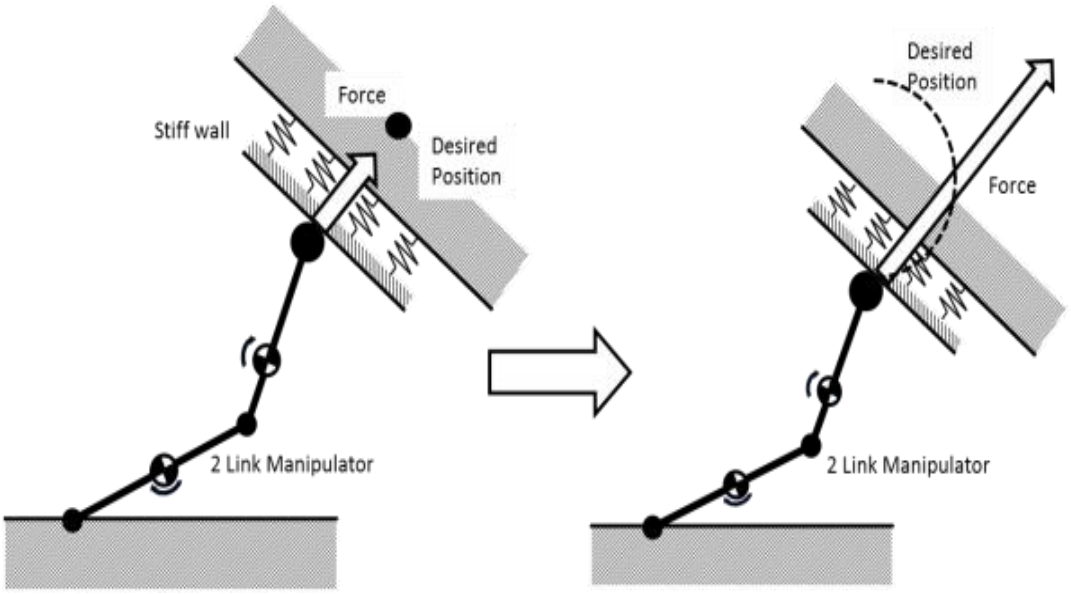

Fig. 3.2 Comparison between the invariant and varying desired position

4.2 Passive Impedance Control (PIC)

4.2.1 Control Law of PIC

In order to keep the passivity of the robot controlled by impedance control law while performing the trajectory tracking task, it is necessary to appropriately adjust the desired impedance center so as to limit the energy exerted by robot.

In [17], under the condition that the robot's physical parameters are all known, it was proposed to switch a scaling parameter of the robot's desired velocity as follows. Here, the velocity of the desired impedance center is set as

$$\dot{\boldsymbol{x}}_{\boldsymbol{d}} = \alpha \boldsymbol{V} \tag{4.2.1}$$

where α is the scaling parameter satisfying $\alpha > 0$, V was defined as the tangent

velocity vector of impedance center trajectory designed previously without considering the environmental uncertainties.

Then, if we adjust the scaling parameter α satisfying the condition

$$\alpha \begin{cases} \leq -\frac{\gamma S + \dot{\boldsymbol{x}}^{\boldsymbol{T}} \boldsymbol{D_d} \dot{\boldsymbol{x}}}{z} & when\ z < 0 \\ \geq -\frac{\gamma S + \dot{\boldsymbol{x}}^{\boldsymbol{T}} \boldsymbol{D_d} \dot{\boldsymbol{x}}}{z} & when\ z > 0 \end{cases} \tag{4.2.2}$$

the robot would be passive. Here, γ is a positive value and a new value z was defined as

$$z \coloneqq \boldsymbol{V^T K_d (x - x_d)} \tag{4.2.3}$$

To understand this control approach, let's define a new value S, or accurate to say, the derivative of S as

$$\dot{S} \coloneqq \dot{\boldsymbol{x}}^{\boldsymbol{T}} \boldsymbol{D_d} \dot{\boldsymbol{x}} + \dot{\boldsymbol{x}}_{\boldsymbol{d}} \boldsymbol{K_d (x - x_d)} \tag{4.2.4}$$

where the initial value of S has been set as $S_0 > 0$.

If we make

$$\dot{S} \geq -\gamma S \tag{4.2.5}$$

Since the initial value of S be set as $S_0 > 0$, we have

$$S > S_0 e^{-\gamma t} \ > 0 \quad \forall t > 0$$

Base on this setting, α's condition can be derived as (4.2.2). and one possible choice of α can be given as

$$\alpha = (\gamma S + \dot{\boldsymbol{x}}^{\boldsymbol{T}} \boldsymbol{D_d} \dot{\boldsymbol{x}})(1 + \frac{1 - e^{-cz}}{1 + e^{-cz}}) \tag{4.2.6}$$

Therefore, from Eq. (4.1.4.2) and Eq. (4.2.4), we get

$$\frac{d}{dt}(E+S) = \dot{\boldsymbol{x}}^{\boldsymbol{T}}\boldsymbol{f_e} \tag{4.2.7}$$

Since $S > 0$, Eq. (4.1.33) becomes

$$\int_0^t \dot{\boldsymbol{x}}^{\boldsymbol{T}}\boldsymbol{f_e}\,\boldsymbol{ds} = E + S - (E_0 + S_0) > -(E_0 + S_0) \tag{4.2.8}$$

Thus, energy served to the environment can be limited by $E_0 + S_0$ so that the impedance controlled robot remains passive.

4.2.2 Influences of Model Uncertainties for Passive Impedance Control

Here, we further consider the case that the robot's dynamics M and C are unknown. We set their estimations as $\widehat{\boldsymbol{M}}$ and $\widehat{\boldsymbol{C}}$, respectively. We also define $\widetilde{\boldsymbol{M}}$ and $\widetilde{\boldsymbol{C}}$ as error terms as

$$\widetilde{\boldsymbol{M}} \coloneqq \boldsymbol{M} - \widehat{\boldsymbol{M}}, \widetilde{\boldsymbol{C}} \coloneqq \boldsymbol{C} - \widehat{\boldsymbol{C}}.$$

Then, from Eq. (4.1.30), now the robot's control input becomes

$$\boldsymbol{\tau} = \widehat{\boldsymbol{M}}\boldsymbol{J}^{-1}(\boldsymbol{q})\{\boldsymbol{M_d}^{-1}(-\boldsymbol{D_d}\dot{\boldsymbol{x}} - \boldsymbol{K_d}(\boldsymbol{x} - \boldsymbol{x_d}) + \boldsymbol{f_e}) - \boldsymbol{J}(\dot{\boldsymbol{q}})\dot{\boldsymbol{q}}\} + \widehat{\boldsymbol{C}}\dot{\boldsymbol{q}} - \boldsymbol{J}^{\boldsymbol{T}}\boldsymbol{f_e} \tag{4.2.9}$$

Put this control into Eq. (4.1.2), then we get

$$\boldsymbol{M_d}\ddot{\boldsymbol{x}} + \boldsymbol{D_d}\dot{\boldsymbol{x}} + \boldsymbol{K_d}(\boldsymbol{x} - \boldsymbol{x_d}) = \boldsymbol{f_e} + \boldsymbol{f_m} \tag{4.2.10}$$

where $\boldsymbol{f_e}$ is the external force while $\boldsymbol{f_m}$ represents the force term caused by the robot's model uncertainties as

$$\boldsymbol{f_m} \coloneqq -(\boldsymbol{M_d}\boldsymbol{J}\widehat{\boldsymbol{M}}^{-1}\widetilde{\boldsymbol{M}}\ddot{\boldsymbol{q}} + \boldsymbol{M_d}\boldsymbol{J}\widehat{\boldsymbol{M}}^{-1}\widetilde{\boldsymbol{C}}\dot{\boldsymbol{q}}) \tag{4.2.11}$$

From Eq. (4.2.11), it is clear that model errors actually may have effects on the results of impedance control and the passivity of the robot as follows:

$$\int_0^t \dot{\boldsymbol{x}}^T \boldsymbol{f}_e \, \boldsymbol{ds} = E + S - (E_0 + S_0) - \int_0^t \dot{\boldsymbol{x}}^T \boldsymbol{f}_m \, \boldsymbol{ds} \tag{4.2.12}$$

Since the term $\int_0^t(-\dot{\boldsymbol{x}}^T \boldsymbol{f}_m)$ds exists, besides of time-varying impedance center, the robot's model uncertainties also influence the change of the energy which is provided by the robot to the environment. Therefore, robot may lose its passivity even under the control frame of passive impedance control method.

4.3 Robust Passive Impedance Control (RPIC)

In order to solve this problem, we propose a novel robust control approach based on an appropriate selection of the estimation of $\boldsymbol{M}$ and $\boldsymbol{C}$ so that to keep the robot's passivity during impedance control even if there are model uncertainties of the robot.

Considering the robot's model error term of $\boldsymbol{f}_m$, here we set the new energy as

$$E = \frac{1}{2}\dot{\boldsymbol{x}}^T \boldsymbol{M}_d \dot{\boldsymbol{x}} + \frac{1}{2}(\boldsymbol{x} - \boldsymbol{x}_d)^T \boldsymbol{K}_d (\boldsymbol{x} - \boldsymbol{x}_d) + E_m \tag{4.3.1}$$

where $E_m = \frac{1}{2}\dot{\boldsymbol{q}}^T \tilde{\boldsymbol{M}} \dot{\boldsymbol{q}}$. Note, it is necessary to keep E_m be positive, therefore we have to carefully select the estimation $\widehat{\mathbf{M}}$ so that $\widetilde{\mathbf{M}}$ can always be positive definite matrix. In this paper, we select $\widehat{\boldsymbol{M}} := \boldsymbol{J}^T \boldsymbol{M}_d \boldsymbol{J}, \widehat{\boldsymbol{C}} = \frac{1}{2}\dot{\widehat{\boldsymbol{M}}} = \boldsymbol{J}^T \boldsymbol{M}_d \dot{\boldsymbol{J}}$ and set small $\boldsymbol{M}_d$ so that $\widetilde{\boldsymbol{M}} := \boldsymbol{M} - \widehat{\boldsymbol{M}}$ can be positive definite.

Then, the time variation of the energy can now be obtained as

$$\frac{\boldsymbol{d}}{\boldsymbol{dt}} E = -\dot{\boldsymbol{x}}^T \boldsymbol{D}_d \dot{\boldsymbol{x}} - \dot{\boldsymbol{x}}_d \boldsymbol{K}_d (\boldsymbol{x} - \boldsymbol{x}_d) + \dot{\boldsymbol{x}}^T \boldsymbol{f}_e + \dot{W}_m \tag{4.3.2}$$

With $\dot{W}_m = \dot{\boldsymbol{x}}^T \boldsymbol{f}_m + \dot{E}_m = -\dot{\boldsymbol{x}}^T \left(\boldsymbol{M}_d \boldsymbol{J} \widehat{\boldsymbol{M}}^{-1} \tilde{\boldsymbol{M}} \ddot{\boldsymbol{q}} + \boldsymbol{M}_d \boldsymbol{J} \widehat{\boldsymbol{M}}^{-1} \tilde{\boldsymbol{C}} \dot{\boldsymbol{q}}\right) + \dot{\boldsymbol{q}}^T \left(\tilde{\boldsymbol{M}} \ddot{\boldsymbol{q}} + \tilde{\boldsymbol{C}} \dot{\boldsymbol{q}}\right) = \mathbf{0}$. The time variation of energy now becomes

$$\frac{\boldsymbol{d}}{\boldsymbol{dt}} E = -\dot{\boldsymbol{x}}^T \boldsymbol{D}_d \dot{\boldsymbol{x}} - \dot{\boldsymbol{x}}_d \boldsymbol{K}_d (\boldsymbol{x} - \boldsymbol{x}_d) + \dot{\boldsymbol{x}}^T \boldsymbol{f}_e \tag{4.3.3}$$

Then, by using the same passive impedance control in section II, we can keep the

robot's passivity.

And by substituting of $\widehat{\boldsymbol{M}} := \boldsymbol{J}^{\boldsymbol{T}}\boldsymbol{M}_{\boldsymbol{d}}\boldsymbol{J}, \widehat{\boldsymbol{C}} = \frac{\mathbf{1}}{\mathbf{2}}\dot{\widehat{\boldsymbol{M}}} = \boldsymbol{J}^{\boldsymbol{T}}\boldsymbol{M}_{\boldsymbol{d}}\dot{\boldsymbol{J}}$ into the control input eq. (4.2.9), $\boldsymbol{\tau}$ becomes

$$\boldsymbol{\tau} = -\boldsymbol{J}^{\boldsymbol{T}}\left(\boldsymbol{D}_{\boldsymbol{d}}\dot{\boldsymbol{x}} + \boldsymbol{K}_{\boldsymbol{d}}(\boldsymbol{x} - \boldsymbol{x}_{\boldsymbol{d}})\right) - \boldsymbol{J}^{\boldsymbol{T}}\boldsymbol{f}_{\boldsymbol{e}} \tag{4.3.4}$$

This is a very smart and simple PD like control+force feedback which is even simple that the original control of eq.(4.1.2) that has nonlinear feedback compensation using the robot's dynamic parameters of $\boldsymbol{M}$ and $\boldsymbol{C}$. The only condition here is that we have to set small M_d so $\widehat{\boldsymbol{M}} := \boldsymbol{J}^{\boldsymbol{T}}\boldsymbol{M}_{\boldsymbol{d}}\boldsymbol{J}$ can make $\widetilde{\boldsymbol{M}} := \boldsymbol{M} - \widehat{\boldsymbol{M}}$ be positive definite as well as $\widehat{\boldsymbol{C}} = \frac{\mathbf{1}}{\mathbf{2}}\dot{\widehat{\boldsymbol{M}}} = \boldsymbol{J}^{\boldsymbol{T}}\boldsymbol{M}_{\boldsymbol{d}}\dot{\boldsymbol{J}}$.

However, even in this study, we proposed an approach to select the estimation of M and C so as the robot can keep its passivity under the model uncertainties. However, the performance of impedance control still be influenced by the model error term f_m and thus remain to be improved.

4.4 Observer based Passive Robust Impedance Control (PRIC)

In this section, we propose a novel observer based passive robust impedance control approach which designs an observer to detect the model error f_m so that to decrease the effect of the term $\int_0^t \dot{\boldsymbol{x}}^{\boldsymbol{T}}\boldsymbol{f}_{\boldsymbol{m}}\,ds$ in eq. (4.3.4) to make the robot passive as well as realize the robot's impedance control performance.

By introducing f_c as a new input force, we select the robot's control law as

$$\boldsymbol{\tau}' = \widehat{\boldsymbol{M}}(\boldsymbol{q})\boldsymbol{J}^{-\mathbf{1}}(\boldsymbol{q})\left\{\boldsymbol{M}_{\boldsymbol{d}}{}^{-\mathbf{1}}(-\boldsymbol{D}_{\boldsymbol{d}}\dot{\boldsymbol{x}} - \boldsymbol{K}_{\boldsymbol{d}}(\boldsymbol{x} - \boldsymbol{x}_{\boldsymbol{d}}) + \boldsymbol{f}_{\boldsymbol{e}} + \boldsymbol{f}_{\boldsymbol{c}}) - \boldsymbol{J}(\dot{\boldsymbol{q}})\dot{\boldsymbol{q}}\right\} + \widehat{\boldsymbol{C}}(\boldsymbol{q}, \dot{\boldsymbol{q}})\dot{\boldsymbol{q}} - \boldsymbol{J}^{\boldsymbol{T}}\boldsymbol{f}_{\boldsymbol{e}} \tag{4.4.1}$$

$\boldsymbol{f}_{\boldsymbol{c}}$ is mainly designed to eliminate the model error force $\boldsymbol{f}_{\boldsymbol{m}}$ in the impedance equation which will be shown later.

By applying this control input, the robot's impedance becomes:

$$\boldsymbol{M_d\ddot{x} + D_d\dot{x} + K_d(x - x_d) = f_e + f_c + f_m} \tag{4.4.2}$$

On the other hand, we also introduce a new reference $\boldsymbol{x_r}$ and set the ideal impedance as

$$\boldsymbol{M_d\ddot{x}_r + D_d\dot{x}_r + K_d(x_r - x_d) = f_e} \tag{4.4.3}$$

where $\boldsymbol{\ddot{x}_r, \dot{x}_r}$and $\boldsymbol{x_r}$ represent the robot's ideal acceleration, velocity and position, respectively.

By calculating eq. (4.4.2) –eq. (4.4.3), we can obtain

$$\boldsymbol{M_d\ddot{x}_e + D_d\dot{x}_e + K_dx_e = f_c + f_m} \tag{4.4.4}$$

where $x_e \coloneqq x - x_r$.

Since the robot's real position x as well as the interaction force f_e from the environment to the robot can all directly be measured, then we can obtain $\boldsymbol{x_r}$ from eq.(4.4.3) and in turn, the error position $\boldsymbol{x_e}$. By filtering this error position $\boldsymbol{x_e}$ using the following transfer function:

$$\boldsymbol{O(s) = \frac{M_ds^2 + D_ds + K_d}{Ts^2 + bs}} \tag{4.4.5}$$

then we can design the new control force

$$\boldsymbol{f_c = -O(s)Ix_e} \tag{4.4.6}$$

so that

$$\boldsymbol{f_c = \frac{-1}{Ts^2 + bs + 1} If_m}$$

By set the parameters T and b, we can make sure that $\boldsymbol{f_c + f_m \to 0}$. Therefore, the robot's model error will not influence the impedance control of eq. (4.4.2). Here, I

is an unit matrix. The overall observer design is shown in Fig.4.3.

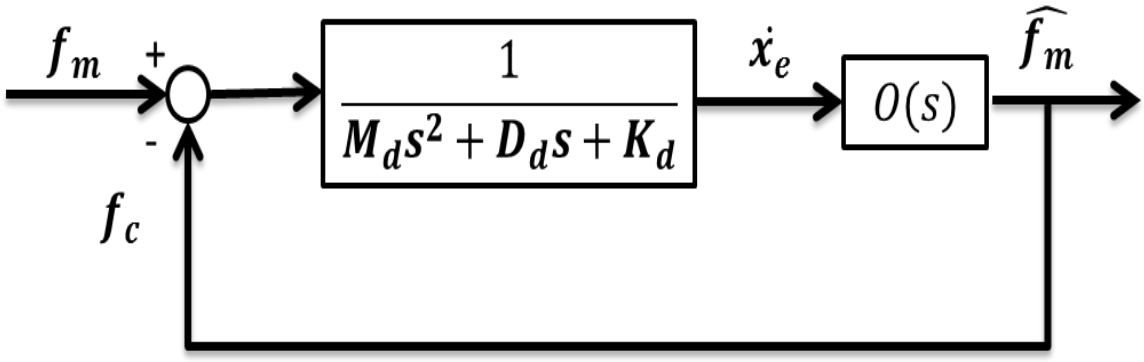

Fig. 4.3 Block Diagram of the Disturbance Observer Design

4.5 Simulation Studies

In this section, we perform computer simulations to show the effectiveness of the RPIC and PRIC method respectively. In the simulations, we consider a 2 D.O.F robot arm interacting with an unknown stiff wall as shown in Fig.4.4.

The robot's all physical parameters used for simulation are listed in Table.1.

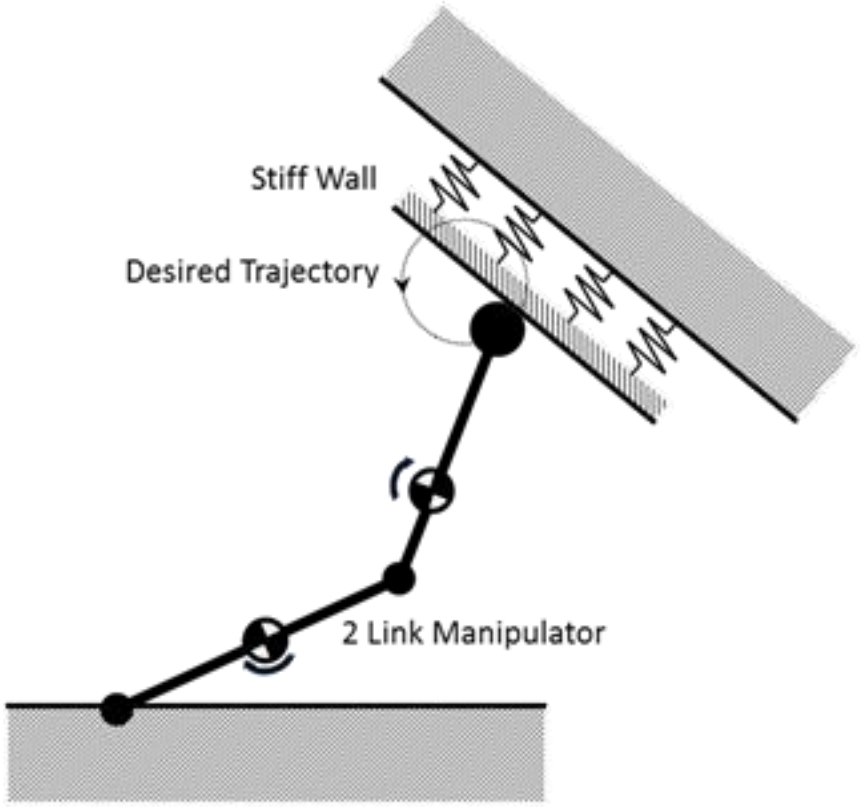

Fig.4.4 Computer simulations of a 2 D.O.F robot arm moving on a dynamic wall

I_1	0.3125	kgm^2
I_2	0.3125	kgm^2
m_1	5	kg
m_2	5	kg
l_1	0.25	m
l_2	0.25	m
L_1	0.5	m
L_2	0.5	m

Table. 4.1 Simulation Parameters of the Robot

4.5.1 Simulations of RPIC method

Here, we mainly performed three types of simulations. The first type and the second type use same previous passive impedance control, but in different cases: (1) when there is no model error $\widehat{m_i} = 1.0 \times m_i$ and (2) when the estimated $\widehat{m_i} = 1.8 \times m_i$. The third type uses our robust passive impedance control method when the estimated inertial matrix $\widehat{M} = J^T M_d J$ and the estimated Coriolis and centrifugal force term of $\hat{C} = J^T M_d \dot{J}$.

In addition, we also set the parameter in the matrix (K_d, D_d, M_d) of the impedance equation and the parameter in the matrix (K_e, D_e) of the stiff wall as $k_d = 25, d_d = 10, m_d = 1$ and $k_e = 375, d_e = 200$.The initial value of S has been defined as $S_0 = 0.02$. Considering the initial value of mechanic energy E_0 is 0, the value $E_0 + S_0$ is 0.02.

Figs.4.5 to 4.7 shows the result using passive impedance control on robot without model errors, while Figs.4.8 to 4.10 are for the case when we set $\widehat{m_i} = 1.8 \times m_i$, and Figs.4.11 to 4.13 are results of our robust passive impedance control. From Fig.4.5, We can see that the external force converges to the value of 1N after the contact. Fig.4.6 shows the time change of the mechanic energy of the robot, it is clear that the energy didn't exceed the initial value $E_0 + S_0 = 0.02$, the robot can keep the passivity by using PIC method.

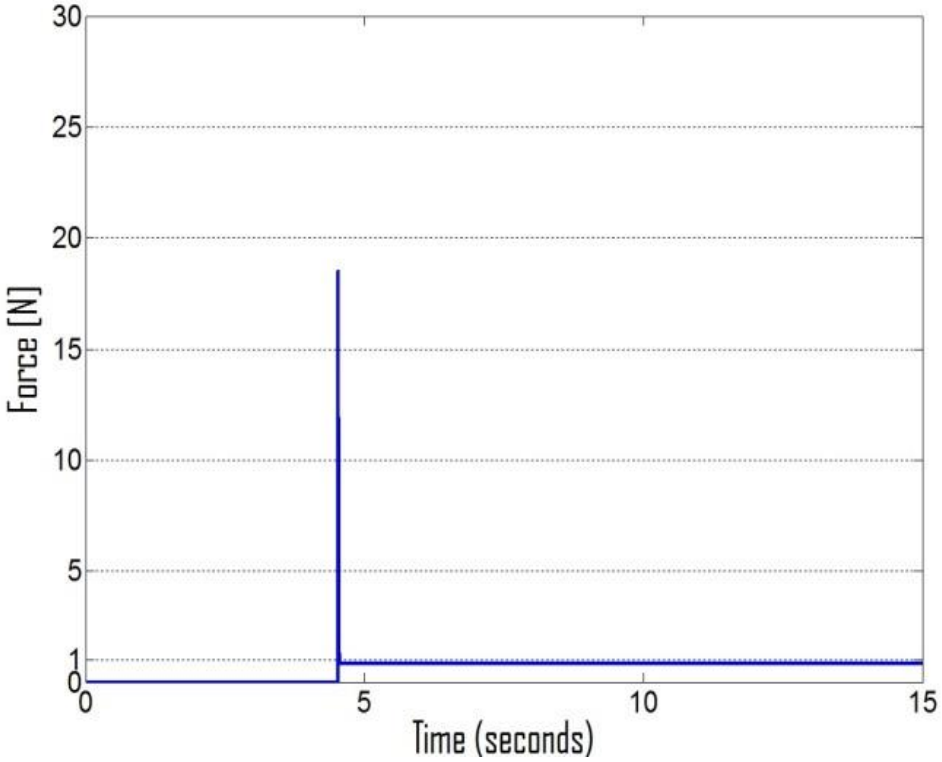

Fig.4.5 The contact force by PIC with real inertial parameter

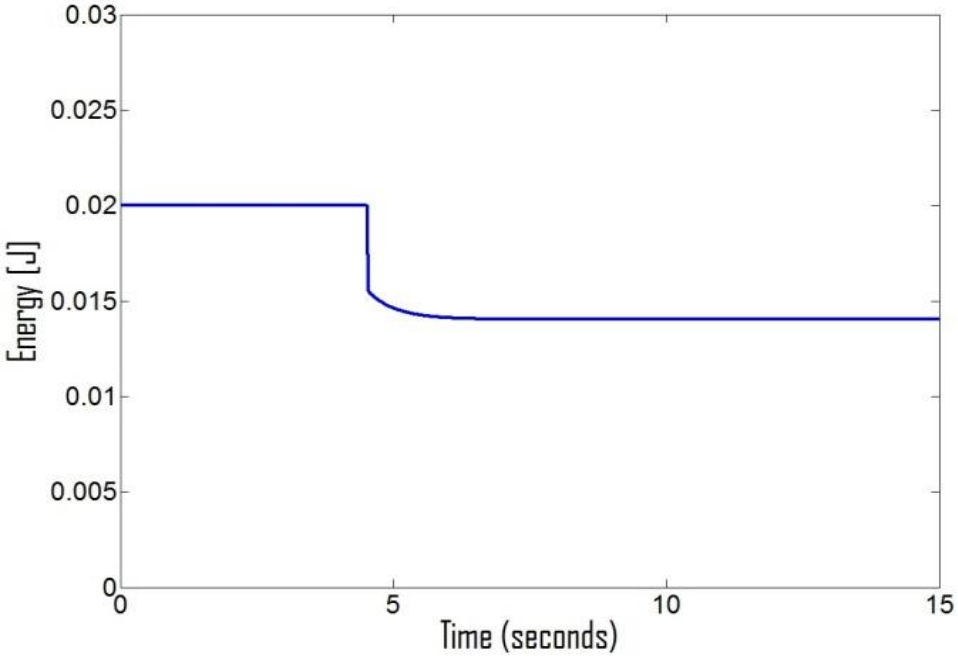

Fig.4.6 The mechanic energy by PIC with real inertial parameter

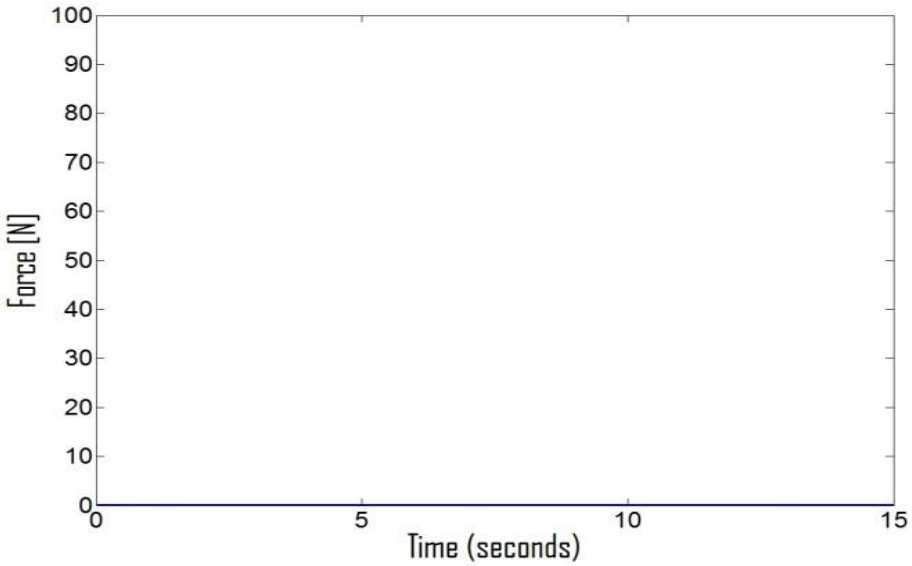

Fig.4.7 f_m by PIC with real inertial parameter

When there are model errors, from Fig. 4.8, the external forces exceed the line of 1N when and after the end-effector punches the wall. From Fig. 4.9, the mechanic energy always over the initial energy of 0.02J. And, from Eq. (4.1.33), the robot lost its passivity when interacting with the environment.

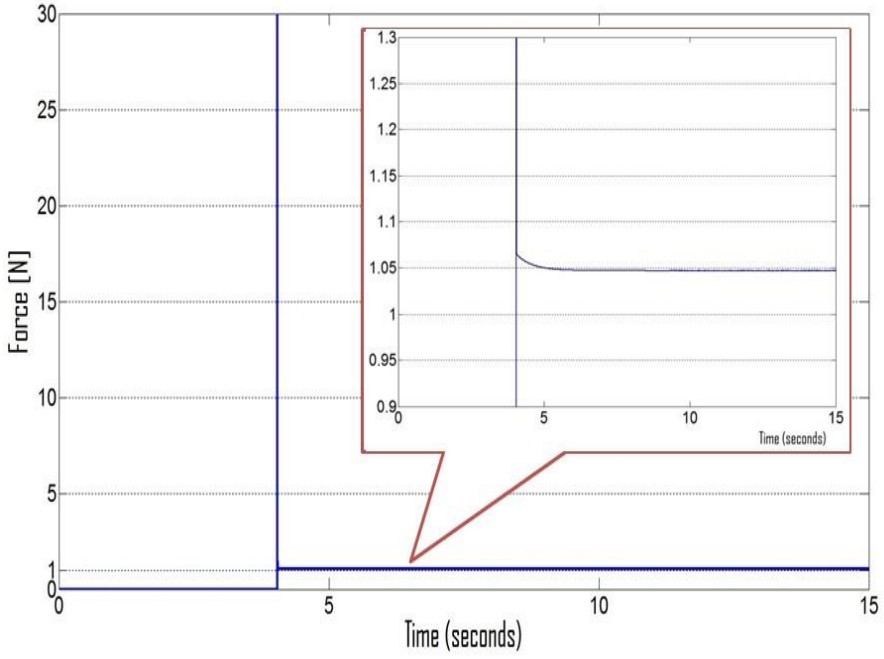

Fig.4.8 The contact force by PIC with Estimate inertial =1.8×real inertial parameter

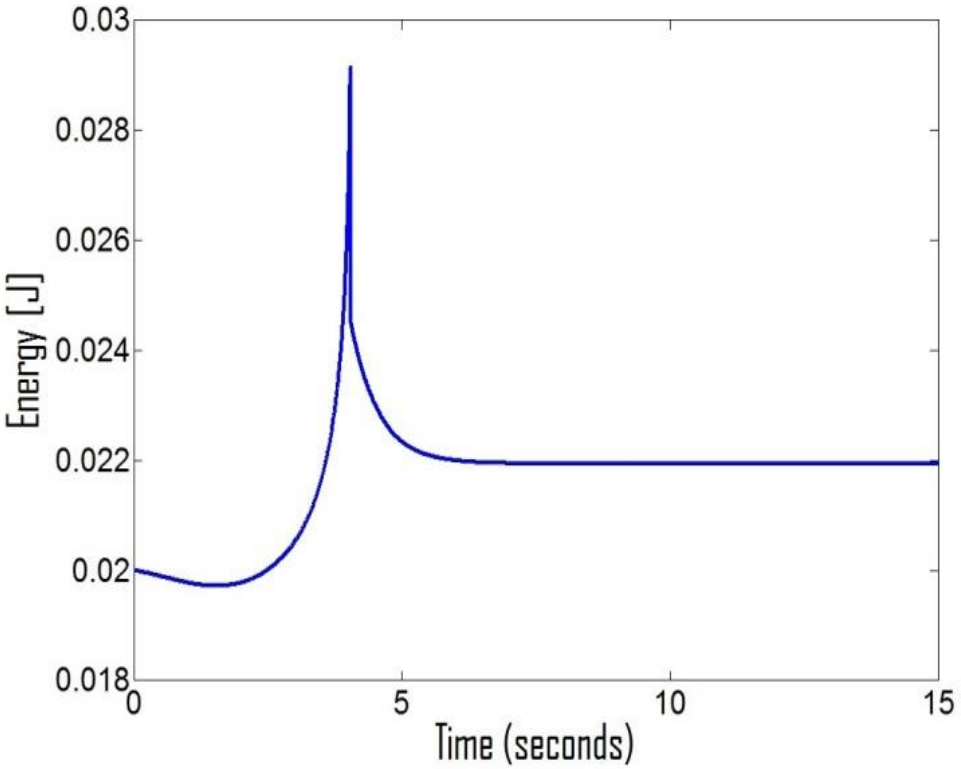

Fig.4.9 The mechanic energy by PIC with Estimate inertial =1.8×real inertial parameter

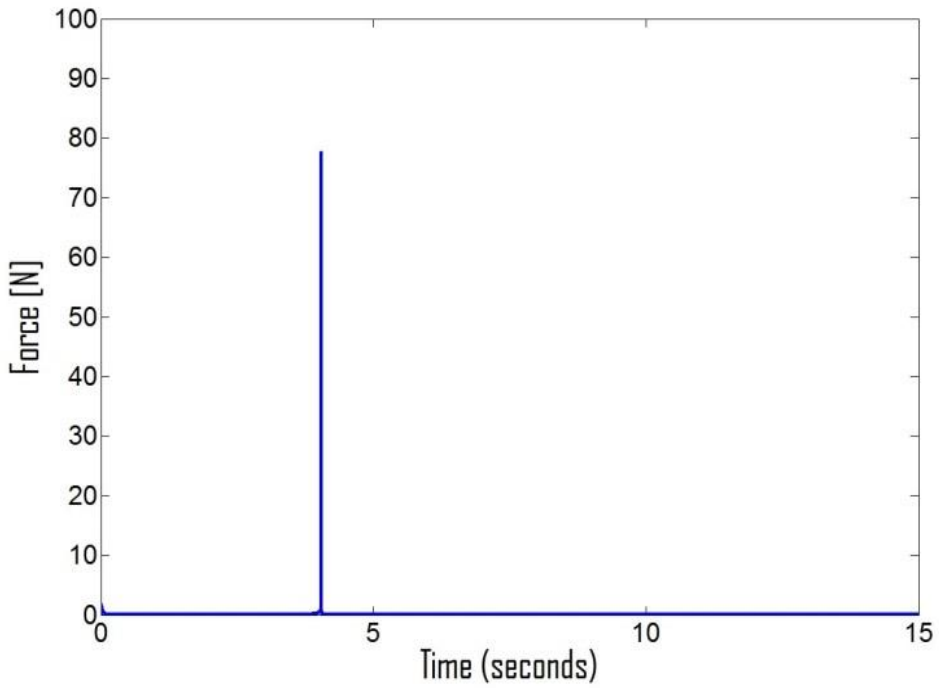

Fig.4.10 f_m by PIC with Estimate inertial =1.8×real inertial parameter

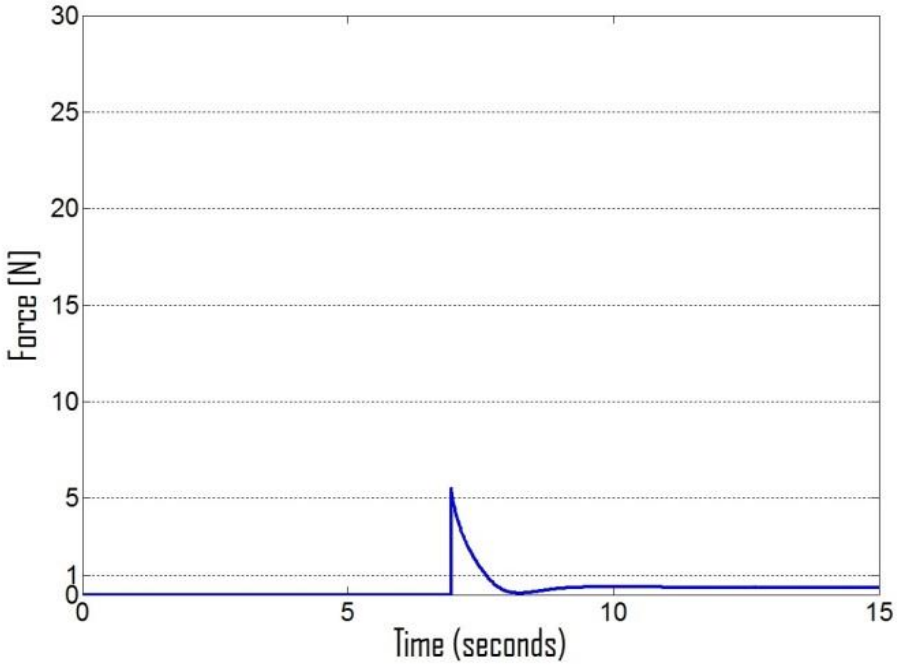

Fig.4.11 The contact force by RPIC with Estimate inertial =1.8×real inertial parameter

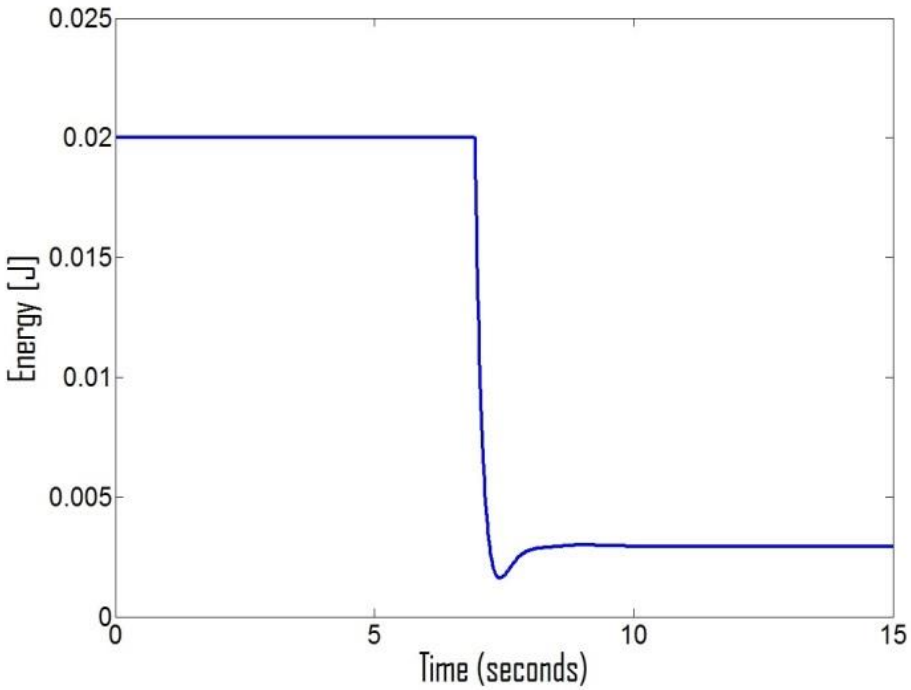

Fig.4.12 The mechanic energy by RPIC with Estimate inertial =1.8×real inertial parameter

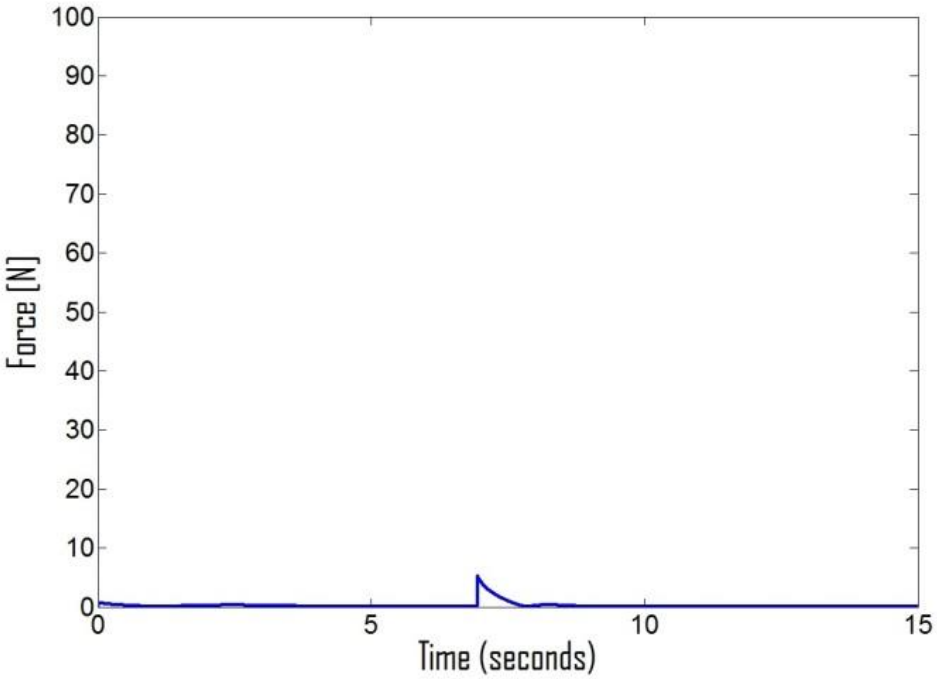

Fig.4.13 f_m by RPIC with Estimate inertial =1.8×real inertial parameter

Figs. 4.11 to 4.13 show the result using our robust passive impedance control. It is clear that, even if there are model errors, the contact forces converges to the value below 1N after the robot punched the stiff wall and the mechanic energy of the robot has been limited below the initial value of 0.02J.

By comparing this result with Figs. 4.8 to 4.10, it shows that the robot keeps passivity.

On the other hand, by comparing f_m under PIC with model errors and RPIC (Figs.4.10 and 4.13), it is clear that RPIC method actually reduced the error force term f_m when end-effector of robot punch the stiff wall.

4.5.2 Simulations of PRIC

In order to show the effectiveness of this PRIC method, we mainly performed simulation for four different conditions as follows, respectively:

(1) There are no model errors, and the robot is controlled by passive impedance control method.

(2) There are model errors, and the robot is controlled by the same passive

impedance control method as in (1). The estimated mass and center of the link's gravity, which are used in the calculation of the estimated inertial matrix, is set as

$$\widehat{m_i} = 0.5 \times m_i \ , \qquad \widehat{lg_i} = 0.5 \times lg_i$$

where m represent the mass of the link and lg represents the position of the center of the gravity of the link.

(3) There are model errors, and the control method is the RPIC method proposed in the previous section.

(4) There are model errors, and the control method is our observer-based passive impedance control.

In addition, we also set the parameter in the matrix K_d, D_d and M_d of the impedance equation as

$$M_d = \begin{bmatrix} 1 & 0 \\ 0 & 1 \end{bmatrix}, D_d = \begin{bmatrix} 2 & 0 \\ 0 & 2 \end{bmatrix}, K_d = \begin{bmatrix} 1 & 0 \\ 0 & 1 \end{bmatrix}$$

and the parameter in the matrix K_e and K_e of the stiff wall as $k_e = 15, d_e = 1$. The initial value of S and the mechanic energy E has been defined as $S_0 = 0.5\text{J}, \ E_0 = 0\text{J}$.

The parameter in observer is set as $T = 0.0001, \ b = 0.02$.

- ***Simulation Results***

a) Effects of the impedance control method in different cases

The blue line denotes the results of the case (1). The orange line and the red dot line represent the results of the cases (2) and (3), and the black dot lines are the results of the case (4).

The trajectory tracking results of four cases are shown in Fig. 4.14. The grey line shown in this figure represents the stiff wall whose spring and damping ratio are set as $k_e = 15$ and $d_e = 3$ respectively.

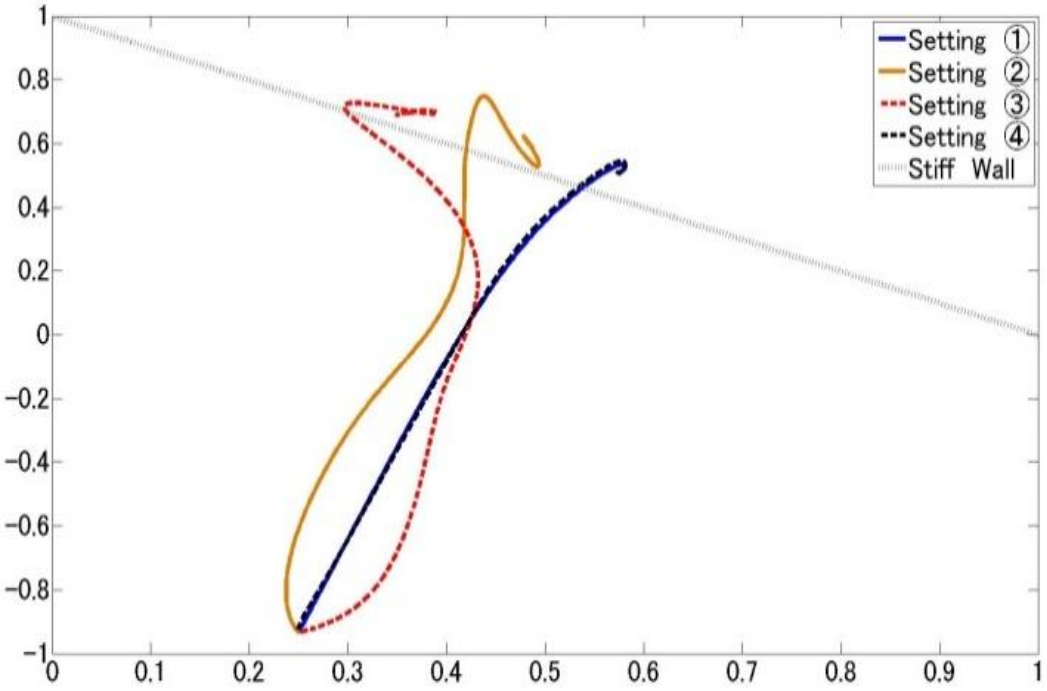

Fig.4.14 Trajectory of the robot in four different cases

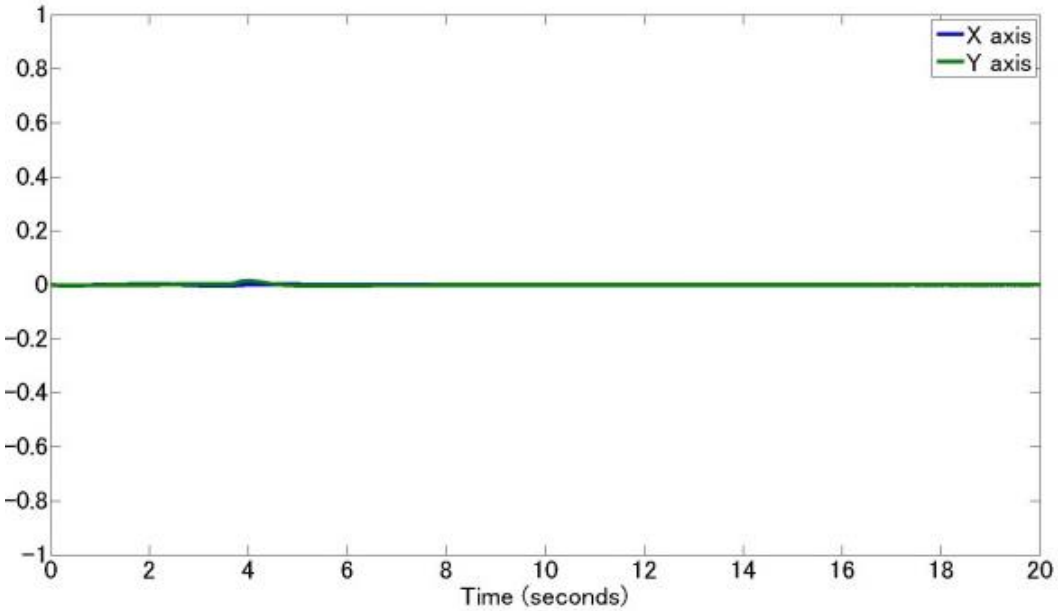

(a) Time responses of position errors x_e in the case (4)

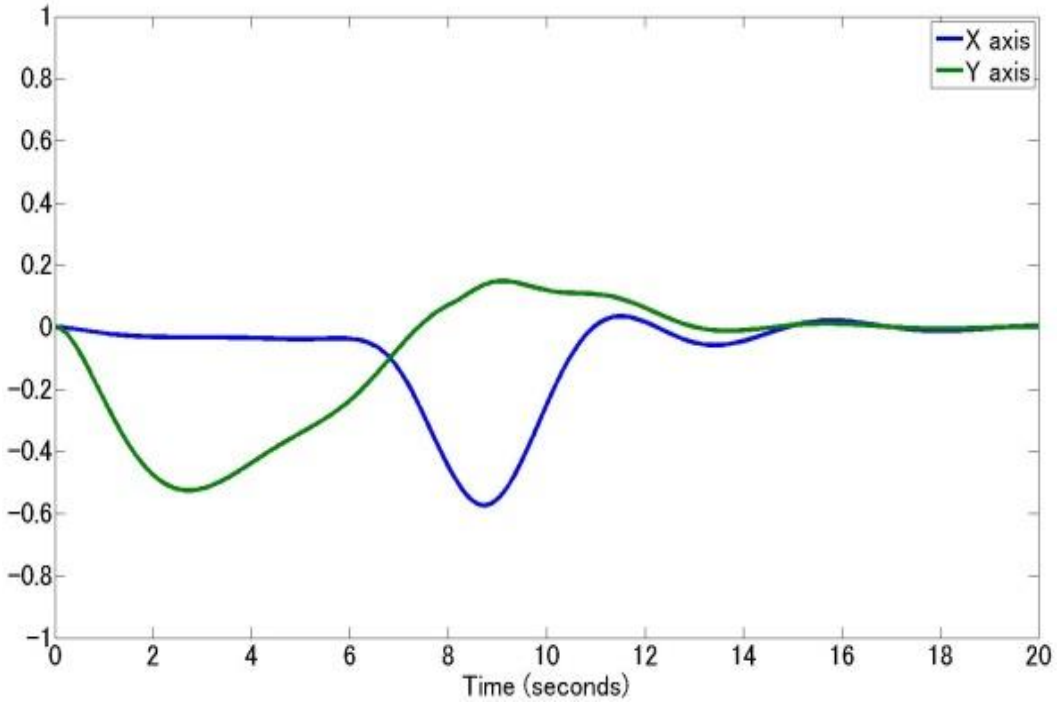

(b) Time responses of position errors x_e in the case (3)

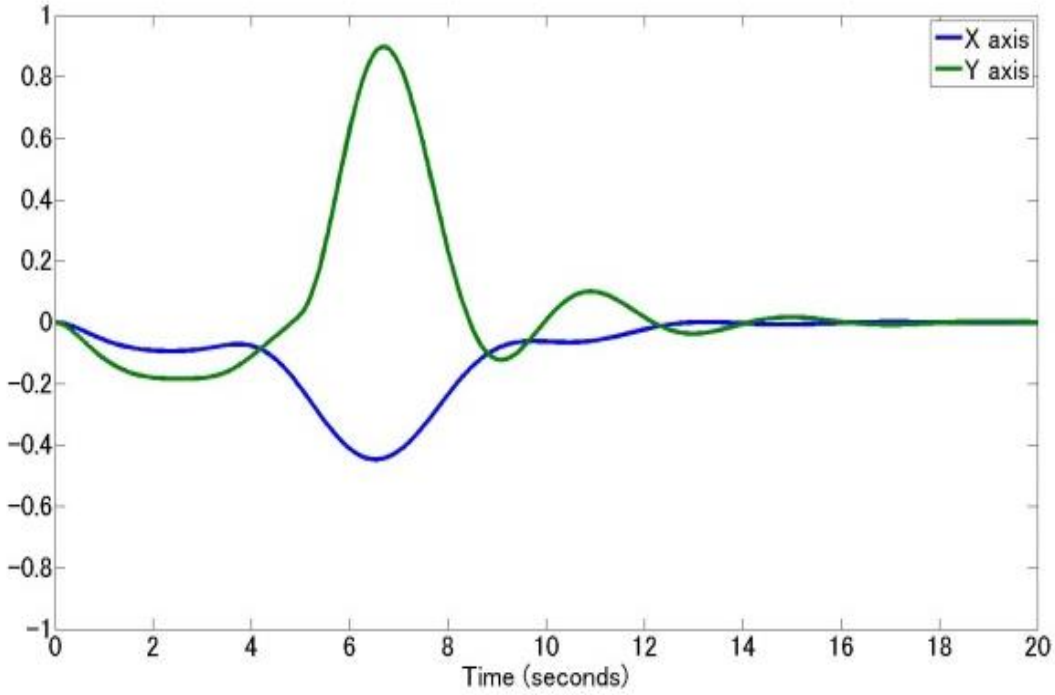

(c) Time responses of position errors x_e in the case (2)

Fig.4.15 Time responses of position errors x_e in different cases

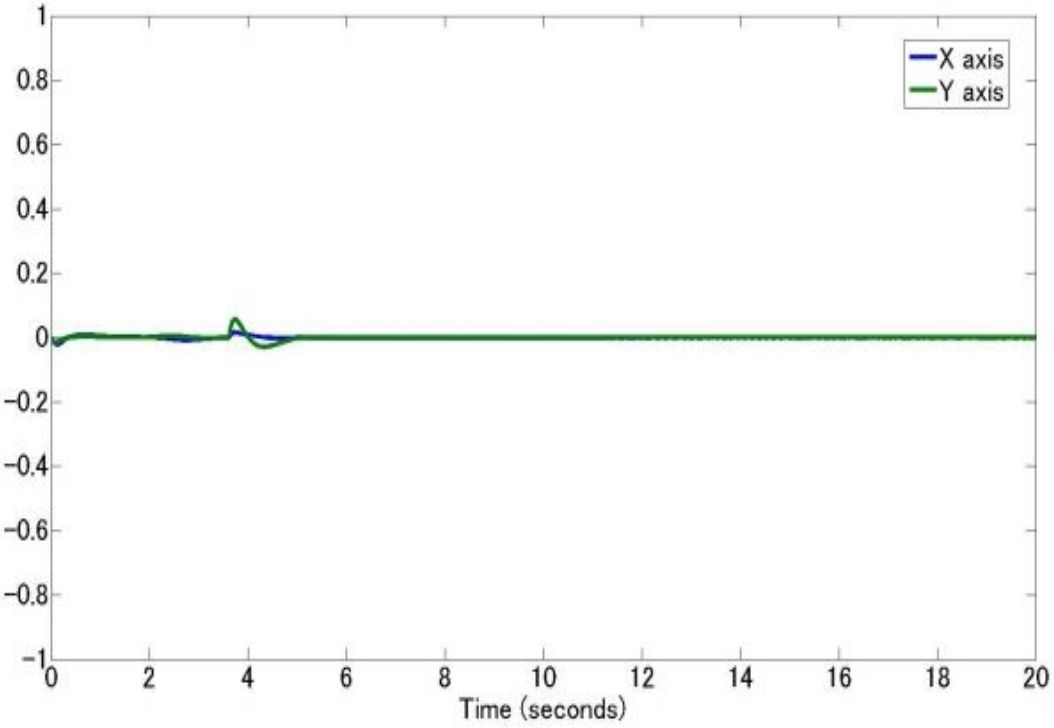

(a) Time responses of velocity errors $\dot{x}_e$ in the case (4)

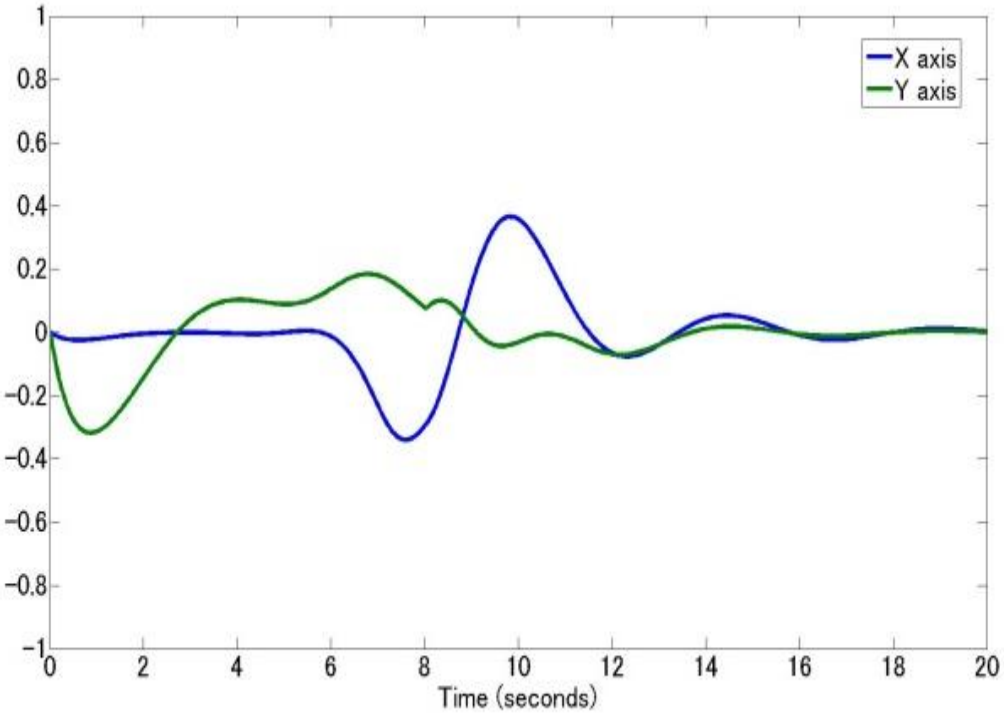

(b) Time responses of velocity errors $\dot{x}_e$ in the case (3)

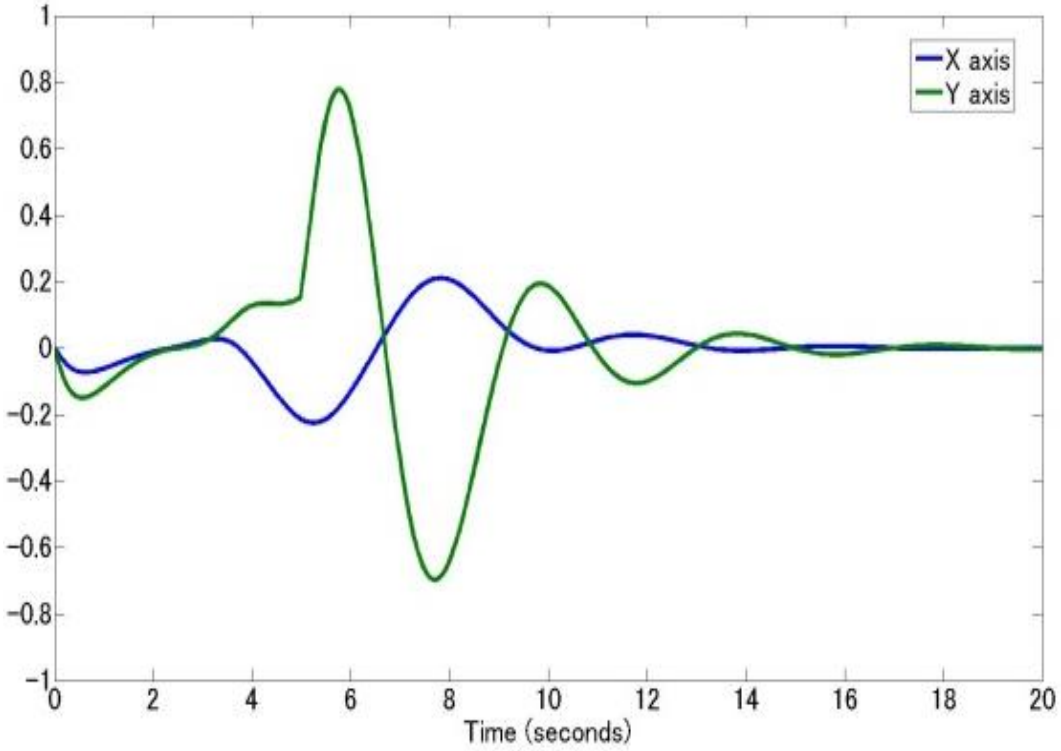

(c) Time responses of velocity errors $\dot{x}_e$ in the case (2)

Fig.4.16 Time responses of velocity errors $\dot{x}_e$ in different cases

As seen from the trajectory of the orange line in Fig. 4.14, we can find that the robot's model errors seriously influence the tracking ability of the robot. The trajectory of the red line shows that previous RPIC method do not contribute to the performance of trajectory tracking. From the trajectory tracking results of the black dot line and the blue line in Fig. 4.14, it is clear that, by utilizing our method, the effects of the model error on the trajectory tracking can be eliminated.

Figs. 4.15 and 4.16 shows the errors between the real value of the robot's position and velocity in task space and the ideal value when there exists no model error in control system. From these results, it is obvious that the observer-based method can effectively decrease the tracking errors caused by the model errors, which are even better than the results of our previous RPIC method in case (3).

Fig. 4.17 shows the response of external forces in four different cases. It is clear that model errors may have some effects on the response time and the vibration of the force. Also, it is shown that the observer-based controller can lead the external force approach the ideal value.

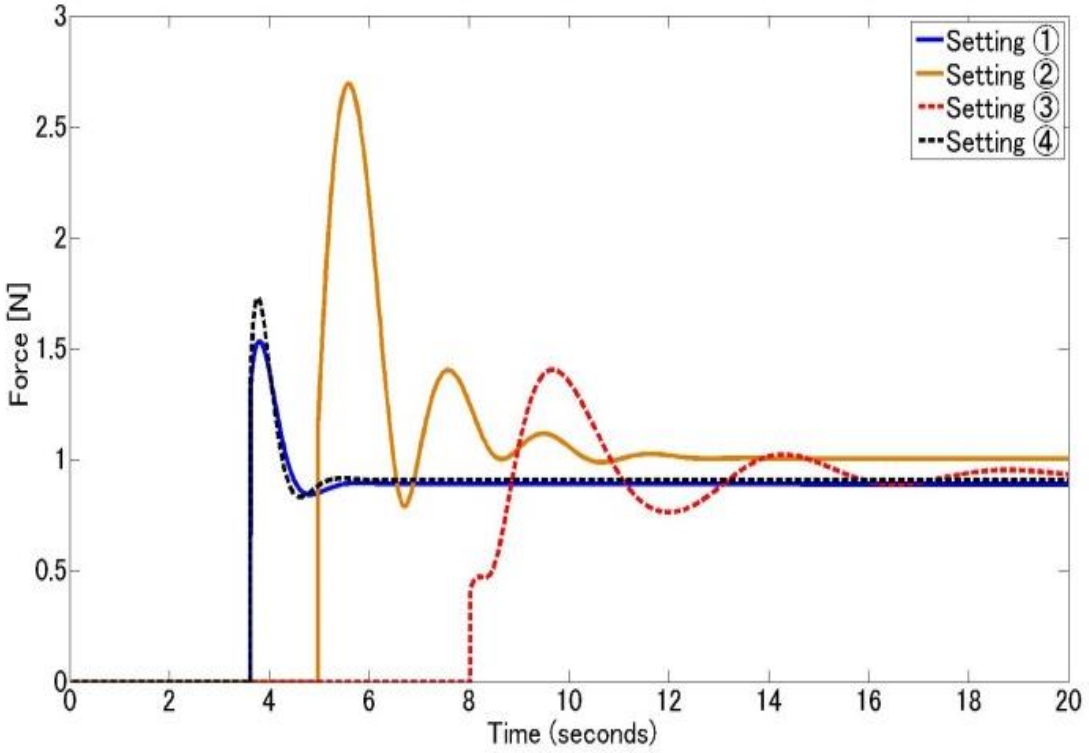

Fig.4.17 The external force responses of the robot in four different cases

From Figs. 4.14 to 4.17, it is found that the previous method (3) could not decrease the effect from the model errors on impedance control law and observer-based method could eliminate this effect and help the robot to realize the ideal impedance.

b) Passivity Analysis

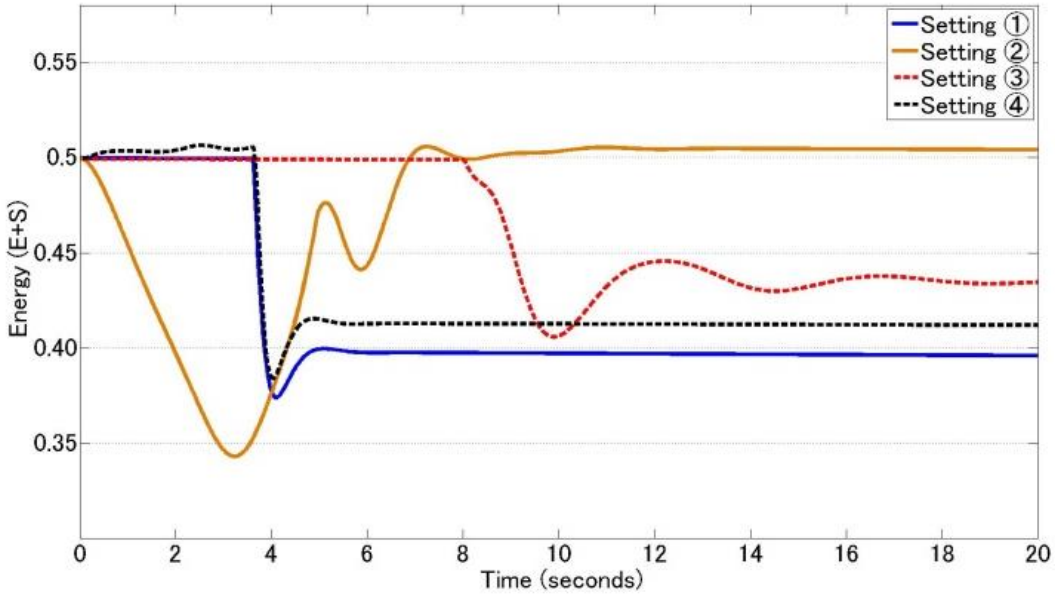

Fig.4.18 The Energy (E+S) in four different cases

Fig. 4.18 shows the energy results of E+S in different cases. The orange line shows that model errors could affect the energy's variation so as to make the energy (E+S) exceed the its initial value 0.5J, which means that the robot is not passive. By using the previous RPIC method with a special estimation adjustment, from red dot line, we see that the passivity can be satisfied. The black dot line shows that the robot is passive by using our proposed observer-based method. By comparing the black dot line and the orange line, we see that our proposed controller could effectively decrease the influence of model errors on the energy E+S, therefore, the robot can keep its passivity under the model errors.

Chapter 5 Passive Velocity Field Control of a Redundant Cable-Driven Robot with Tension Limitations

Considering the possibility of the robotic rehabilitation, this chapter pay attention to the fitness between the robot and human, a passivity based control design is performed for a robot with cable-driven structure to realize better fitness with the complex human body joint structure. Taking into account of the limitations that the cable driven robot has high redundant actuation and cable tension limitations, the passive velocity field control (PVFC) method is extended for the redundant cable-driven robot system to realize not only passivity but also tracking performance.

In this Chapter, we first describe the dynamics and the constrain conditions of the cable driven robot and then utilize the previous proposed PVFC control approaches to overcome the redundancy problem of the cable-driven robot and satisfy the robot's passivity while complete the trajectory tracking. The cable's tension limitation problem can be solved by adapting and adjusting a parameter in the control input basing on some analysis. Simulation results shown in section 4 verify the effectiveness of our method.

5.1 Dynamics of a Cable-driven Robot

The dynamics of a robot manipulator interacting with its environment can be denoted as

$$\boldsymbol{M}(\boldsymbol{q})\ddot{\boldsymbol{q}} + \boldsymbol{C}(\boldsymbol{q}, \dot{\boldsymbol{q}})\dot{\boldsymbol{q}} = \boldsymbol{\tau} + \boldsymbol{J}^{\boldsymbol{T}}\boldsymbol{f} \tag{5.1.1}$$

where $\boldsymbol{M}(\boldsymbol{q}) \in \mathfrak{R}^{\mathbf{m}\times\mathbf{m}}$is the inertial matrix of rigid link, $\boldsymbol{C}(\boldsymbol{q}, \dot{\boldsymbol{q}})\dot{\boldsymbol{q}} \in \mathfrak{R}^{,\mathbf{m}\times\mathbf{m}}$is the Coriolis and centrifugal force vector. $\boldsymbol{\tau} \in \mathfrak{R}^{\mathbf{m}}$ is the applied joint wrench exerted by the cables.$\boldsymbol{J}(\boldsymbol{q}) \in \mathfrak{R}^{\mathbf{m}\times\mathbf{m}}$ is a Jacob matrix and f is the interaction force vector between the robot and the environment such as human body.

In order to control the cable-driven robot, it is necessary to specify the mathematic

relationship between the cable tension and wrench acting at the end-effector/joints of the robot, which can be represented as

$$\boldsymbol{AT} = \boldsymbol{\tau} \tag{5.1.2}$$

where $\mathrm{T} \in \Re^{\mathrm{n}}$ is the cable tension vector of n-dimension satisfying the inequality

$$\boldsymbol{T_{min}} \leq \boldsymbol{T} \leq \boldsymbol{T_{max}} \tag{5.1.3}$$

$\boldsymbol{T_{max}} = (T_{max1}, \cdots, T_{maxn})^T \in \Re^{\mathrm{n}}$ is the maximum toleration of the cable and is related to the material of the cable, $\boldsymbol{T_{min}} = (T_{min1}, \cdots, T_{minn})^T \in \Re^{\mathrm{n}}$ denotes the minimum limitation of the tension which is nonnegative, regularly. τ represents the wrench vector (torque/force). $\boldsymbol{A} \in \Re^{\mathrm{m}\times\mathrm{n}}$ represents the structure matrix which can be calculated as $\boldsymbol{A} = \begin{pmatrix} -l_1 & \cdots & -l_n \\ -w_1 \times l_1 & \cdots & -w_n \times l_n \end{pmatrix}$,
where l_n denote the tendon vector and w_n represent the center of the platform which is formed by several connection point between the cable and the rigid link (human arm) to each connection point.

Basically, for the given wrench vector $\boldsymbol{\tau} \in \Re^{\mathrm{m}}$, the inverse relation to compute the tension $\mathrm{T} \in \Re^{\mathrm{n}}$ with $\mathrm{m} < \mathrm{n}$ can be calculated as

$$\boldsymbol{T} = \boldsymbol{A}^{+}\boldsymbol{\tau} + (\boldsymbol{I} - \boldsymbol{A}^{+}\boldsymbol{A})\boldsymbol{p} \tag{5.1.4}$$

Here $\boldsymbol{A}^{+}$ denotes the pseudo-inverse of $\boldsymbol{A}$, and $(\boldsymbol{I} - \boldsymbol{A}^{+}\boldsymbol{A}) = \boldsymbol{N}(\boldsymbol{A})$ is the orthogonal complement of $\boldsymbol{A}$, and $\boldsymbol{p}$ can be selected as any vector, $\boldsymbol{I}$ is a unit matrix.

Due to the input constraint of the tension of Eq. (5.1.3), from Eq. (5.1.2), wrench will also have a limitation. The relation between tension constraint and wrench constraint is shown in Fig. 5.1 with the simple setting that tension space has 2-dimensions and wrench has 1-dimension.

Note that, the angular φ between two spaces is totally dependent on the matrix $\boldsymbol{A}$.

As shown in Fig.5.1 that for a given wrench $\boldsymbol{\tau_\gamma}$, there exit plenty of tension choices to execute due to the multi selection of $\boldsymbol{p}$ in Eq.(5.1.4). Hence, a lot of works has been contributed to the optimization of tension distribution to ensure all tension has been located into the constraint box constructed by tension's limitation. Meanwhile, for a given tension constraint and a given pose (structure matrix $\boldsymbol{A}$), wrench $\boldsymbol{\tau}$ can be denoted as the feasible wrench satisfies the range $\boldsymbol{\tau} \in [\boldsymbol{\tau_{min}}, \boldsymbol{\tau_{max}}]$. However, this range of the wrench may limit the objective task of the robot. For example, if there are a large error between the robot's initial position and its objective target, when using usual PD control, we may not possible to generate a necessary large wrench τ outside the constraint range $\boldsymbol{\tau} \in [\boldsymbol{\tau_{min}}, \boldsymbol{\tau_{max}}]$.

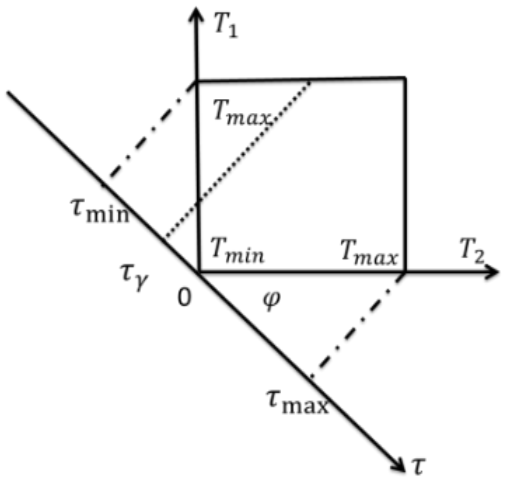

Fig. 5.1 Relationship between the Tension Space and Torque Space

5.2 Previous Works

First of all, considering the redundant actuation problem that $\boldsymbol{m < n}$, in some previous researches [38], LP as well as QP programming has been used to solve the limitation problem of the tension. This idea can be formulated as following:

$$min\, \boldsymbol{f(p)}$$

$$s.t. \qquad \boldsymbol{T_{min} \le A^{+}\tau + (I - A^{+}A)p \le T_{max}} \tag{5.2.1}$$

If the objective function is selected as $\boldsymbol{f(p) = c^T p}$ ($\boldsymbol{c}$ is a constant vector), it is a LP problem. If $\boldsymbol{f(p) = p^T Y p}$ ($\boldsymbol{Y}$ is a positive definite matrix), it is a QP problem.

However, no matter what the objective function is chosen as and how the vector $\boldsymbol{p}$ varies, there may exit some infeasible $\boldsymbol{\tau}$ that makes unsatisfactory of the tension's condition. Moreover, since we need iterative computation to solve LP or QP objective functions subjected to some conditions with inequalities, it may be difficult to perform within real time control of the robot.

Secondly, considering the tension limitation problem, in order to keep the cables to satisfy the tension constraint while the robot is executing some tasks, it is necessary to consider the term composing control input $\boldsymbol{\tau}$(wrench). For tracking task, we cannot set the desired position too far to make the designed wrench too large for robot to handle it. Hence, tracking the desired position outside the tolerance scope is necessary to be considered.

Oh and Agrawal [9] proposed a method to solve this problem for a 6 DOF cable-driven parallel robot with 6 cables. The robot's dynamics in the task space can be determined as

$$\boldsymbol{M}(\boldsymbol{X})\ddot{\boldsymbol{X}} + \boldsymbol{C}\left(\boldsymbol{X}, \dot{\boldsymbol{X}}\right)\dot{\boldsymbol{X}} + \boldsymbol{g}(\boldsymbol{X}) = \boldsymbol{AT} \tag{5.2.2}$$

where $\boldsymbol{X} = (\boldsymbol{x}, \boldsymbol{y}, \boldsymbol{z}, \boldsymbol{\psi}, \boldsymbol{\theta}, \boldsymbol{\phi})$ describes the position and orientation of the end-effector, $\boldsymbol{g}(\boldsymbol{X})$ represent the gravity vector. Note that, since we have $m = n = 6$ here, the matrix $\mathbf{A}$ is invertible.

They first set the control input tension vector $\boldsymbol{T}$ as

$$\boldsymbol{T} = \boldsymbol{A}^{-1}(\boldsymbol{C}\left(\boldsymbol{X}, \dot{\boldsymbol{X}}\right)\dot{\boldsymbol{X}} + \boldsymbol{g}(\boldsymbol{X}) - \boldsymbol{M}(\boldsymbol{X})\boldsymbol{\lambda}\dot{\boldsymbol{X}} - \boldsymbol{M}(\boldsymbol{X})\boldsymbol{\eta}\boldsymbol{s}) \tag{5.2.3}$$

where $\boldsymbol{\lambda} = \lambda_0\boldsymbol{I}$, $\boldsymbol{\eta} = \eta_0\boldsymbol{I}$, $\boldsymbol{s}$ is the control surface defined by

$$\boldsymbol{s} = \dot{\boldsymbol{X}} + \boldsymbol{\lambda}(\boldsymbol{X} - \boldsymbol{X_d}) \tag{5.2.4}$$

By imposed a relation that $\dot{\boldsymbol{s}} = -\boldsymbol{\eta}\boldsymbol{s}$, the equilibrium at the $\boldsymbol{X_d}$ will be exponentially stable and we have

$$\ddot{\boldsymbol{X}} = -\boldsymbol{\lambda}\dot{\boldsymbol{X}} - \boldsymbol{\eta}\boldsymbol{s} \tag{5.2.5}$$

Let the $\boldsymbol{X_d}$ as the input, considering the first term of the robot's position vector $\boldsymbol{X}$, the transfer function can be written as

$$x(r) = \frac{\eta_0\lambda_0}{r^2+(\lambda_0+\eta_0)r+\eta_0\lambda_0} x_d(r) \tag{5.2.6}$$

After some analysis of the transfer function, it is possible to obtain the damping ratio $\zeta \geq 1$ and the natural frequency $\omega_n = \sqrt{\eta_0\lambda_0}$.

Then, based on the analysis of time domain solution of the transfer function, we can get the bounds on states:

$$x(t) \in [x_0, x_d]$$

$$\ddot{x}(t) \in (x_0 - x_d){\omega_n}^2[Z_m, -1]$$

where x_0 is the initial value of the position and Z_m represent the maximum of the term

$$\frac{1}{2\sqrt{\zeta^2-1}}\left[-\left(\zeta+\sqrt{\zeta^2-1}\right)e^{-\left(\zeta+\sqrt{\zeta^2-1}\right)\omega_n t} + (\zeta+\sqrt{\zeta^2-1})e^{\left(-\zeta+\sqrt{\zeta^2-1}\right)\omega_n t}\right] \tag{5.2.7}$$

Thus, we can compute the bounds on other components of vector x and $\ddot{x}$.

Then, this research considered the translation motion of the robot and simplified the tension constraint as

$$\boldsymbol{T = A^{-1}\left(M(x)\ddot{x} + g(x)\right) \geq 0} \tag{5.2.8}$$

This inequality is determined by $\mathbf{x}$ $\ddot{\mathbf{x}}$ and some coefficient. In order to make this inequality satisfied, it is necessary to calculate the minimum value of $\boldsymbol{T}$ by substituting the bounds of $\boldsymbol{x}$ $\ddot{\boldsymbol{x}}$ into this inequality. Note that when the coefficient in front of the variable is minus, we need to substitute the maximum value of this valuable and when the coefficient is positive, we should substitute the minimum value. After substituting, we can get

$$\boldsymbol{D_1}\begin{bmatrix} x_d \\ y_d \end{bmatrix} \leq \boldsymbol{D_2}\begin{bmatrix} x_0 \\ y_0 \end{bmatrix} + \boldsymbol{b} \tag{5.2.9}$$

Note that, this research simplified the problem as robot only move in the x-y plane. Matrix $\boldsymbol{D_1}$ $\boldsymbol{D_2}$ and vector $\boldsymbol{b}$ can be calculated by the bounds of each components in $\boldsymbol{X}$ and $\ddot{\boldsymbol{X}}$. Thus, the ineq. (5.2.9) determines a feasible domain of $\boldsymbol{X_d}$ based on the initial position.

In order to tracking the final objective position, it is necessary to select the closest one in the feasible domain of $\boldsymbol{x_d}$ to the final objective position. In the research of [38], they further offered an iteration optimization method to perform the iteration calculation with the movement of the robot and choose the most appropriate desired position in the calculated scope, which is closest to the final desired position.

Although this work shows some efficiency on the position control task, it is impossible to be used for the trajectory tracking control problem of cable-driven robot, especially with high dimensional redundant tension due to the massive computation time and its complicate analysis.

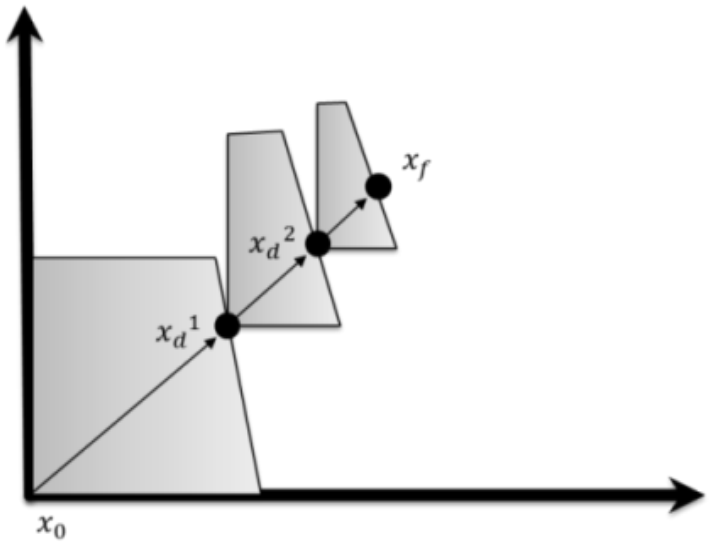

Fig.2 Reachable domains in a x-y plane

As mentioned in the previous analysis, the cable's tension constraint condition as well as its actuation redundancy are two fundamental problems that we should considered in the control design of the cable-driven robot. If we do not design the proper control, these two problems may constrain the possible selection of the robot's objective target position for some given initial positions so as to serious limit the

robot's task performance. By now, the researches mainly considered only one side of the problems, static solution of the redundancy or dynamic control under tension limitations. In order to make real application of a cable driven robot to perform wider range of tasks, we need to solve the two problems simultaneously for the dynamics of the robot.

5.3 Dynamic Control of Cable-Driven Robot Using PVFC

In order to solve the redundancy problem as well as the tension limitation problem so as the robot can realize more dynamic task performance under cable-driven actuation, in this paper, we propose a novel dynamic control approach. Here, we specify the robot's objective motions in a form of the velocity vector field in the work space instead of the usual time function. We then set an augmented virtual dynamic subsystem with dimension n-m. For the n- dimensional augmented dynamic system, we apply Li's passive velocity field control (PVFC)[10] to design the control input. PVFC can realize not only the motion tracking performance for the real robot's velocity to approach the objective velocity field vector in free motion space but also the passivity when the robot is interacting with the environment. Finally, to keep the real robot's cable tension limitation, we adjust the PVFC's control parameter and clarify the control parameter's possible range.

5.3.1. Augmented Mechanical System

In order to overcome the difficulty brought by the redundancy characteristic of the robot's cable actuation of Eqs. (5.1.1) and (5.1.2) with m<n, we propose to augment the system with a n-m dimensional virtual dynamic subsystem.

$$\boldsymbol{M_F}\ddot{\boldsymbol{q}}_{\boldsymbol{n-m}} = \boldsymbol{\tau_{n-m}} = \boldsymbol{BT} \tag{5.3.1}$$

where we set $\boldsymbol{M_F} = diag(m_f, \cdots, m_f) \in \Re^{(\mathrm{n-m})\times(\mathrm{n-m})}$ and $\boldsymbol{B}$ represents a $(\mathrm{n}-\mathrm{m})\times\mathrm{n}$ matrix, $\boldsymbol{q_{n-m}} \in \Re^{(\mathrm{n-m})}$ is the position vector of the virtual augmented subsystem.

Therefore, the dynamic of the overall augmented system can be formulated as

$$\bar{\boldsymbol{M}}(\bar{\boldsymbol{q}})\ddot{\bar{\boldsymbol{q}}} + \bar{\boldsymbol{C}}(\bar{\boldsymbol{q}}, \dot{\bar{\boldsymbol{q}}})\dot{\bar{\boldsymbol{q}}} = \bar{\boldsymbol{\tau}} + \bar{\boldsymbol{\tau}_e} \tag{5.3.2}$$

where $\bar{\boldsymbol{M}}(\bar{\boldsymbol{q}}) = \begin{bmatrix} \boldsymbol{M}(\boldsymbol{q}) & \boldsymbol{0} \\ \boldsymbol{0} & \boldsymbol{M_F} \end{bmatrix}$, $\bar{\boldsymbol{C}}(\bar{\boldsymbol{q}}, \dot{\bar{\boldsymbol{q}}}) = \begin{bmatrix} \boldsymbol{C}(\boldsymbol{q}, \dot{\boldsymbol{q}}) & \boldsymbol{0} \\ \boldsymbol{0} & \boldsymbol{0} \end{bmatrix}$, $\bar{\boldsymbol{q}} = \begin{bmatrix} \boldsymbol{q} \\ \boldsymbol{q_{n-m}} \end{bmatrix}$, $\bar{\boldsymbol{\tau}_e} = \begin{bmatrix} \boldsymbol{\tau_e} \\ \boldsymbol{0} \end{bmatrix}$

In detail, $\bar{\boldsymbol{q}} = [q_1, \cdots, q_m, q_{m+1}, \cdots, q_n]^T$, and by combining the Eq. (5.1.2) and (5.3.2), we have

$$\bar{\boldsymbol{\tau}} = \bar{\boldsymbol{A}}\boldsymbol{T} = \binom{\boldsymbol{A}}{\boldsymbol{B}}\boldsymbol{T} \tag{5.3.3}$$

Notice that, in order to avoid appearance of redundancy, we should select the matrix $\boldsymbol{B}$ so that to keep the augmented matrix $\binom{\boldsymbol{A}}{\boldsymbol{B}}$ full rank.

The objective velocity vector $V_{n-m}(q)$ for the augmented subsystem can be specified as follows.

Firstly, we define

$$\bar{\boldsymbol{V}}(\bar{\boldsymbol{q}}) = [\boldsymbol{V}(\boldsymbol{q})^{\boldsymbol{T}}, \boldsymbol{V_{n-m}}(\boldsymbol{q})]^{\boldsymbol{T}} \tag{5.3.4}$$

as the objective velocity vector of the augmented system, then the total objective kinetic energy can be denoted as

$$k\big(\bar{q}, \bar{V}(\bar{q})\big) = \frac{1}{2}\overline{\boldsymbol{V^T}}(\bar{\boldsymbol{q}})\bar{\boldsymbol{M}}(\bar{\boldsymbol{q}})\bar{\boldsymbol{V}}(\bar{\boldsymbol{q}}) = \frac{1}{2}(\boldsymbol{V^T M}(\boldsymbol{q})\boldsymbol{V} + \boldsymbol{V_{n-m}}^{\boldsymbol{T}}\boldsymbol{M_F V_{n-m}}) = \bar{E} > 0 \tag{5.3.5}$$

where $\boldsymbol{V_{n-m}} = \rho[1, \cdots, 1]^T$ and ρ is a scalar. For the given $\boldsymbol{V}(\boldsymbol{q})$ and constant $\bar{E}$, we then can calculated

$$\rho = \sqrt{\frac{2}{m_f}\left(\bar{E} - \frac{1}{2}\boldsymbol{V^T M}(\boldsymbol{q})\boldsymbol{V}\right)} \tag{5.3.6}$$

Then, based on ρ, it is possible to calculate the virtual subsystem's desired velocity $\boldsymbol{V_{n-m}}$ and further the desired velocity of total augmented system $\bar{\boldsymbol{V}}$.

5.3.2 Coupling Control Law

Before considering the cable tension limitation problem, for the control design of the augmented system such that the original cable robot system can realize not only the tracking of the objective velocity vector $\bar{\mathbf{V}}$ in the free motion space (when $\boldsymbol{\tau_e} = \mathbf{0}$) but also be passive when interacting with environment, we simply apply Li's PVFC control rule. From [12], we can set a control input as

$$\bar{\boldsymbol{\tau}}(\bar{\boldsymbol{q}}, \dot{\bar{\boldsymbol{q}}}) = \boldsymbol{G}\dot{\bar{\boldsymbol{q}}} + \boldsymbol{\gamma}\boldsymbol{R}\dot{\bar{\boldsymbol{q}}} = \bar{\boldsymbol{\tau}}_{\boldsymbol{c}}(\bar{\boldsymbol{q}}, \dot{\bar{\boldsymbol{q}}}) + \bar{\boldsymbol{\tau}}_{\boldsymbol{f}}(\bar{\boldsymbol{q}}, \dot{\bar{\boldsymbol{q}}}) \tag{5.3.7}$$

defining G and R as two skew symmetric matrices

$$\boldsymbol{G} = \frac{\mathbf{1}}{\mathbf{2}\bar{\boldsymbol{E}}}(\bar{\boldsymbol{w}}\bar{\boldsymbol{P}}^{\boldsymbol{T}} - \bar{\boldsymbol{P}}\bar{\boldsymbol{w}}^{\boldsymbol{T}}) \tag{5.3.8}$$

$$\boldsymbol{R} = (\bar{\boldsymbol{P}}\bar{\boldsymbol{p}}^{\boldsymbol{T}} - \bar{\boldsymbol{p}}\bar{\boldsymbol{P}}^{\boldsymbol{T}}) \tag{5.3.9}$$

where

$$\bar{\boldsymbol{p}}(\bar{\boldsymbol{q}}, \dot{\bar{\boldsymbol{q}}}) = \bar{\boldsymbol{M}}(\bar{\boldsymbol{q}})\dot{\bar{\boldsymbol{q}}}$$

$$\bar{\boldsymbol{P}}(\bar{\boldsymbol{q}}) = \bar{\boldsymbol{M}}(\bar{\boldsymbol{q}})\bar{\boldsymbol{V}}(\bar{\boldsymbol{q}})$$

$$\bar{\boldsymbol{w}}(\bar{\boldsymbol{q}}, \dot{\bar{\boldsymbol{q}}}) = \bar{\boldsymbol{M}}(\bar{\boldsymbol{q}})\dot{\bar{\boldsymbol{V}}}(\bar{\boldsymbol{q}}) + \bar{\boldsymbol{C}}(\bar{\boldsymbol{q}}, \dot{\bar{\boldsymbol{q}}})\bar{\boldsymbol{V}}(\bar{\boldsymbol{q}})$$

This control input leads to two results:

1) The trajectory tracking error of the total augmented robot system ($\overline{\boldsymbol{e_a}} = \dot{\bar{\boldsymbol{q}}} - \boldsymbol{\beta}\bar{\boldsymbol{V}}$) can be globally exponentially stable which also make the original system exponentially convergent to the desired trajectory.
2) System can be passive when there are external forces acting at the system.

The proof of these two results can refer to [12].

5.3.3 Satisfaction of the Tension Condition

① Analysis of the Tension's Condition

The important thing left here is to adjust $\bar{\boldsymbol{\tau}}$ of Eq.(5.3.7) to satisfy the tension condition $(\boldsymbol{T_{min} \le T \le T_{max}})$ which can be also represented as

$$(\boldsymbol{T - T_0})^{\boldsymbol{T}}\boldsymbol{E}(\boldsymbol{T - T_0}) \le \mathbf{1} \tag{5.3.10}$$

where $\boldsymbol{T_0} = \frac{\boldsymbol{T_{max}+T_{min}}}{\mathbf{2}}$, $\boldsymbol{E} = \boldsymbol{diag}(\frac{\mathbf{1}}{\boldsymbol{r^2}}, \cdots, \frac{\mathbf{1}}{\boldsymbol{r^2}})$, *and* $\boldsymbol{r} = \frac{\boldsymbol{max(T_{maxi})-min(T_{minj})}}{\mathbf{2}}$.

From Eq. (5.3.3), since we select the B so that $\bar{\boldsymbol{A}} = \binom{\boldsymbol{A}}{\boldsymbol{B}}$ is full rank, we have

$$\boldsymbol{T} = \bar{\boldsymbol{A}}^{-\mathbf{1}}\bar{\boldsymbol{\tau}} \tag{5.3.11}$$

For $\boldsymbol{T_0}$, there exists an corresponding $\bar{\boldsymbol{\tau}}_{\mathbf{0}}$ that

$$\bar{\boldsymbol{\tau}}_{\mathbf{0}} = \bar{\boldsymbol{A}}\boldsymbol{T_0} \tag{5.3.12}$$

Then, the cycle constraint Eq. (5.3.10) can be represented as

$$\left(\bar{\boldsymbol{A}}^{-\mathbf{1}}\left(\boldsymbol{G}\dot{\boldsymbol{q}} + \gamma\boldsymbol{R}\dot{\boldsymbol{q}}\right) - \boldsymbol{T_0}\right)^{\boldsymbol{T}}\left(\bar{\boldsymbol{A}}^{-\mathbf{1}}\left(\boldsymbol{G}\dot{\boldsymbol{q}} + \gamma\boldsymbol{R}\dot{\boldsymbol{q}}\right) - \boldsymbol{T_0}\right) - r^{\mathbf{2}} \le \mathbf{0} \tag{5.3.13}$$

by considering Eq.(5.3.8).

From ineq. (5.3.13), it is clear that we can change the value of γ to make the tension condition be satisfied. Based on this design, we can regard the left side of ineq. (5.3.13) as a function with variable γ

$$f(\gamma) = \gamma^2\boldsymbol{a}^{\boldsymbol{T}}\boldsymbol{a} - 2\gamma\boldsymbol{a}^{\boldsymbol{T}}\boldsymbol{b} + \boldsymbol{b}^{\boldsymbol{T}}\boldsymbol{b} - r^2 = 0 \tag{5.3.14}$$

where $\boldsymbol{a} = \bar{\boldsymbol{A}}^{-\mathbf{1}}\boldsymbol{R}\dot{\boldsymbol{q}}$ and $\boldsymbol{b} = \boldsymbol{T_0} - \bar{\boldsymbol{A}}^{-\mathbf{1}}\boldsymbol{G}\dot{\boldsymbol{q}}$

If there is no real solution of this function, the adjustable range of γ should not be existed. Therefore, besides the appropriate adjustment of γ, we also need to select an appropriate $\bar{A}$.

② Method to Satisfy Tension Condition

In order to satisfy the constraint (5.3.10), we need to minimize the norm of the vector

$$\Delta \boldsymbol{T_c} = \boldsymbol{T_0} - \bar{\boldsymbol{A}}^{-1}(\boldsymbol{G}\dot{\bar{\boldsymbol{q}}} + \boldsymbol{\gamma R}\dot{\bar{\boldsymbol{q}}})$$

as possible as we can.

If we select the inverse of the $\bar{A}$ as

$$\bar{\boldsymbol{A}}^{-1} = (\boldsymbol{A}^{+} \quad \boldsymbol{N_A K}) \tag{5.3.15}$$

where $K = diag(k_1, \cdots, k_{n-m})$ can be selected to satisfied the equation, the vector ΔT_c can be rewritten as

$$\Delta \boldsymbol{T_c} = \boldsymbol{T_0} - \boldsymbol{A}^{+}(\bar{\boldsymbol{\tau}}_{\boldsymbol{Gm}} + \boldsymbol{\gamma}\bar{\boldsymbol{\tau}}_{\boldsymbol{Rm}}) - \boldsymbol{N_A K}(\bar{\boldsymbol{\tau}}_{\boldsymbol{Gnm}} + \boldsymbol{\gamma}\bar{\boldsymbol{\tau}}_{\boldsymbol{Rnm}}) \tag{5.3.16}$$

where $\bar{\boldsymbol{\tau}}_{\boldsymbol{Gm}}$ and $\bar{\boldsymbol{\tau}}_{\boldsymbol{Rm}}$ represent the first $\boldsymbol{m}$ elements of the vector $\boldsymbol{G}\dot{\bar{\boldsymbol{q}}}$ and $\boldsymbol{R}\dot{\bar{\boldsymbol{q}}}$, $\bar{\boldsymbol{\tau}}_{\boldsymbol{Gnm}}$ and $\bar{\boldsymbol{\tau}}_{\boldsymbol{Rnm}}$ represent the remaining $\boldsymbol{n-m}$ elements of the $\boldsymbol{G}\dot{\bar{\boldsymbol{q}}}$ and $\boldsymbol{R}\dot{\bar{\boldsymbol{q}}}$. $\boldsymbol{N_A}$ represents the null space of the matrix $\boldsymbol{A}$.

Notice that, if we select $\bar{\mathbf{A}}^{-1}$ as Eq. (28), $\bar{\mathbf{A}}$ would satisfy $\bar{\boldsymbol{A}} = \begin{pmatrix} \boldsymbol{A} \\ \boldsymbol{B} \end{pmatrix}$ which is proved in [41].

Based on this Eq. (5.3.16), it is easily to know that, when we have a certain $\bar{\boldsymbol{\tau}}$, the norm of $\Delta \boldsymbol{T_c}$ could have the minimum value by appropriately selecting each element of the diagonal matrix $\boldsymbol{K}$ to make it satisfy

$$\boldsymbol{K}(\bar{\boldsymbol{\tau}}_{\boldsymbol{Gnm}} + \boldsymbol{\gamma}\bar{\boldsymbol{\tau}}_{\boldsymbol{Rnm}}) = \boldsymbol{N_A}^{+}(\boldsymbol{T_0} - \boldsymbol{A}^{+}(\bar{\boldsymbol{\tau}}_{\boldsymbol{Gm}} + \bar{\boldsymbol{\tau}}_{\boldsymbol{Rm}})) \tag{5.3.17}$$

Thus, the minimum value of $\Delta \boldsymbol{T_c}$ can be formulated as

$$\Delta \boldsymbol{T_c} = (\boldsymbol{I} - \boldsymbol{N_A N_A}^{+})\,(\boldsymbol{T_0} - \boldsymbol{A}^{+}(\bar{\boldsymbol{\tau}}_{\boldsymbol{Gm}} + \boldsymbol{\gamma}\bar{\boldsymbol{\tau}}_{\boldsymbol{Rm}})) \tag{5.3.18}$$

From this result, ineq. (5.3.13) can be written as

$$\|\gamma \boldsymbol{w} - \boldsymbol{v}\| \leq r \tag{5.3.19}$$

where $\boldsymbol{w} = (\boldsymbol{I} - \boldsymbol{N_A N_A}^{+})\boldsymbol{A}^{+}\bar{\boldsymbol{\tau}}_{\boldsymbol{Rm}}$,$\boldsymbol{v} = (\boldsymbol{I} - \boldsymbol{N_A N_A}^{+})\,(\boldsymbol{T_0} - \boldsymbol{A}^{+}\bar{\boldsymbol{\tau}}_{\boldsymbol{Gm}})$.

Result from the reverse triangular inequality, we can get

$$r \geq \|\gamma \boldsymbol{w} - \boldsymbol{v}\| \geq |\gamma \|\boldsymbol{w}\| - \|\boldsymbol{v}\|| \tag{5.3.20}$$

Thus, after some algebra analysis, we obtain the condition for the control parameter γ as

$$\frac{\|\boldsymbol{v}\| - r}{\|\boldsymbol{w}\|} \leq \gamma \leq \frac{r + \|\boldsymbol{v}\|}{\|\boldsymbol{w}\|} \tag{5.3.21}$$

Consequently, we can solve the tension's problem following two steps:

1. Select $\boldsymbol{\gamma}$ satisfying (5.3.21).
2. Select the inverse of $\bar{\boldsymbol{A}}$ as (5.3.15)~(5.3.17).

Thus, we can overcome the problem brought by the limitation of cable tension so that to control the cable-driven robot tracking trajectory while keep the passivity contemporarily.

5.4 Simulation Studies

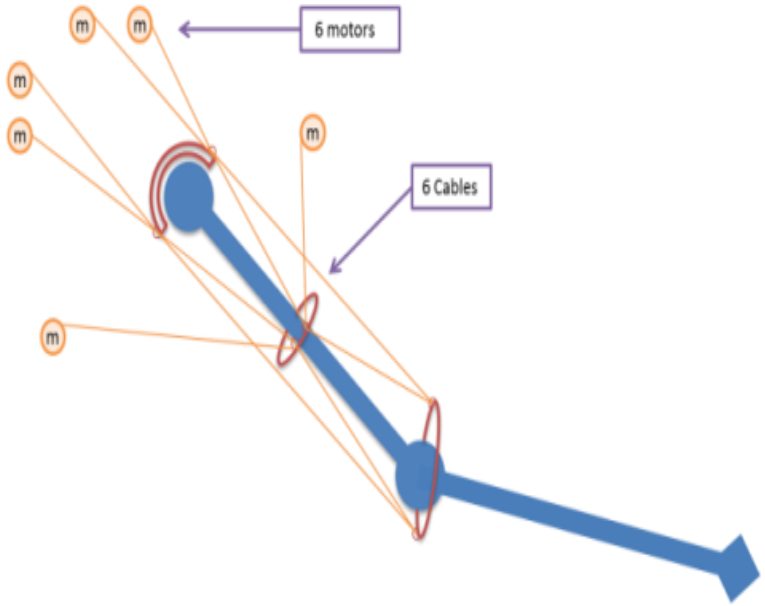

Fig.5.4 A 2-link cable driven manipulator

We performed simulations to verify the effectiveness of our method for a 2-DOF robot driven by 6 cables shown in Fig. 5.4 tracking a desired trajectory in the xy plane. The robot's physical parameters used for simulation are listed in Table 5.1, where I_1 and I_2 represent the inertial moment of each link's center of gravity, m_1 and m_2 represent mass of link, and L_1 and L_2 represent the length of each link.

I_1	0.625	kgm^2
I_2	0.625	kgm^2
m_1	1	kg
m_2	1	kg
L_1	1	m
L_2	1	m

Table 5.1 Physical parameter of the robot arm

Trajectory Tracking Ability

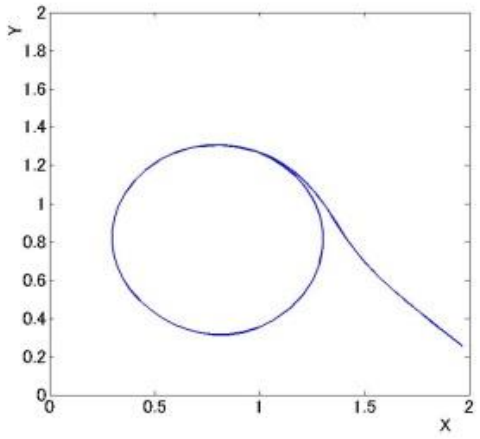

(a) $\gamma = 1$

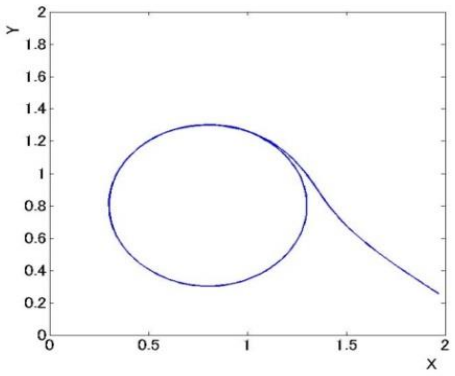

(b) $\gamma = 5$

Fig. 5.6 Trajectory of the manipulator's end-effector

Figs. 5.5 and 5.6 shows the position tracking results of the cable-driven robot while the control input tension T has been designed following Eq. (5.3.11). Fig.5.5 shows the desired velocity field of a circle trajectory with center point (0.8, 0.8) and radius 0.5. In Figs. 5.6(a) and 5.6(b), γ is selected as $\gamma = 1$ and $\gamma = 5$ respectively, it is obvious that both selection have a good property of tracking the desired trajectory.

Satisfaction of Tension's Condition

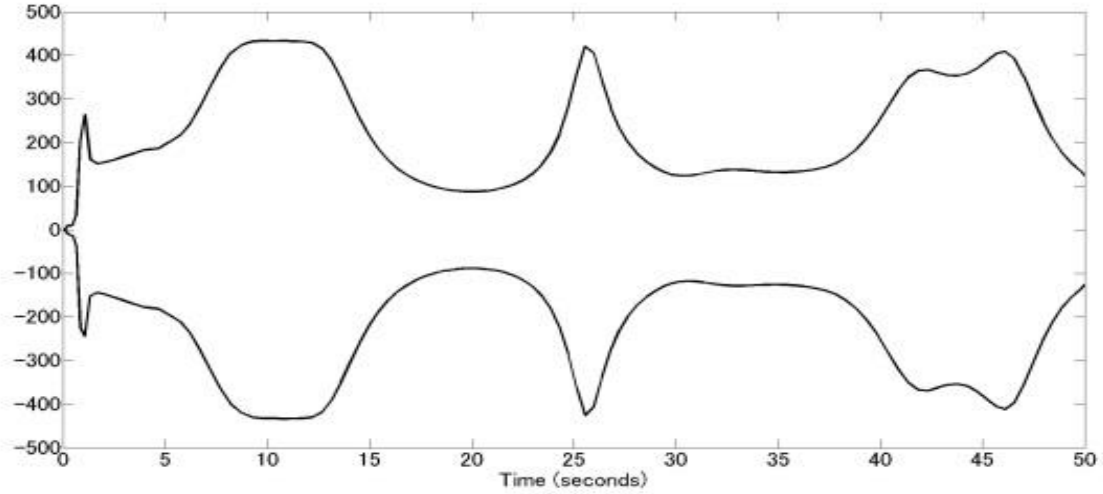

Total Upper and Lower bound

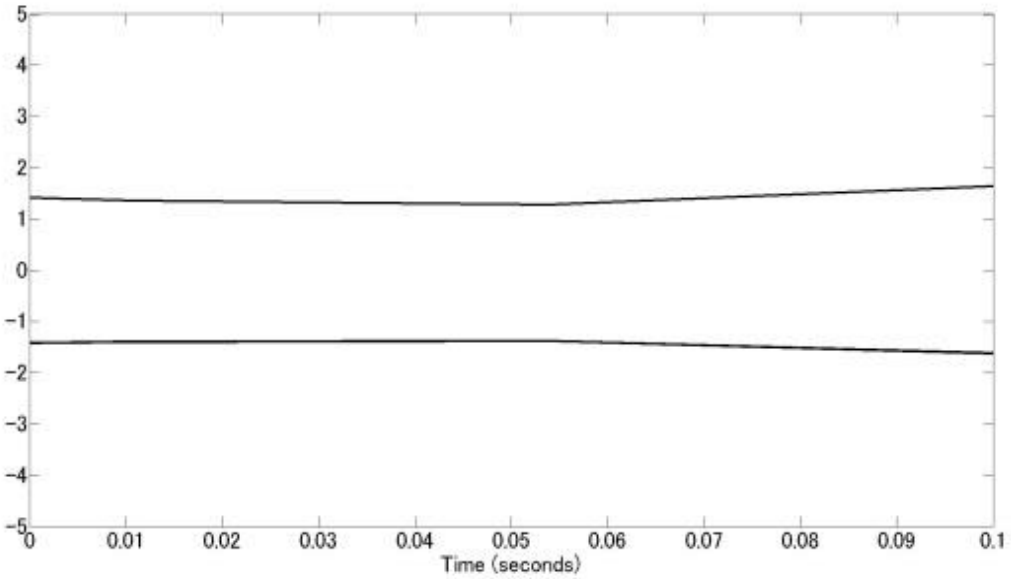

Upper and Lower bound at the Initial time

Fig.5. 7 Upper and Lower Bound of the γ when γ is selected as $\gamma = 1$

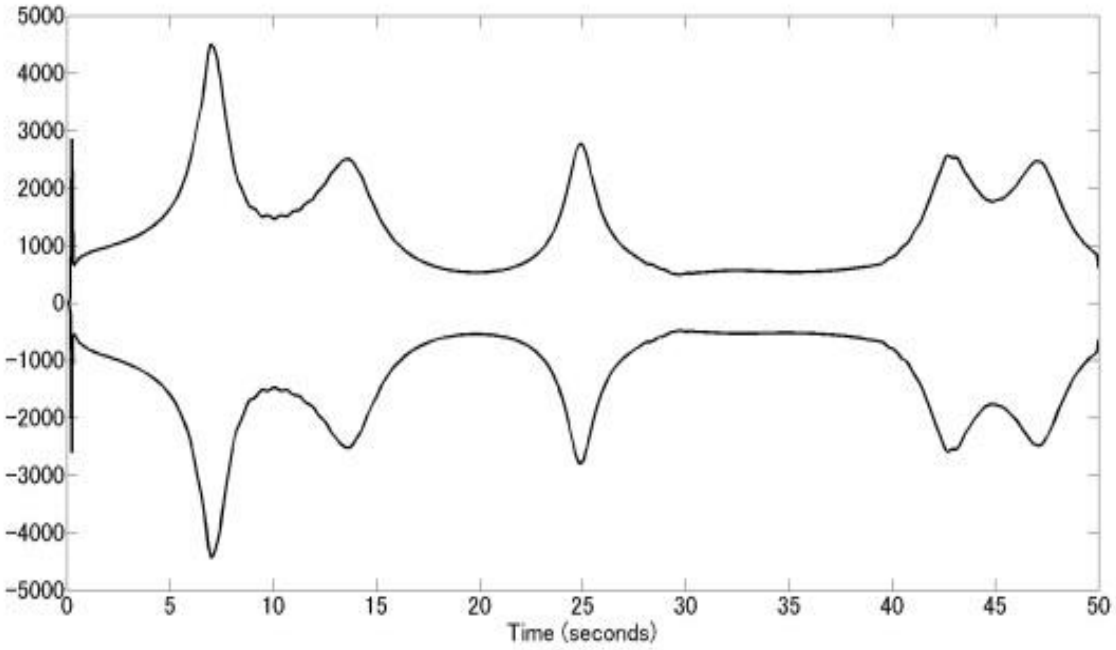

Total Upper and Lower bound

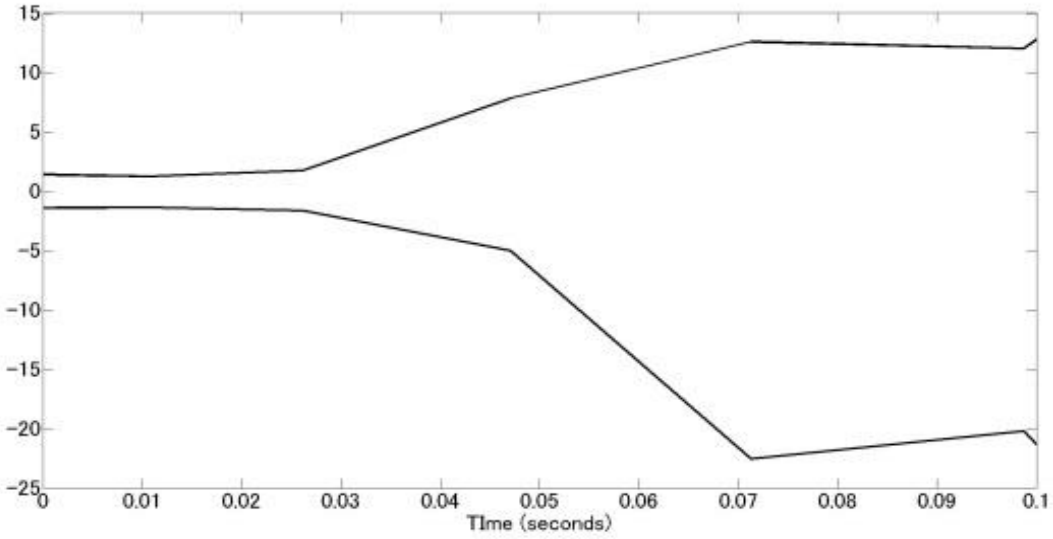

Upper and Lower bound at the Initial time

Fig. 5.8 Upper and Lower Bound of the γ when γ is selected as $\gamma = 5$

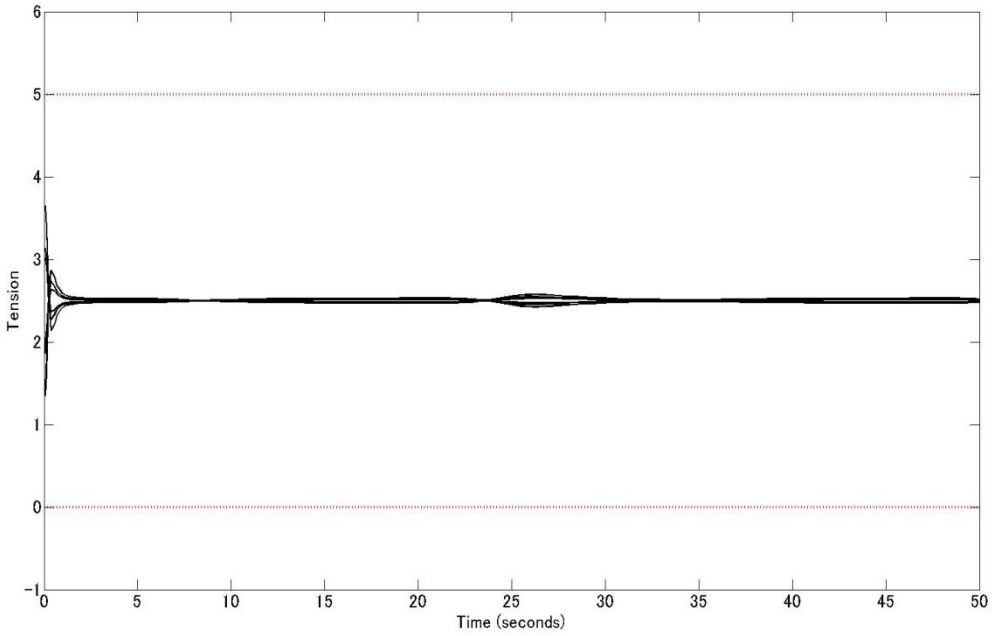

Tension's Result of total motion

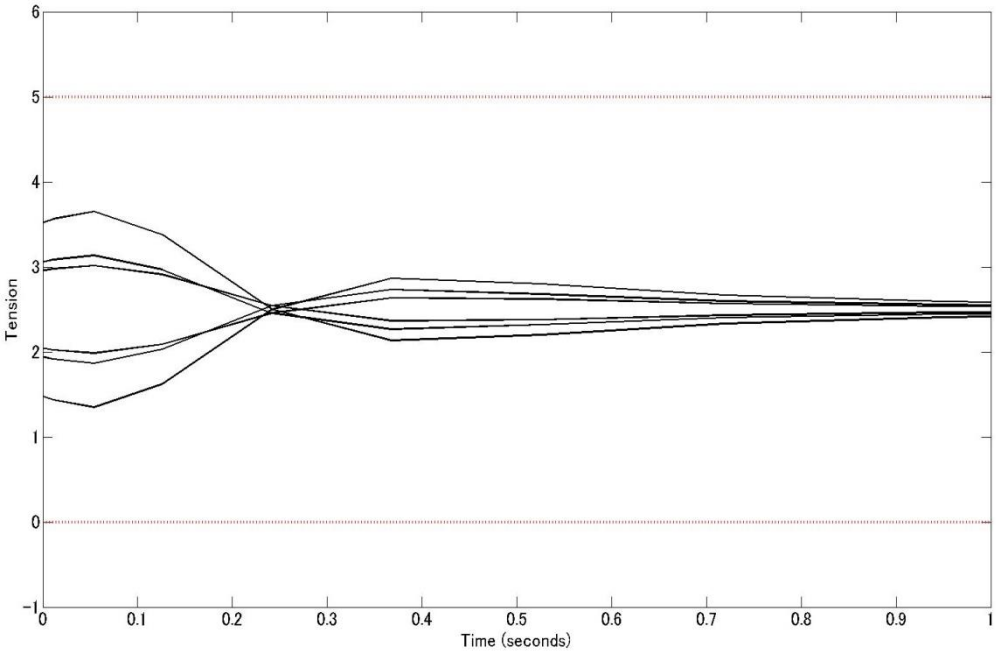

Tension's Result of the Initial Time

Fig. 5.9 Value of the cable's tension when γ is selected as $\gamma = 1$

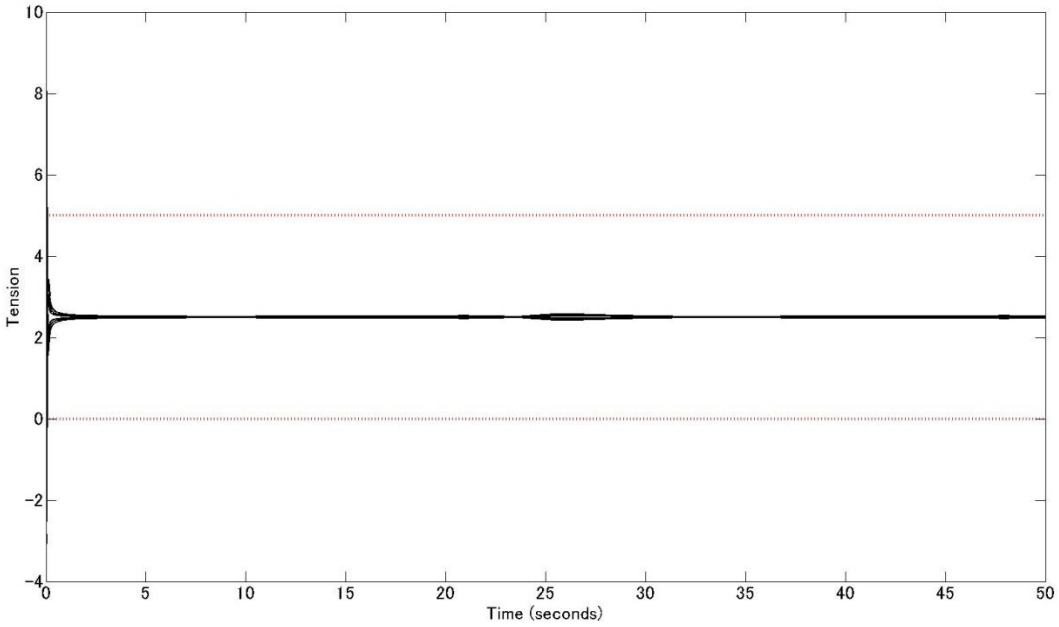

Tension's Result of total motion

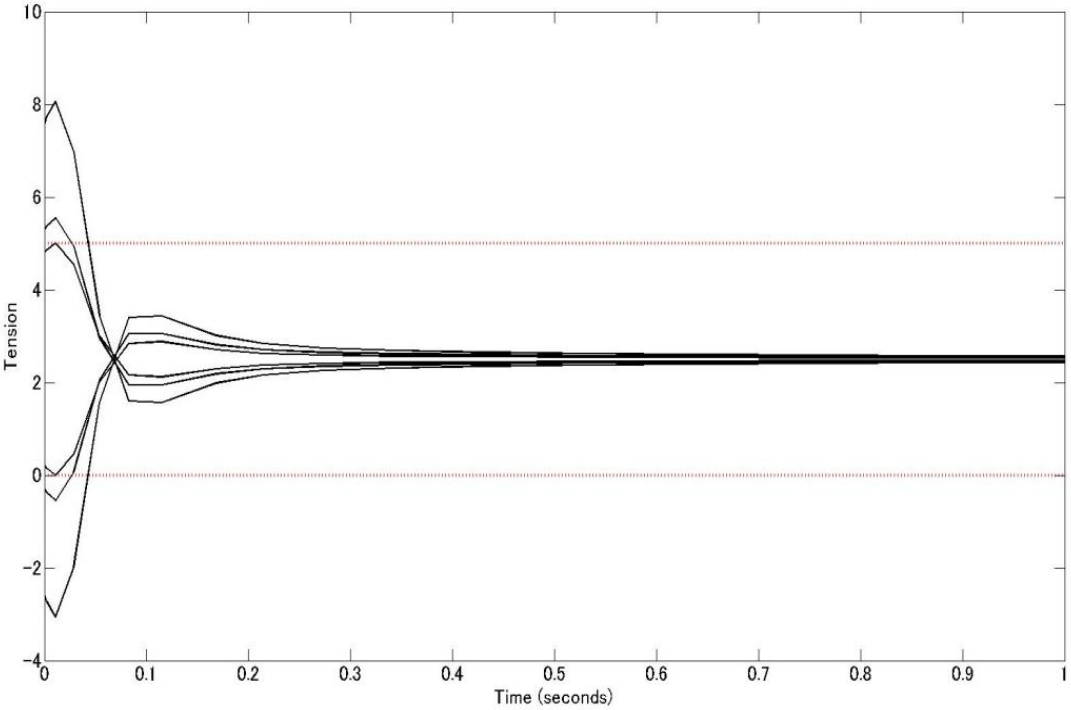

Tension's Result of the Initial Time

Fig. 5.10 The value of the cable tension ($\gamma = 5$)

In these two selection of γ, $\gamma = 1$ can satisfy ineq.(5.3.13) while $\gamma = 5$ is disable to satisfy this condition. We can check this following Figs. 5.7~5.8 representing upper and lower bound in Eq. (5.3.13) while using each γ.

From Figs. 5.7~5.8, it is clear that the selection of γ=1 satisfies the condition

ineq.(5.3.13) in total trajectory tracking's procedure while the selection of $\gamma = 5$ is not in the γ's selectable range at the initial time.

Figs. 9 ~10 show the cable tension's result while robot is tracking the desired circle with different selection of γ in control input (Eq. (5.3.11)). The upper and lower bound of the tension value is set as 0N and 5N.

From Fig.5.9, it is clear that when γ is properly selected, the cable tension may satisfy the tension constraint using our method. From Fig. 5.10, we see that, if γ is out of the range proposed in ineq. (5.3.13), the cable tension may not satisfy the constraint and cables cannot generate such a PVFC's control torque in Eq.(5.3.11) at manipulator's joint.

Passivity of Total Robot System

In xy plane, we set a stiff wall at the line $x + y = 1$ with a stiffness ratio $ke = 100$ and damper ratio $de = 20$ to test robot's passivity after punching the wall. We select appropriate $\gamma = 1$ in the control torque. The trajectory tracking's result can be shown as below.

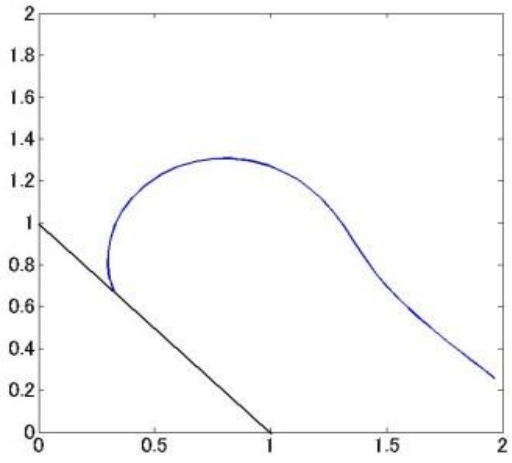

Fig. 5.11 Trajectory of the manipulator interacting with a stiff wall

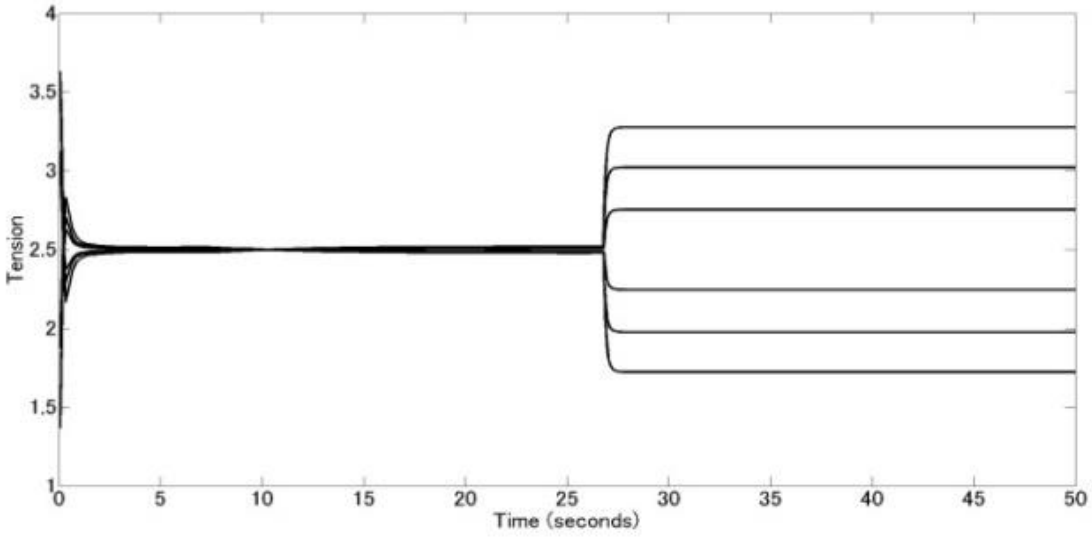

Fig. 5.12 Cable's Tension when robot interacting with a stiff wall

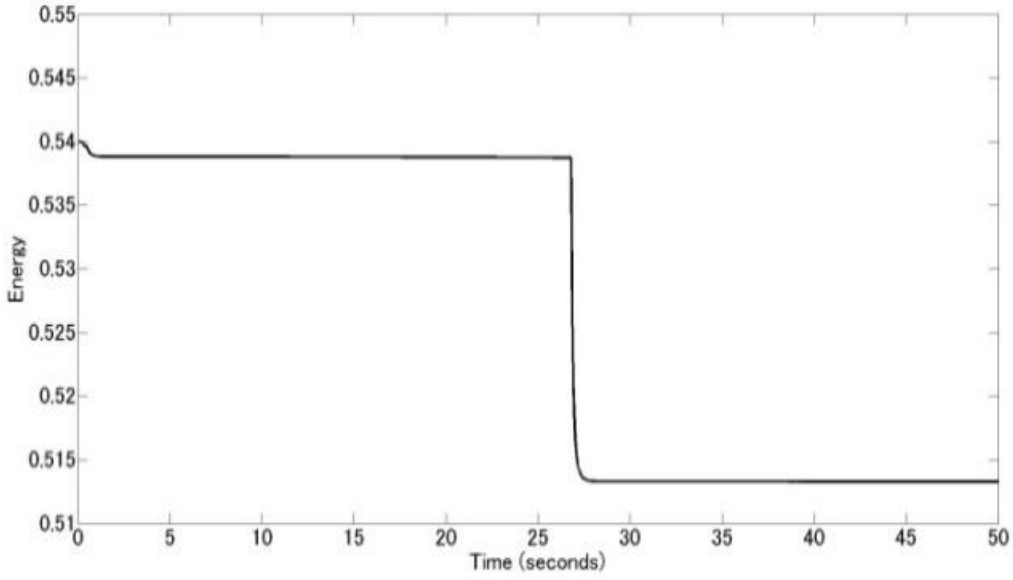

Fig. 13 Total Kinetic Energy of the whole System

From Fig. 5.11, we see that cable-driven manipulator perform well in trajectory tracking task while interacting with the environment. Meanwhile, from Fig.5.12, cables' tension does not violate the constraint in this procedure. From Fig. 5.13, it is clear that the whole system's kinetic energy would not exceed its initial value after punching the wall, which means that the passivity of the manipulator is satisfied.

Chapter 6 Conclusion

In this thesis, in order to properly design the human friendly robot considering the possible application in human care and rehabilitation, three basic researches are performed to realize human friendly robot interaction.

In the chapter 3, the optimal estimation of the position of object's center of gravity has been performed using the force sensors installed on the upper arms of a nursing care robot. It is worth to notice that, here, the problem of the different position of the sensors and the contact points during the human robot interaction has been solved in this research. In order to verify the effectiveness of the research, we perform the simulation and experiment for two situations (single contact point and dual contact point). The results of simulation and experiment show that it can steady estimate the position of gravity center with little error. Since the model errors of the robot may also introduce some errors on the estimation, hence, in the future work, it is necessary to correct the model of the robot so as to estimate more accurately.

On the other hand, in chapter 4, the thesis studied how to satisfy the robot's passivity when the robot with model uncertainties to interact with its environment so as for the robot to keep its safety. In the first place of this research, robust passive impedance control approach was proposed. This approach adjusts the estimations of the robot's dynamic parameters in a simple way. Thus, it can keep robot's passivity under the existence of the model errors. However, the impedance control performances, such as tracking responses, still be influenced by the model errors. Then, we proposed a novel control approach for a robot with model uncertainties to perform dynamic interaction with environment. By introducing a reference impedance model as well as an observer, this approach can not only keep the robot's passivity even for the time-varying impedance center, but also greatly improved the impedance control performances.

Lastly, in chapter 5, focused on the fitness between the robot and human, a control method on cable driven robot system was proposed, which can adapt the human structure better than the traditional robot. The dynamic control of a cable driven robot

with the cable's tension limitation as well as the cable's redundancy were studied in order to complete the passive trajectory tracking control while keeping the passivity. Here, a virtual subsystem was applied to eliminate the redundancy of the original system so that it can easily transfer the tension constraint condition into the wrench space. Then, using PVFC control method, the convergence of the trajectory tracking and the passivity can be achieved. After analyzing this PVFC's control input in the wrench space, a condition to adjust the control parameter was derived so as to solve the cable's tension limitation. Compared with other previous researches, this method enables the trajectory tracking control of the cable-driven robot with an easy wrench adjustment algorithm and no heavy optimization for tension distribution. Simulations were performed to verify the effectiveness of this research. The comparison results showed that robot driven by cables can track the trajectory while keep its passivity at the same time very well.

Human friendly robot is more and more popular nowadays and no doubt it can support more and more tasks in human's daily life in the near future. It is expected that, these three researches can help the development of next human friendly robot.

There still remain problems needs to be considered in the human friendly robot's design. For example, in order to generalize the robot's use, we need to make the robot to adapt to different individuals. Considering the passivity research, in the previous and this research, we mainly discuss how to keep the robot's passivity. We select a certain limitation of the energy transferring form robot to the environment. Nevertheless, sometimes, we have to change this power's limitation to adapt the varying situation. For instance, for a rehabilitation robot, we can make robot to adapt to patients with different degree of motion ability lost by providing different degree of support power. In the future, we need to discuss about how to determine the energy limitation and how to change the limitation. Moreover, when we consider the cable-driven robot's design, how to optimize the cable-driven robot's structure to adapt individual's different body structure is also a big problem.

We cannot say that the research on human friendly robot is perfectly complete now. Actually, research on the human friendly robot can also be named as human

centered robot and it is a rethink of ourselves. Further consideration of this design from the inspiration in our daily life is expected to make it more comfortable and useful.

Acknowledgements

I have received a lot of help and encouragement from many people during these three years. Without their support and encouragement, I could not complete this thesis. Here, I have a chance to express my great gratitude to them.

Firstly, I would like to express my deep and sincere gratitude to my supervisor, Prof. Zhiwei Luo for his constant encouragement and guidance. He set a good example to me about how to make a research more scrupulously and scientifically. Without his patience, consistent and illuminating instruction, my research should not reach its present form. During my academic writing process, he pointed out some weakness in my paper kindly. Because of this, my paper can be improved step by step.

Next, thanks Prof. Uehara and Prof. Matoba for the effort in reviewing the dissertation. Without their help, this dissertation would not be so logically structured and accurately written.

At the same time, I want to show my sincere thanks to Prof. Quan. She provided me many useful instructions and ideas about my research. Her intelligent instruction is the strong driving force of my research.

In addition, it is my pleasure to thank my colleagues in CS11 laboratory. Without their advices and cooperation, my research cannot be worked out smoothly.

Finally, I would like to thank my family and dear friends for their generous supporting. I will give my best wishes to my parents for their mental support in three years. I thank my friends, because of their patient comforts when I was disappointed.

.

Reference

[1] F. Asano, Z.W. Luo, M. Yamakita, S. Hosoe "Modeling and bio-mimetic control for whole-arm dynamic cooperative manipulation", Advanced Robotics 19.9, 2005,pp.929-950.

[2] T. Odashima, M. Onishi, K. Tahara, K. Takagi, F. Asano, H. Nakashima, Y. Kabayashi, T. Mukai, Z.W. Luo, S. Hosoe "A soft human-interactive robot ri-man", In Proc. IEEE/RSJ Int. Conf. Intelligent Robots and Systems Intelligent Robots and Systems, 2006,pp. 1-1.

[3] M. Onishi, Z.W. Luo, T. Odashima, S. Hirano, T. Mukai "Generation of human care behaviors by human-interactive robot RI-MAN ", In Proc. IEEE Int. Conf. Robotics and Automation, 2007,pp.3128-3129.

[4] F. Asano, Z.W. Luo, M. Yamakita, Hosoe S "Modeling and bio-mimetic control for whole-arm dynamic cooperative manipulation ", Advanced Robotics 19.9, 2005, pp.929-950.

[5] T. Mukai, Y. Kato "1 ms soft areal tactile giving robots soft response.", Journal of Robotics and Mechatronics 20.3 ,2008, pp.473.

[6] K. Nagase, K. Yoshinaga, A. Nakashima, Y. Hayakawa "Estimation of contact point by force sensor with measurement noise ", Journal of the Robotics Society of Japan 23.6, 2005, pp. 725-731.

[7] H.W. Dong, Z.W. Luo, A. Nagano " Reduced model adaptive force control for carrying human beings with uncertain body dynamics in nursing care ", In Proc. IEEE/ASME Int. Conf. Advanced Intelligent Mechatronics (AIM), 2010,pp.193-200.

[8] G. Hirzinger, N. Sporer, A. Albu-Schaffer, M. Hahnle, and A. Pascucci "DLR's torque-controlled light weight robot III—Are we reaching the technological limits now? " In Proc. Int. Conf. Robotics Automation, 2002, pp. 1710–1716.

[9] M. Zinn , O. Khatib , B. Roth , J.K. Salisbury "Playing it safe [human-friendly robots]." IEEE Robotics & Automation Magazine 11.2, 2004, pp. 12-21.

[10] D. Vischer, O. Khatib "Design and development of high-performance

torque-controlled joints", IEEE Transactions on robotics and automation 11.4 ,1995,pp.537-544.

[11] N. Hogan "Impedance control: An approach to manipulation: Part II—Implementation." Journal of dynamic systems, measurement, and control 107.1,1985,pp. 8-16.

[12] P.Y. Li, R. Horowitz "Passive velocity field control of mechanical manipulators." , IEEE Transactions on robotics and automation 15.4,1999, pp. 751-763.

[13] M. Yamakita, K. Suzuki, X. Z. Zheng, M. Katayama, K. Ito "An extension of passive velocity field control to cooperative multiple manipulator systems", In Proc. IEEE Int. Conf. Intelligent Robots and Systems Vol. 1. 1997,pp.11-16

[14] P.Y. Li "Adaptive passive velocity field control", In Proc. IEEE Int. Conf. American Control Conference Vol. 2, 1999.

[15] P.Y. Li, R. Horowitz "Passive velocity field control (PVFC). Part I. Geometry and robustness", IEEE Transactions on Automatic Control 46.9 , 2001,pp. 1346-1359.

[16] P.Y. Li, R. Horowitz "Passive velocity field control (PVFC). Part II. Application to contour following", IEEE Transactions on Automatic Control 46.9 ,2001, pp. 1360-1371.

[17] Y. Kishi, Z.W. Luo, F. Asano, S. Hosoe "Passive impedance control with time-varying impedance center.", In Proc. IEEE Int. Conf. Computational Intelligence in Robotics and Automation Vol. 3, 2003.

[18] K. Kido, Z.W. Luo, and A. Nagano "Passive control of a Dual-Arm cooperative robot." , In Proc. IEEE Int. Conf. SICE Annual Conference, 2010.

[19] J.J. E.Slotine, W.P Li "Applied Nonlinear Control", Prentice Hall，1991

[20] B. Bobath "Adult Hemiplegia: Evaluation and Treatment. ", London: Butterworth-Heinemann Medical, 1990

[21] M.F. Levin, E. Panturin “Sensorimotor integration for functional recovery and the Bobath approach.”, Motor Control 15, 2011, pp.285–301.

[22] L. Dipietro, H. I. Krebs, S. E. Fasoli, B. T. Volpe, J. Stein, C. Bever, N. Hogan "Changing motor synergies in chronic stroke.", Journal of neurophysiology 98.2 , 2007, pp. 757-768.

[23] P. Tropea, V. Monaca, M. Coscia, F. Posteraro, S. Micera, "Effects of early and intensive neuro-rehabilitative treatment on muscle synergies in acute post-stroke patients: a pilot study.", Journal of neuroengineering and rehabilitation 10.1, 2013, pp.103.

[24] M.D. Ellis, T. Sukal-Moulton, J. P. Dewald "Progressive shoulder abduction loading is a crucial element of arm rehabilitation in chronic stroke." Neurorehabilitation and neural repair 23.8, 2009, pp.862-869.

[25] T. Krabben, G.B Prange, B.I. Molier, A.HA. Stienen, M.JA Jannink, J.H. Buurke, J.S. Rietman "Influence of gravity compensation training on synergistic movement patterns of the upper extremity after stroke, a pilot study." Journal of neuroengineering and rehabilitation 9.1, 2012, pp. 44.

[26] T. Nef, M. Guidali, and R. Riener "ARMin III–arm therapy exoskeleton with an ergonomic shoulder actuation.", Applied Bionics and Biomechanics 6.2, 2009, pp.127-142.

[27] C. Carignan, M. Liszka "Design of an arm exoskeleton with scapula motion for shoulder rehabilitation", In Proc. IEEE Int. Conf. Advanced Robotics, 2005.

[28] T. Noritsugu, T. Tanaka "Application of rubber artificial muscle manipulator as a rehabilitation robot", IEEE/ASME Transactions On Mechatronics 2.4 ,1997, pp. 259-267.

[29] T. Nakamura, N. Saga, K. Yaegashi "Development of a pneumatic artificial muscle based on biomechanical characteristics.", In Proc. IEEE Int. Conf. Industrial Technology Vol. 2 , 2003.

[30] Y. Mao, S.K. Agrawal "Design of a cable-driven arm exoskeleton (CAREX) for neural rehabilitation.", IEEE Transactions on Robotics 28.4, 2012, pp. 922-931.

[31] Y. Mao, X. Jin, G.G. Dutta, J. P.Scholz, S.K. Agrawal "Human movement training with a cable driven arm exoskeleton (carex).", IEEE Transactions on Neural Systems and Rehabilitation Engineering 23.1,2015,pp. 84-92.

[32] A.B. Alp, S.K. Agrawal "Cable suspended robots: design, planning and control", In Proc. IEEE Int. Conf. Robotics and Automation, 2002. pp. 4275–4280.

[33] C.B. Pham, S.H. Yeo, G. Yang, M. S. Kurbanhusen, I.M. Chen "Force-closure workspace analysis of cable-driven parallel mechanisms.", Mechanism and Machine Theory 41.1,2006, pp. 53-69.

[34] S.K. Mustafa, S.K. Agrawal "On the force-closure analysis of n-DOF cable-driven open chains based on reciprocal screw theory." IEEE Transactions on Robotics 28.1, 2012, pp. 22-31.

[35] Q.J. Duan, V. Vashista, and S.K. Agrawal "Effect on wrench-feasible workspace of cable-driven parallel robots by adding springs.", Mechanism and Machine Theory 86, 2015, pp. 201-210.

[36] P. Bosscher, T. R. Andrew, I. Ebert-Uphoff "Wrench-feasible workspace generation for cable-driven robots." IEEE Transactions on Robotics 22.5 ,2006, pp. 890-902.

[37] S.R. Oh, S.K. Agrawal "Cable suspended planar robots with redundant cables: controllers with positive tensions ", IEEE Transactions on Robotics 21.3, 2005, pp. 457-465.

[38] S.R. Oh, S.K. Agrawal "Generation of feasible set points and control of a cable robot ", IEEE Transactions on Robotics 22.3, 2006, pp. 551-558.

[39] S. Fang, D. Franitza, M. Torlo, F. Bekes, M. Hiller "Motion control of a tendon-based parallel manipulator using optimal tension distribution", IEEE/ASME Transactions On Mechatronics 9.3, 2004,pp. 561-568.

[40] P.H. Borgstrom, B.L. Jordan, G.S. Sukhatme, M.A. Batalin, W.J. Kaiser "Rapid computation of optimally safe tension distributions for parallel cable-driven robots", IEEE Transactions on Robotics 25.6 , 2009,pp.1271-1281.

[41] L. Ros, A. Sabater, F. Thomas “An ellipsoidal calculus based on propagation and fusion.”, IEEE Transactions on Systems, Man, and Cybernetics, Part B (Cybernetics) 32.4, 2002, pp. 430-442.

[42] S. Arimoto, F. Miyazaki. "Stability and robustness of PD feedback control with gravity compensation for robot manipulator", ASME Winter Meeting., 1986.

Publications

[1] Sheng Cao, Zhiwei Luo, Changqin Quan "On Energy-based Robust Passive Impedance Control of a Robot Manipulator", Journal of Mechanics Engineering and Automation 7.2, 2017, pp.65-70

[2] Sheng Cao, Zhiwei Luo, Changqin Quan "On Observer-based Passive Robust Impedance Control of a Robot Manipulator", Journal of Mechanics Engineering and Automation 7.2, 2017, pp.71-78

[3] Sheng Cao, Zhiwei Luo, Changqin Quan "Estimaion of an Object's Physical Parameter by Force Sensors of a Dual-arm Robot", Journal of Mechanics Engineering and Automation 7.3, 2017, pp.120-131

[4] Sheng Cao, Zhiwei Luo, Changqin Quan "Passive Velocity Field Control of a Redundant Cable-Driven Robot with Tension Limitations", Journal of Mechanics Engineering and Automation 7.3, 2017, pp.132-144

Doctor Thesis, Kobe University

"Optimal Estimation and Passivity based Control for Human Friendly Robots",

100 pages Submitted on July, 1st, 2017

The date of publication is printed in cover of repository version published in Kobe University Repository Kernel.